

**T-Pos247** CORRELATIVE MORPHOLOGIC AND PHYSIOLOGIC FEATURES OF IDENTIFIED SYNAPSES BETWEEN INDIVIDUAL SENSORY AND MOTOR NEURONS OF *APLYSIA* CO-CULTURED ON POLYLYSINE-COATED ACLAR SUBSTRATES. E.B. Masurovsky, D. Glanzman, and S. Schacher, Center for Neurobiology and Behavior, Columbia Univ. Coll. of P&S, and NYS Psychiatric Inst., New York, N.Y. 10032.

Sensory and motor neurons isolated from the abdominal ganglion of *Aplysia californica* reliably form chemical connections *in vitro* and can undergo both short-term and long-term alterations in synaptic strength (Rayport and Schacher, *J. Neurosci.*, 6:759, 1986; Montarolo et al., *Science*, 234:1249, 1986). In an attempt to examine the structural changes that may accompany the various forms of plasticity at the sensory-motor synapse, we have combined electron microscopic analysis with the fluorescence microscope methodology recently developed by Purves and Hadley (*Nature*, 315:404, 1985) for visualizing the structural features of a single identified neuron. Individual sensory and motor neurons isolated from the abdominal ganglion of *Aplysia* were plated in close proximity on polylysine-coated Aclar plastic coverslips (Masurovsky and Bunge, *Stain Tech.*, 43:161, 1968). After 4-5 days *in vitro*, synaptic strength was assayed electrophysiologically. Sensory neurons that had formed strong chemical connections (10-40 mV) were injected with the fluorescent dye 5(6)-carboxyfluorescein and viewed with a fluorescence microscope coupled to a low-light level video camera to delineate putative synaptic varicosities and boutons. The cultures were then fixed for correlative electron microscope analysis using a 3-step fixation protocol (Masurovsky et al., *Soc. Neurosci.* 7th Annu. Mtg. Abstr., p. 374, 1977)  $\pm$  10% or 20% sucrose (Schacher and Proshansky, *J. Neurosci.*, 2:2403, 1983). We saw synaptic configurations containing  $\sim$ 65-90  $\pm$  5 nm variably-lucent and some  $\sim$ 100  $\pm$  8 nm dense-cored presynaptic vesicles near membrane- and synaptic cleft-specializations reminiscent of *Aplysia* synapses *in vivo* (Bailey and Chen, *Science*, 220:91, 1983), which were correlatable with fluorescent images suggestive of synaptic locales. These sites appeared accessible for antibody and biochemical probes. (Supported by the McKnight Foundation.)

**T-Pos248** DYNAMICS OF AN OPTIMAL LEARNING ALGORITHM Daniel Ruderman and William Bialek, Departments of Physics and Biophysics, University of California, Berkeley, CA 94720.

Many perceptual tasks, such as the detection and recognition of sounds or images in a noisy background, can be approximated by the mathematical problem of discriminating among signals chosen randomly from two or more categories given by probability distributions. There is a well developed theory of such problems from the point of view of an observer who knows essentially everything about the relevant probability distributions. We are trying to develop the corresponding theory for an observer who lacks knowledge of the probability distributions and thus must *learn* to perform recognition tasks using only a finite set of samples from each category of signals. For one-dimensional signals in two categories we have been able to formulate the optimal learning strategy in a simple fashion easily amenable to simulation. Results show that the minimum rate of incorrect recognitions  $f_{inc}$  after learning from  $N$  samples of each category varies approximately as  $f_{inc}(N) = f_{inc}(\infty) + AN^{-\alpha}$ , where the exponent  $\alpha$  decreases monotonically as the 'signal-to-noise ratio' for the recognition task decreases; there appears to be a critical signal-to-noise ratio at which this scaling behavior is exact for all  $N$ , and we always find  $\alpha < 1$ . Qualitative arguments suggest that the exponent  $\alpha$  will decline in higher dimensional problems such as the recognition of speech sounds or complex images, and we hope to support these arguments with detailed simulations. These results raise several important questions: Do humans approach optimal learning performance? Can near-optimal learning be achieved through simple algorithms? Are there rather natural tasks which are of such high dimensionality that they become essentially unlearnable ( $\alpha \rightarrow 0$ )?

This work is supported in part by grants from the NSF and the USPHS.

**T-Pos249** PERFORATED PATCH RECORDING TO PREVENT WASH-OUT. Richard Horn, Alain Marty and Stephen J. Korn (Intr. by Carole Bailey). Ecole Normale Supérieure, 75005 Paris; Dept. of Neurosci., Roche Inst. of Mol. Biol., Nutley, NJ 07110.

A new method is introduced to prevent wash-out of membrane currents which disappear during usual whole-cell recording. The method, which is a variation of "slow whole-cell recording" (Lindau & Fernandez, 1986, *Nature* 319:150), makes use of the pore-forming antibiotic nystatin, which is introduced into the patch pipette in the cell-attached patch configuration. Nystatin permeabilizes the patch with a multitude of tiny pores that provide electrical continuity between the pipette and the cell interior without loss or alteration of cytoplasmic compounds necessary for the maintenance of membrane currents. The conductance induced by nystatin is reversible and monovalent cation selective. Thus, small monovalent cations (e.g. Cs<sup>+</sup> or K<sup>+</sup>) may be exchanged between the pipette and the cell. The series resistance following application of nystatin is concentration-dependent and varies from  $\sim$ 83 M $\Omega$  at 50  $\mu$ g/ml nystatin to  $\sim$ 13 M $\Omega$  at 100  $\mu$ g/ml. We have examined two currents that wash-out within 5-10 min in typical whole-cell recordings: i) K<sup>+</sup> and Cl<sup>-</sup> currents induced by the muscarinic action of acetylcholine (ACh) in rat lacrimal gland cells, and ii) Ca<sup>++</sup> currents in GH3 cells. In both cases the currents were maintained for >50 min. The ACh-induced currents were unchanged during this period whereas the Ca<sup>++</sup> currents showed a greatly slowed decrease.

**T-Pos250 MODULATION OF MEMBRANE CURRENTS IN GH3 PITUITARY CELLS BY DOPAMINE.**  
Stephen J. Korn and Richard Horn, Dept. of Neurosci., Roche Inst. of Mol. Biol., Nutley, NJ 07110.

Dopamine (DA) inhibits both basal and stimulated prolactin release from anterior pituitary cells in a dose-dependent manner, possibly through one or more second messenger systems. We are using GH3 cells, which are lactotrophs cloned from a rat anterior pituitary tumor, to study the effects of DA on membrane currents, and the relationship between membrane currents and prolactin release. GH3 cells, like pituitary cells in primary culture, spontaneously fire action potentials mediated by  $\text{Ca}^{++}$  and  $\text{Na}^+$ , and host a variety of membrane currents, including voltage- and  $\text{Ca}^{++}$ -activated  $\text{K}^+$  currents. Application of DA (1  $\mu\text{M}$ ) reversibly hyperpolarizes GH3 cells and decreases the frequency of action potential firing. We observed two effects of DA on  $\text{Ca}^{++}$ -activated  $\text{K}^+$  currents in whole-cell recordings: an immediate, reversible potentiation and a much larger, irreversible potentiation. The reversible effect was also observed in cell-attached patches as an increased probability of opening of single  $\text{Ca}^{++}$ -activated  $\text{K}^+$  channels. Since  $\text{Ca}^{++}$  currents steadily "wash out" of GH3 cells following the onset of whole cell recording, we are using the perforated-patch technique, described in the previous abstract, to study the effects of DA on  $\text{Ca}^{++}$  currents, and the possible involvement of second messenger systems whose function may also be impaired by "wash-out."

**T-Pos251 NERVE GROWTH FACTOR (NGF) TREATMENT OF PC12 CELLS INCREASES THE PROPORTION OF VOLTAGE-ACTIVATED K CHANNELS THAT ARE TEA-SENSITIVE.**

Daniel Kalman and Paul H. O'Lague, Department of Biology, UCLA, Los Angeles CA

PC12 cells treated with NGF, the trophic substance for developing sympathetic neurons, undergo neuron-like differentiation. They develop neurites and express functional Na channels. We report that NGF also initiates significant alterations in the relative numbers of two types of voltage-activated K channels as judged by patch clamp studies of dialyzed cells and membrane patches. Before NGF treatment, ~50% of the macroscopic K current elicited by depolarizing from -60 mV ( $V_h$ ) to +40 mV for 160 ms was blocked by TEA (20 mM). The remaining current was blocked by 4-aminopyridine (4-AP, 5mM), inactivated strongly during the step ( $t_{1/2}$  ~100 ms), and underwent steady-state inactivation at more positive holding potentials. The 4-AP-sensitive current closely resembles the A-type K current described in many excitable cells whereas the TEA-sensitive current resembles that of the delayed rectifier. Following NGF treatment for five days, over 90% of the current became TEA-sensitive. Single channel recordings from both treated and untreated cells revealed two classes of K channels in cell-attached patches: one class with a large conductance blocked by TEA; the other with a small conductance blocked by 4-AP. The probability of opening of the small conductance channel decreased both during depolarization and with holding potentials more positive than -60 mV. In NGF-treated cells we observed an increase only in the number of large conductance channels per patch (n=14). These results indicate that the pharmacological changes observed with NGF treatment arises from an increase in the relative number of TEA-sensitive K channels.

**T-Pos252 PALYTOXIN INDUCES A RELATIVELY NON-SELECTIVE CATION PERMEABILITY IN FROG MYELINATED NERVE WHICH CAN BE INHIBITED BY CARDIAC GLYCOSIDES.** N.A. Castle and G.R. Strichartz. Anesthesia Research Labs, Brigham & Women's Hospital, Harvard Medical School, Boston, MA 02115.

Palytoxin (PTX) is a non-peptide toxin (MW 2678) present in marine soft corals of the *Palythoa* genus. It causes both nerve and muscle to depolarize and also stimulates  $\text{K}^+$  release from erythrocytes. Recent studies on erythrocytes suggest that PTX actions may be inhibited by cardiac glycosides. In the present study we have examined the actions of PTX on frog sciatic nerve using the sucrose-gap technique. In Ringer solution containing 12 mM tetraethylammonium and 50 nM saxitoxin (to block voltage-gated  $\text{K}^+$  and  $\text{Na}^+$  channels), PTX (1-100 nM) evokes a dose-dependent irreversible depolarization of up to 25 mV. This depolarization can also be observed when extracellular  $\text{Na}^+$  is replaced by  $\text{Li}^+$ ,  $\text{Cs}^+$ , methylamine, hydroxylamine, methylhydroxylamine but not by tetramethylammonium or choline. The cardiac glycoside, cymarin inhibits the PTX evoked depolarization in a dose-dependent manner, half maximal inhibition being observed at ~10  $\mu\text{M}$ . Interestingly, strophanthidin, the aglycon of cymarin, which reportedly exhibits a similar potency for inhibiting  $\text{Na}^+/\text{K}^+$  ATPase fails to produce a significant inhibition of PTX action even when present at 1 mM.

We conclude that PTX induces the opening or formation of a cation permeable pore which exhibits less selectivity than the  $\text{Na}^+$  channel. The inhibitory action of cymarin suggests that this pore may be associated with the  $\text{Na}^+/\text{K}^+$  pump although the exact mechanism of PTX/cardiac glycoside interaction remains uncertain.

**T-Pos253** AN ANALYSIS OF THE PHASE-DETECTOR TECHNIQUE FOR STUDYING EXOCYTOSIS. Chaya Joshi and Julio M. Fernandez, Univ. of Pennsylvania, Philadelphia, PA 19104-6085. Intr. by D.H. Kim.

Using patch-clamp and circuit analysis techniques, we studied the admittance of degranulating mast cells. We found they are described by four circuit elements: membrane capacitance,  $C$ , membrane conductance,  $G$ , access conductance,  $G_s$ , and stray capacitance. Current,  $I$ , can be measured using a two-phase detector either at phase-angle  $\alpha$  ( $\Delta I$  due to  $\Delta G$ , other elements constant) and  $\alpha-90^\circ$ , or at  $\theta$  ( $\Delta I$  due to  $\Delta G_s$ ) and  $\theta-90^\circ$ . The relative contribution of  $\Delta G_s$  and  $\Delta C$  to  $\Delta I_{\alpha-90^\circ}$  is  $\frac{2GC}{G_s^2} \frac{\Delta G_s}{\Delta C}$ . While that of  $\Delta G$  and  $\Delta C$  to  $\Delta I_{\theta-90^\circ}$  is  $\frac{2G}{\omega^2 C} \frac{\Delta G}{\Delta C}$ . Typically, mast cells have few ion channels (small  $\Delta G$ ) while  $\Delta G_s$  is large. Therefore,  $\Delta G_s$  dominates  $\Delta I_{\alpha-90^\circ}$  while  $\Delta C$  dominates  $\Delta I_{\theta-90^\circ}$ . In contrast with present methods, to study capacitance changes in mast cells,  $\Delta I$  must be monitored at  $\theta-90^\circ$ . Since the system is changing,  $\theta$  is changing while the detector remains fixed. For a typical 7 pF cell containing 1000, 14 fF granules, if the cell is properly compensated, and the appropriate phase-angle has been found before degranulation, then the size of the first few granules can be accurately determined. However, due to the change in cell capacitance, the measured size of the 500th granule would be 8.75 fF instead of the true 14 fF. We have derived a closed-form expression for these errors in the granule size as the cell degranulates. Finally, we present an algorithm for a software-based phase detector which simplifies capacitance measurements.

**T-Pos254** THE FORMATION OF SECRETORY GRANULES AS REVEALED BY MEMBRANE CAPACITANCE MEASUREMENTS, G. Alvarez de Toledo and J.M. Fernandez, Department of Physiology, School of Medicine University of Pennsylvania, Phila., PA 19104-6085

The membrane area of secretory granules was measured in developing mast cells by monitoring the size of step increases in the cell membrane capacitance during exocytosis. The cell membrane capacitance was monitored using patch-clamp techniques and a software based phase detector (see abstract by Joshi & Fernandez). Simple inspection of the capacitance records frequently revealed a striking periodicity in the size of the granules. The capacitance step amplitude histograms done for individual cells revealed, in newborn and adult rats, a periodic multimodal distribution with a first peak at  $11.85 \pm 3.8$  fF ( $n=7$ ). A periodicity in secretory granule volumes has been reported (Hammel, I., Lagunoff, D., Bauza, M. & Chi, E. *Cell and Tissue Research* 228:51-59, 1983). A periodicity in membrane areas and volumes implies that secretory granules are formed by the multiple fusion of "unit granules" which have the dimension of condensing vacuoles. As the cells matured, the number of granules per cell was followed by measuring the amount of vesicular membrane added to the plasma membrane, expressed as the ratio of  $C_f/C_i$  (final value of capacitance after complete degranulation versus the initial one). This ratio increased gradually from 1, reaching 2 for three week old rats and saturating at 4 after eight weeks, indicating a completed granulogenesis. During this time the capacitance step size distribution remained unchanged.

**T-Pos255** DEFECTIVE SECRETORY GRANULE FORMATION IN CHEDIAK-HIGASHI MICE, J.M. Fernandez, and G. Alvarez de Toledo, Department of Physiology, School of Medicine, University of Pennsylvania, Phila., PA 19104-6085 (Spon. by M. White).

We have studied the formation of secretory granules in peritoneal mast cells of mice with the Chediak-Higashi syndrome (beige mice) and normal controls. Individual granule sizes as well as total number of granules per cell were monitored by measuring the increase in membrane capacitance of single cells undergoing exocytosis (see abstracts by Alvarez de Toledo & Fernandez and by Joshi & Fernandez). Capacitance step amplitude histograms of individual cells obtained from newborn and adult control mice were identical in shape. In contrast to rat mast cells, we were not able to resolve a clear periodicity of granule sizes in control mice, this is probably due to a much smaller "unit granule" in mice as compared to rats. As before, the total amount of vesicular membrane contained in single mast cells was measured by the ratio  $C_f/C_i$ . This ratio grew from 1, reaching 2 for two week old mice and saturating at about 4 after twelve weeks again indicating a completed granulogenesis in control mice. In sharp contrast, in mast cells from mice with the Chediak-Higashi syndrome this ratio reached 1.7 at two weeks of age without increasing thereafter, indicating an impaired synthesis of new granule membrane. The capacitance step amplitude histogram obtained from newborn beige mice was similar to that of controls but as the mice aged a dramatic increase in the size of the granules was observed. This increase in size was due to the continued fusion of the secretory granules among themselves.

**T-Pos256** STOICHIOMETRY OF ACETYLCHOLINE/ATP RELEASE FROM PRESYNAPTIC CHOLINERGIC NERVE ENDINGS.

C. Unsworth and R.G. Johnson, Dept of Med, Physiol., and Biochem. and Biophys, and Howard Hughes Med. Inst, Univ of Penna. Medical Center, Philadelphia, PA 19104

Central to the investigation of the presynaptic regulation of acetylcholine release by neuromodulators or neurotransmitters is the issue of whether acetylcholine release occurs from secretory vesicles via an exocytotic event, from the cytosol via a membrane "transporter", or as combination of both mechanisms. Highly purified and homogeneous cholinergic synaptosomes from the electric ray *Narcine braziliensis* were isolated from intact electric organ using differential and density gradient centrifugation and Percoll and Ficoll gradients. Contamination by postsynaptic membranes was minimal and the acetylcholine content approached 150 nmoles/mg of protein. Using phospholine to block the ecto-ATPase activity, the ATP and acetylcholine release were measured by sensitive on-line quantitative spectrophotometric techniques. The ratio of acetylcholine/ATP release was found to be 6.5 to 6.9 for a variety of secretagogues including KCl, veratridine and calcium ionophores. The stoichiometry was constant over a wide variety of  $K^+$  and  $Ca^{++}$  concentrations and external pH values. The ratio of release of acetylcholine to ATP compared favorably with the ratio found in highly purified secretory vesicles (6.5 to 7.0) and unfavorably with that of intact synaptosomes. The data is consistent with the conclusion that calcium dependent acetylcholine release is from secretory vesicles and no significant secretion of acetylcholine from the cytosol occurs in highly purified intact synaptosomes. These studies will provide a basis for investigations into presynaptic regulation of neurotransmitter release.

**T-Pos257** EFFECTS OF DIVALENT CATIONS ON STIMULATION-INDUCED CHANGES IN TRANSMITTER RELEASE AT THE FROG NEUROMUSCULAR JUNCTION. Zengel, J.E., Lee, D.T., Van Veelen, M.-L., and Mosier, D.R. VA Med. Ctr. and Depts. Neurosci./Neurosurg., Univ. of Fla. Coll. of Med., Gainesville, Fla. 32610.

End-plate potentials (EPPs) were recorded from frog (*Rana pipiens*) sartorius muscles under conditions of reduced release (0.4-0.7 mM Ca, 5 mM Mg). The nerve was conditioned with trains of 10-200 impulses (20 impulses/sec).

Previous experiments had shown that small decreases in  $[Ca^{++}]_o$  can reduce the increase in release seen during short trains of repetitive stimulation. If this effect is related to a decreased entry of  $Ca^{++}$  during nerve stimulation, then agents which block  $Ca^{++}$  entry should have the same effect as decreasing  $[Ca^{++}]_o$ . To test this, low concentrations (0.1-0.3 mM) of  $Co^{++}$  or  $Zn^{++}$  were added to the bathing solution. As expected, the addition of either of these ions led to a small decrease in the stimulation-induced increase in EPP amplitude normally seen during 10 impulse trains. This effect could be reversed by increasing  $[Ca^{++}]_o$ .

Similar experiments were also done using cadmium ( $Cd^{++}$ ), another Ca channel blocker, but with much different results.  $Cd^{++}$  produced a large, and sometimes complete, blockage of the increase in EPP amplitude normally seen during repetitive stimulation, even at extremely low concentrations (1-30  $\mu$ M). The effect of  $Cd^{++}$  on stimulation-induced changes in EPP amplitude was dose-dependent and resulted from a decrease in the amount of transmitter released during the conditioning train. It is not known at this time whether this effect of  $Cd^{++}$  results from a block of the stimulation-induced increases in release normally observed during repetitive stimulation, or whether it arises from an increase in depression which could mask any underlying increases in EPP amplitude.

**T-Pos258** CHARACTERIZATION OF A TOXIC COMPONENT FROM THE VENOM OF *CONUS DELISSERTII*. Nutter, T.J. (Intro. by R.P. Boyce) Dept. of Neurosci., Univ. of Fla. Coll. of Med., Gainesville, Fla. 32610.

The venom of *Conus delissertii*, a Western Atlantic cone snail, was examined for bioactivity in representative vertebrates and invertebrates. Injection of the crude venom into arthropods produced paralysis and death. The onset and severity of symptoms were dose-dependent. Common shore shrimp (*Palaemonetes vulgaris*) exhibited 50% mortality at doses of 35  $\mu$ g venom/gram (dry weight).

The action of the venom was examined on isolated crayfish (*Procambarus clarkii*) walking legs. Discrete "twitches" of the dactyl segment elicited through nerve stimulation were prevented in the presence of venom. No effect was observed on the nerve conduction velocity or compound action potential waveform. Excitatory junctional potentials (EJP's) recorded intracellularly from the crayfish abductor were eliminated following venom administration. Extensive washing of the muscle failed to restore the EJP's. The site of venom action (pre- or postsynaptic) has not yet been determined.

The venom was fractionated through gel filtration and reversed-phase high pressure liquid chromatography (RPHPLC). The lethal component appears to be a single polypeptide with an apparent molecular weight of 15,000 daltons, as determined by SDS-PAGE. Toxic activity is retained following treatment with acid (pH 2.0, 5 days, 4°C), repeated freeze-thaws and lyophilization.

**T-Pos259** PASSIVE ELECTRICAL PROPERTIES OF ACUTELY EXPOSED HIPPOCAMPAL NEURONS.

Nelson Spruston and Daniel Johnston; Prog. Neurosci., Baylor Coll. Med., Houston, TX

The whole-cell patch clamp technique was applied to a preparation of acutely exposed hippocampal neurons prepared from adult guinea pig (Gray & Johnston *J. Neurophysiol.* 54:134,1985) to investigate their passive electrical properties. Voltage and current steps were given to dentate granule cells, and the resulting current and voltage transients were fit with up to three exponentials by DISCRETE (Provencher *J. Chem. Phys.* 64:2772,1976).

Three criteria were used for the selection of the transients: 1) the responses to the steps were within the linear region of the I-V curve, 2) the time constants derived from the depolarizing transients were similar to those derived from the hyperpolarizing transients, and 3) the time constants derived from the charging transients were similar to those derived from the discharging transients. Cells under voltage clamp and in normal bath and cytoplasmic salines had a mean input resistance of  $1.04 \pm 0.19$  Gohms ( $n=21$ ). Higher input resistances (mean  $R_n = 2.52 \pm 1.01$  Gohms;  $n=3$ ) were obtained in the presence of drugs to block voltage-dependent conductances (bath: 1  $\mu$ M TTX, 200  $\mu$ M Cd, 100  $\mu$ M 3,4-DAP, 5 mM TEA; cyto: 100  $\mu$ M 3,4-DAP, 15 mM TEA). Most of the current transients were well fit by two time constants ( $0.59 \pm 0.12$  ms and  $0.07 \pm 0.01$  ms;  $n=13$ ), although an additional slower time constant was occasionally needed ( $2.17 \pm 0.45$  ms,  $0.49 \pm 0.08$  ms, and  $0.07 \pm 0.01$  ms;  $n=8$ ). These values for the time constants did not appear to be dependent on the presence of the drugs. The fastest of the time constants ( $\sim 0.07$  ms) can be attributed to the speed of the clamp, while the slower time constants are caused by the redistribution of charge to dendritic processes.

Voltage charging curves were also obtained from 8 of these cells (mean  $R_n = 0.57 \pm 0.17$  Gohms). The average membrane time constant was  $7.85 \pm 0.84$  ms with the first equalizing time constant equal to  $1.25 \pm 0.23$  ms ( $n=8$ ). Our results using patch-clamp methods will be compared to those obtained previously with microelectrodes. Supported by NIH grants NS11535 and HL31164 and AFOSR 85-0178.

**T-Pos260** NEW DATA CONCERNING D<sub>2</sub>O EFFECTS ON SOME EXCITABLE BIOSYSTEMS

V. Vasilescu, Mioara Tripsa, Cornelia Zaciuc &amp; Eva Katona

Department of Biophysics, Medical Faculty, Bucharest, Romania

The earlier investigations on the structure-function relationship in various excitable biosystems revealed D<sub>2</sub>O as a strong inhibitory agent. Under quasi-total deuteration an excessive stress on the tissue energetic equipment, inhibition of bioelectrogenesis processes and abolishment of the function of excitable membranes were observed, the more and the sooner the activity of the system observed was higher. All these inhibitory effects appeared to be at least partially reversible, some of them being possible to be prevented or antagonised if external ATP supply is available.

Analysis of data concerning D<sub>2</sub>O effects on excitation processes of axonal membranes and neuromuscular junctions as well allowed the correlation of the macroscopic and microscopical events involved in the nerve fibre functioning. As a consequence a modelling of some molecular mechanisms characteristic to the ionic channels behaviour is proposed.

Having in view the differences between hydrogen bond energy and deuterium bond energy the role of protons in stabilizing the interaction of shell water molecules with permeating cations into the channel is pointed out.

**T-Pos261** THE MOTILE NERVOUS SYSTEM: CONTRACTIONS OF THE SQUID STELLATE GANGLION. Maria Elena

Sanchez and George J. Augustine. Dept. Ciencias Fisiologicas, Univ. Valle, Cali, Colombia, Dept. Biological Sciences, Univ. Southern California, Los Angeles, CA 90089 and MBL, Woods Hole, MA.

Physiological studies of the 'giant' synapse in the squid stellate ganglion often are impeded by the presence of ganglionic contractions. We have used optical recording methods to characterize these contractions and evaluate various strategies for eliminating contractions without interfering with synaptic transmission. Contractions of isolated stellate ganglia of *Loligo pealei* were detected by measuring changes in light transmission through the ganglion with a photodiode. With this arrangement it usually was possible to observe spontaneous, rhythmic contractions of variable amplitude and a frequency of about 8/minute (range 2-16/min). These contractions were very temperature sensitive, with lower rates of contraction observed at temperatures below the normal recording temperature of 24°C. The rate and amplitude of these contractions were very sensitive to external Ca concentration ( $[Ca]_o$ ), both progressively declining as  $[Ca]_o$  was lowered. At  $[Ca]_o$  below about 0.1 mM contractions ceased. Inorganic Ca channel blockers, such as Cd<sup>2+</sup> (2 mM) and Mn<sup>2+</sup> (12.5 mM) completely blocked contractile activity. The organic Ca channel blocker, nitrendipine (10-20  $\mu$ M), produced a variable reduction in contractions. In summary, we have demonstrated spontaneous, rhythmic contractions in the squid stellate ganglion. These contractions require external Ca and are blocked by several Ca channel blockers. Among the several treatments that we have found to eliminate contraction, only organic Ca channel blockers selectively spare synaptic transmission (Charlton & Augustine, *Biol. Bull.* 173, in press). Supported by NIH Grant NS-21624 to GJA.

T-Pos262 REGULATION OF RETINAL EXTRACELLULAR pH: IMPORTANCE OF THE BICARBONATE/CO<sub>2</sub> BUFFER SYSTEM IN BUFFERING METABOLICALLY-PRODUCED ACID IN DARKNESS AND DURING ILLUMINATION.  
R. Wen and B. Oakley II. NBB Program and ECE Dept., University of Illinois at Urbana-Champaign.

We measured extracellular H<sup>+</sup> concentration, H<sup>+</sup>, in the isolated retina of the toad, *Bufo marinus*, using H<sup>+</sup>-selective microelectrodes. We used a superfusate with a poor buffering capacity (phosphate buffered solution, PBS), to detect optimally H<sup>+</sup>, and we compared the results to those observed using a physiological buffer with a 75-times greater buffering capacity (bicarbonate-CO<sub>2</sub> buffered solution, BBS). In darkness, there was a gradient of H<sup>+</sup> from the inner retina (high H<sup>+</sup>) to the bathing solution (low H<sup>+</sup>). This gradient was 0.7 pH units in PBS, but only 0.2 pH units in BBS; it increased to 1.0 pH unit during anoxia (N<sub>2</sub>-bubbled PBS), suggesting that lactic acid from glycolysis is the acid source. Light evoked changes in H<sup>+</sup> with two major components: a light-on acidification and a light-off alkalization. These components varied with retinal depth and with the intensity and duration of illumination. Aspartate (2 mM), which blocked the ERG b-wave, diminished the light-on acidification, while amiloride (2 mM), an inhibitor of Na<sup>+</sup>/H<sup>+</sup> exchange, diminished all light-evoked components and the H<sup>+</sup> gradient. In BBS, light-evoked changes in H<sup>+</sup> were greatly attenuated; however, addition of acetazolamide (2 mM), a carbonic anhydrase (CA) inhibitor, increased both the H<sup>+</sup> gradient and the light-evoked changes in H<sup>+</sup>. Our data suggest that retinal cells produce lactic acid by glycolysis, and that H<sup>+</sup> is extruded from cells via Na<sup>+</sup>/H<sup>+</sup> exchange. Under physiological conditions (BBS), H<sup>+</sup> is buffered by the HCO<sub>3</sub><sup>-</sup>/CO<sub>2</sub> buffer system, which is dependent upon CA. Since CA is localized to Müller (glial) cells, our data point to a critical role for glial cells in retinal H<sup>+</sup> homeostasis. Supported by NIH grant EY04364.

**T-Pos263** ULTRASTRUCTURE OF RELAXED, RIGOR AND CONTRACTING STRIATED MUSCLE STUDIED BY QUICK FREEZING. Raúl Padrón<sup>1</sup>, Roger Craig<sup>2</sup>, Lorenzo Alamo<sup>1</sup> and Carlo Caputo<sup>1</sup>. <sup>1</sup>Muscle Biophysics Laboratory, IVIC-Biofísica, Apdo 21827, Caracas 1020A, Venezuela and <sup>2</sup>Anatomy Department, U. Mass Medical School, Worcester, MA 01655.

We have developed a quick freezing method, using a copper block cooled with liquid helium or nitrogen, which permits us to freeze muscles at predetermined, precisely measured points in the recorded tension time course of a single twitch or tetanus. Our aim is to arrest structural intermediates of the crossbridge cycle for subsequent observation in the electron microscope. Skinned (detergent treated) or live muscles (frog, tarantula and lobster) have been frozen on the same apparatus (without prior fixation or cryoprotection) in relaxed, rigor or isometrically contracting states. Good freezing has been obtained to depths of 10-20  $\mu\text{m}$ . Freeze substituted relaxed specimens showed excellent preservation of thick filament ultrastructure as revealed by the presence of layer line and meridional reflections in optical diffraction patterns of sections that were similar to those in x-ray diffraction patterns of intact, whole relaxed muscles. Freeze substituted rigor specimens showed actin-based layer lines similar to x-ray patterns of muscles in rigor, while freeze fractured specimens showed clear crossbridge attachments to actin at 38 nm intervals as well as the 5.9 nm actin subunit repeat. Good preservation has also been achieved in muscles which have been rapidly frozen during electrically or chemically stimulated isometric contraction with simultaneous tension monitoring. Supported by grants from NIH (to R.C.), MDA (to R.P., R.C., and C.C.) and CONICIT (to R.P.).

**T-Pos264** ELECTRON MICROSCOPIC STUDIES OF ISOLATED MAMMALIAN SKELETAL MUSCLE THICK FILAMENTS. R. W. KENSLER, DEPARTMENT OF ANATOMY, THE MEDICAL COLLEGE OF PENNSYLVANIA, PHILADELPHIA, PA 19129.

We have previously demonstrated that frog muscle thick filaments (Kensler and Stewart. 1983. *J. Cell Biol.* 96:1797-1802) and fish filaments (Kensler. 1986. *Biophys. J.* 49:263a) can be isolated with the relaxed near-helical arrangement of the myosin heads largely preserved, and a three-dimensional reconstruction of the arrangement of the heads on the frog filaments has been presented (Stewart and Kensler. 1986. *J. Mol. Biol.* 192:831-851). In the present investigation, we have extended these studies to the examination of skeletal muscle thick filaments isolated from the rabbit. Thick filaments were isolated from leg muscles of these animals by slight modifications of the procedures previously employed for the isolation of frog thick filaments (Kensler and Stewart. 1983. *J. Cell Biol.* 96:1797-1802), and the filaments were examined by negative-staining, both in thin stain films and on thin carbon films supported by perforated Formvar coated grids. Although apparently more labile in structure than either frog or fish thick filaments, the rabbit thick filaments in good preparations appear periodic with an apparent repeat every third crossbridge level. Optical diffraction patterns of images of the filaments confirm the periodicity, and show the expected layer lines corresponding to a (near) helical repeat of 43 nm, as expected from X-ray diffraction studies of relaxed vertebrate muscle (Huxley and Brown. 1967. *J. Mol. Biol.* 30:383-434). The isolated rabbit filaments have also been examined by unidirectional platinum shadowing. The shadowed filaments appear periodic with a right-handed (near) helical arrangement of subunits on their surfaces. Optical diffraction studies of the shadowed filaments confirm the periodicity, and show evidence for a perturbation from true helical symmetry, similar to that we previously reported for frog thick filaments (Kensler and Stewart. 1986. *Biophys. J.* 49:343-351). Supported by UPHS grant AR30442.

**T-Pos265** CHANGES IN THE BACKBONE STRUCTURE OF VERTEBRATE SKELETAL MYOSIN FILAMENTS, UNDER DEFINED CONDITIONS OF IONIC STRENGTH AND THE PRESENCE OR ABSENCE OF MgATP OR MgAMPPNP. F. Ashton, J. Weisel and F. Pepe. Dept. of Anatomy, Univ. of Penn. Philadelphia, PA 19104-6058.

The backbone structure of the myosin filaments of chemically skinned chicken pectoralis muscle was studied under different conditions. The subfilament organization in transverse sections was the same on exposure of skinned fibers for 2 hrs (0°C) to rigor solutions at an ionic strength of 20 mM (2.5 mM EGTA, 2.5 mM EDTA, 1 mM DTT, 10 mM imidazole, pH 7.0, Brenner et al. 1984, *Biophys. J.* 46: 299-306) or 200 mM (51.48 mM EGTA, 3.23 mM MgCl<sub>2</sub>, 100 mM TES, pH 7.1 Dantzig and Goldman 1985, *J. Gen. Physiol.* 86: 305-327). In transverse sections, the same arrangements of 9 subfilaments were observed at both ionic strengths (Ashton et al., 1987, *Anat. Rec.* 218: 10A). By comparing the first derivative of the radial density distribution of the image it was possible to detect a shift of mass about 2 nm away from the surface of the filaments on changing the ionic strength from 20 mM to 200 mM. This shift could be related to a similar shift of about 2 nm in the position of an epitope on the S2 portion of myosin recognized by labeling with the Fab fragment of a monoclonal antibody (H1E11) in previous studies (unpublished). Therefore the difference in mass distribution observed in the unlabeled filaments most likely results from the radial movement of S2 with increasing ionic strength. Skinned fibers were also kept at 20 mM ionic strength overnight at 0°C, both in rigor (as above) and in the presence of 1 mM AMPPNP (in 1 mM EGTA, 3 mM MgCl<sub>2</sub>, 1 mM DTT, 10 mM imidazole pH 7.1). In this case the myosin filaments in AMPPNP had exactly the same characteristics as those exposed to the rigor conditions for 2 hrs as above. After overnight exposure in rigor there was movement of the subfilaments to the surface leaving hollow cores.

**T-Pos266** SUBSTRUCTURE AND ACCESSORY PROTEINS IN SCALLOP MYOSIN FILAMENTS.

Peter Vibert and Loriana Castellani, Rosenstiel Center, Brandeis University, Waltham, MA 02254.

Native myosin filaments from scallop striated muscle splay into subfilaments when treated with low ionic strength relaxing buffers. Depending on the extent of treatment and the substrate that supports the filaments, either 2-3 large subfilaments or 5-7 smaller subfilaments are seen in negatively stained samples. The small subfilaments are about as wide as actin filaments, but myosin heads can be seen projecting from them.

Synthetic filaments made from purified scallop myosin by dialysis against relaxing buffers have a uniform width similar to that of native filaments, but are much longer (Castellani et al., *J. Mol. Biol.* 196, 955-960 (1987)). They often bear a well-ordered helical array of crossbridges on the surface. Washing these filaments with low ionic strength buffers also frays them into small subfilaments.

Native filaments in some cases display short protrusions at their tips that are similar in appearance to the "end-filaments" associated with vertebrate striated muscle filaments. SDS polyacrylamide gels of scallop striated muscle homogenates show two proteins with mobilities less than the myosin heavy chain. They have apparent chain weights in the range 0.4 to 1 MD, and may be analogous to nebulin and titin of vertebrate skeletal and cardiac muscles.

Supported by grants from NIH, NSF and MDA.

**T-Pos267** COMPLEX ROTATIONAL MOTION OF MYOSIN HEADS IN FIBERS MEASURED BY TRANSIENT PHOSPHORESCENCE ANISOTROPY

Richard D. Ludescher\*, Peter S. Dahlberg, Piotr G. Fajer, and David D. Thomas, Department of Biochemistry, University of Minnesota Medical School, Minneapolis, MN 55455 and \*Department of Chemistry, The Wichita State University, Wichita, KS 67208.

We are using transient phosphorescence anisotropy (TPA) from a covalently-attached triplet probe to monitor the rotational dynamics of myosin heads on the micro- to millisecond time scale. Glycerinated muscle fibers, treated with eosin-5-maleimide under relaxing conditions, appear to be specifically labeled at the fast-reacting sulfhydryl on myosin S1 when analysed by PAGE, ATPase activity, and dye/protein ratios. The TPA from labeled fibers in rigor is flat and constant from 200 ns to 1 ms, while in relaxation or contraction the TPA exhibits a complex multiexponential decay to a constant value.

The TPA over 1 ms, measured with a time resolution of 1 us/channel, decays biexponentially with time constants of about 20 and 300 us in both relaxing and contracting buffers. Under the same chemical conditions, the TPA, measured at a time resolution of 200 ns/channel, also decays biexponentially but with time constants of about 5 and 40 us. It thus appears that myosin heads in the presence of MgATP undergo complex rotational motion involving at least three time constants over the time scale from 1-1000 us. Although the TPA decays are similar for fibers in relaxing and contracting buffer, the curves differ at both short and long times. Specifically, the TPA decays in contracting buffer are not linear combinations of the decays in rigor and relaxation.

**T-Pos268** STRUCTURE OF ACTIN-ATTACHED MYOSIN HEAD IN THE PRESENCE OF VARIOUS NUCLEOTIDES.

Eisaku Katayama. (Intr. by Frank A. Pepe) Department of Pharmacology, Faculty of Medicine, University of Tokyo, Hongo, Tokyo 113 JAPAN

Recent electron microscopy (Craig et al., 1985; Applegate & Flicker, 1987) showed that myosin head in EDC cross-linked acto-S1 displays various shapes and angles when ATP is added, in contrast to its uniform tilted appearance under rigor condition. Such diversity of conformations in the presence of ATP was confirmed in stereo images of negatively stained samples, though the short and rounded shape predominated the population. It was not easy to objectively rule out the possibility of a fraction of molecules tethered to actin by artificial cross-links. Quick-freeze deep-etch electron microscopy was employed in conjunction with mica flake method (Heuser, 1983) to observe uncross-linked acto-S1 in the presence of ATP. To compensate the lowered affinity of S1 to actin by ATP, protein sample of high concentration was applied to mica flakes whose negative surface charge was converted to positive by chemical modification. Acto-S1 with added ATP exhibited a good correlation with the expected time-course of reversible dissociation and reassociation, ensuring the applicability of this method to examine the structural change of acto-S1. S1 molecule attached to F-actin in rigor or in the presence of ADP showed elongated shape with its long axis tilted about 45° to F-actin in the same manner as seen by negative staining. S1 altered its shape into short and rounded one by the addition of ATP or ADP-Vi. Such conformation of S1 molecule is similar to the one predominated in cross-linked acto-S1 in the presence of ATP and thus likely to occur during active contraction of muscle. Addition of either AMPPNP or PPI showed partial dissociation of S1 from actin as expected from the known properties of those nucleotide analogs.

**T-Pos269 Photon correlation spectroscopy of muscle fibers: A study of the differential polarization signal on the diffraction maximum.** Sui Shen, R. J. Baskin, and Y. Yeh. Depts. of Zoology and Applied Science, University of California, Davis.

Ellipticity of light diffracted from a muscle fiber has been used as a probe to examine the periodic fluctuation of optical anisotropy due to microscopic motion of elements with sarcomeric repeat structure. The dynamics of the difference signal between the two orthogonally polarized electric field components is monitored using a digital autocorrelator. Such a difference signal is sensitive to only the dynamic changes in the sarcomere structure that lead to changes in optical anisotropy. FFT's of these oscillatory signals are studied over the spectral range from 30 Hz to 200 kHz. Signals appearing in the lower frequency end (50-250 Hz) are usually stronger than those found in the higher frequency regime (100-200 kHz). Passive stretch of the fiber shows that while the low frequency signals can change in center frequency by 15 to 20%, the sharp, high frequency signal only changed minimally. This observation suggests that the high frequency signal is due to the averaged motion of crossbridge elements while the low frequency signal may be related to lateral motion of the thick and thin filaments affecting only form anisotropy. The change in the frequency of the high frequency signal between relaxed state and the rigor state is less than that between the relaxed state and the chemically activated state, suggestive of different modes of interaction in these two actomyosin attachment states. Experiments to examine the change in these signals upon  $\alpha$ -chymotrypsin cleavage of S-1 and upon decoration of the thin filament with isolated S-1 will also be reported. Work supported in part by NIH AR-26817.

**T-Pos270 Ellipsometry Studies on the Myosin Subfragments S-1 and HMM: The relative contributions of the form and intrinsic components of birefringence.** H. M. Jones, R. J. Baskin, Y. Yeh. Depts. of Zoology and Applied Science, University of California, Davis.

To more completely understand the role of the S-1 vs. S-2 moieties during force production in the skeletal muscle cross-bridges we have investigated the optical properties of single skeletal muscle fibers under various conditions. We have monitored the first diffraction order of fiber-diffracted light from a He-Ne laser and characterized two parameters, the birefringence ' $\Delta n$ ' and the differential field ratio ' $r$ ', which are sensitive to the structure and spatial distribution of sarcomeric elements. Muscle fibers typically were skinned in a relaxing solution containing 0.5% Triton X-100, mounted in a chamber cooled to 6 degrees centigrade, placed into rigor and irrigated with solutions containing either 2 mg/ml chymotryptic S-1 or HMM. When the S-1 solutions were introduced into the fiber the diffraction pattern was characterized by a steady decline in its intensity, a slight increase in birefringence and a substantial increase in ' $r$ '. This response was stable upon rinsing away unbound S-1 with rigor solution and was completely reversible upon addition of 2.5mM sodium pyrophosphate (PPi). Silver-stained SDS gels demonstrated the binding of S-1 and its release with PPi. Little or no effect on the ' $\Delta n$ ' and ' $r$ ' readings were obtained with HMM; this was due to the inability of HMM to adequately penetrate the fiber. Several attempts using mechanically skinned fibers resulted in only marginal penetration. Further experiments using HMM will focus on producing 'short-HMM', which is about 240 Å and 40 kD smaller than the 'long HMM' used previously. The s-HMM penetrates easier due to the smaller dimensions and potential aggregation into larger masses will be reduced.

**T-Pos271 DIFFERENTIAL FIELD RATIO MEASUREMENTS OF COMPRESSED MUSCLE FIBERS**  
W. L. Kerr, R. J. Baskin, Y. Yeh, Depts. of Zoology and Applied Science, University of California, Davis, California 95616

A new procedure has been developed for measuring the differential field ratio ( $r$ ) from single muscle fibers. Linearly polarized laser light was directed on the fibers with its electric field vector at  $45^\circ$  with respect to the fiber axis. Light which has interacted with the fiber is monitored at the first diffraction order, with its parallel and perpendicular components separated by a Wollaston prism and measured with a photodiode pair. The  $r$  value is defined as  $r = (\sqrt{I_{||}}/\cos\theta_D - \sqrt{I_{\perp}}) / (\sqrt{I_{||}}/\cos\theta_D + \sqrt{I_{\perp}})$ . Values of  $r$  were measured for relaxed, chemically skinned frog muscle fibers as a function of sarcomere length and concentration of polyvinylpyrrolidone (PVP). With no PVP,  $r$  decreased from an average value of .040 at a sarcomere length of 2.48 $\mu$ m to .010 at 3.20 $\mu$ m. Compression of the interlattice spacings with 3% PVP increased  $r$  significantly ( $p < 0.05$ ) at sarcomere lengths between 2.62 and 3.10 $\mu$ m, with the greatest increase occurring at about 3.0 $\mu$ m. No significant changes in  $r$  could be detected at shorter and longer sarcomere lengths. Changes in  $r$  with sarcomere length and interlattice spacing are described by model calculations which account for both the form and intrinsic contributions to  $r$ . Increase in volume fraction would tend to decrease the form contribution to  $r$  while more parallel orientations of crossbridges would increase the intrinsic contribution to  $r$ .

**T-Pos272** THE EFFECT OF TEMPERATURE ON DIFFERENT MODES OF CROSSBRIDGE MOTIONS IN ISOLATED THICK FILAMENTS FROM LIMULUS STRIATED MUSCLE AS DETECTED BY QUASI-ELASTIC LIGHT SCATTERING METHODS. S.F. Fan, M.M. Dewey and B. Chu. Department of Anatomical Sciences and Department of Chemistry, SUNY at Stony Brook, Stony Brook, NY 11794

Using the quasi-elastic light scattering technique, we have described an increase in  $\bar{\Gamma}$  values from a suspension of thick filaments isolated from the myosin-regulated, striated muscles of Limulus following the addition of  $\text{Ca}^{2+}$  (J. Mol. Biol., 166:329, 1983); Biophys. J., 47:809, 1985) or depletion of ATP (Biophys. J., Nov. 1987) in the suspending medium by quasi-elastic light scattering method.  $\bar{\Gamma}$  is the value of the average linewidth of the photoelectron count autocorrelation function of light scattered. The increase of  $\bar{\Gamma}$  values elicited by  $\text{Ca}^{2+}$  is believed to be due to the energy-requiring motion of the crossbridges activated by  $\text{Ca}^{2+}$ . The increase of  $\bar{\Gamma}$  values developed under ATP-depleted conditions is believed to be mainly due to the thermal motion of the crossbridge after it moves radially away from the filament backbone. The percentage increase of  $\bar{\Gamma}$  values from thick filaments isolated from the middle of June to the middle of September is usually smaller. Further, we found that the effect of temperature on the percentage increase of the  $\bar{\Gamma}$  values is different during the summertime from that during the rest of the year or after the depletion of ATP. The percentage increase of  $\bar{\Gamma}$  values by  $\text{Ca}^{2+}$  shows a maximum at about 35°C during the rest of the year. However, the percentage increase of  $\bar{\Gamma}$  values developed under ATP-depleted conditions showed no temperature-related maximum. Supported by NSF DCB8508897

**T-Pos273** CHANGES IN THE THICK FILAMENTS OF LIMULUS STRIATED MUSCLE FOLLOWING SHORTENING. Dewey, M.M., S.-F. Fan and D. Colflesh. Dept. Anatomical Sciences, The Medical School, SUNY at Stony Brook, Stony Brook, NY 11794

Since De Villafranca and Marschaus described A-band shortening in glycerinated fibers of Limulus striated muscle twenty four years ago (J. Ultrastruct. Res. 9:156'63), the issue of whether thick filament shortening during A-band shortening in this muscle has remained highly controversial. The view that the apparent filament shortening is due to differences in intrinsic fiber types has been reiterated (H.E. Huxley, J. Exp. Biol. 115:17, 1985). Here we report further experimental evidence in support of the view that shortening is genuine and is accompanied by change in the internal structure of the filament. We have repeatedly demonstrated that thick filaments can be isolated with average lengths of  $\sim 4.9 \mu\text{m}$  and then shortened in vitro with the addition of  $\text{Ca}^{2+}$  in the presence of ATP to  $\sim 3.0 \mu\text{m}$  (Brann et al., Nature 279:556, 1979). These shortened filaments are remarkably less flexible than the long thick filaments (Fan, Dewey and Colflesh. Biophys. J. 48:859, 1985). As the filament length decreases (1) the mass per unit length of the filament as determined by scanning transmission electron microscope increases and the total mass of the individual filament does not show any statistically significant change; (2) the diameter and the number of subfilaments counted in the cross-section of the individual thick filaments increases and (3) the shape of the cross-section and the cross section density profile of the individual thick filament changes. Supported by NSF DCB8508897

**T-Pos274** DETECTION OF CROSSBRIDGE MOTIONS OF ISOLATED MYOFIBRILS BY QUASI-ELASTIC LIGHT SCATTERING TECHNIQUE. S.F. Fan, M.M. Dewey and B. Chu. Department of Anatomical Sciences and Department of Chemistry, SUNY at Stony Brook, Stony Brook, NY 11794

Using the quasi-elastic light scattering technique, we have described an increase in  $\bar{\Gamma}$  values from a suspension of thick filaments isolated from the myosin-regulated, striated muscles of Limulus and scallop following the addition of  $\text{Ca}^{2+}$  (J. Mol. Biol., 166-329, 1983; Biophys. J. 47:809, 1985).  $\bar{\Gamma}$  is the value of the average linewidth of the photoelectron count autocorrelation function of light scattered. We have demonstrated that this increase of  $\bar{\Gamma}$  values is due to the energy requiring motion of crossbridges activated by  $\text{Ca}^{2+}$ . Since thin filaments are to a large extent removed from the thick filament preparations, it is not clear whether the crossbridge motion we have measured is related to that responsible for muscle contraction. Now we have found that a similar increase of  $\bar{\Gamma}$  values by  $\text{Ca}^{2+}$  can also be detected in isolated myofibrillar preparations. The  $\bar{\Gamma}$  values obtained from isolated myofibrils suspended in a calcium-free relaxing solution are much lower than those obtained from the isolated thick filaments suspended in a similar solution. Yet the  $\bar{\Gamma}$  values also increase tremendously at high scattering angle after the addition of calcium ions (e.g. at a scattering angle of 120° the  $\bar{\Gamma}$  value increases from about 200 to about 1.3k). The  $\bar{\Gamma}$  values decrease appreciably as the ATP is depleted from the suspending medium (e.g. from about 200 to about 50 at a scattering angle of 120°). These results demonstrate that the quasi-elastic light scattering technique can be used to study in situ crossbridge motions. Supported by NSF DCB8508897

**T-Pos275**    **STEPWISE SHORTENING IN SINGLE MYOFIBRILS** Marc L. Bartoo, Tsukasa Tameyasu, David H. Burns, and Gerald H. Pollack. Center for Bioengineering, WD-12, University of Washington, Seattle, WA 98195.

Though controversial, stepwise shortening has now been confirmed using five independent methods in several laboratories: the sarcomere shortening waveform is staircase-like, not smooth. The major question remaining is whether the stepping mechanism resides in some extraneous feature outside the myofibril, or is intrinsic to the myofibrillar sarcomere.

To test this, we measured shortening dynamics in single isolated myofibrils. Honeybee-flight-muscle myofibrils (diameter 2 - 3  $\mu\text{m}$ ) were mounted on an inverted microscope; one end was fixed, the other attached to a piezoelectric motor which could impose ramp length changes. To avoid translation artifacts, we measured sarcomere length very near to the specimen's fixed end. Striations were projected onto a photodiode array, and sarcomere length was computed using a phase-locked loop circuit (Jacobson *et al.*, *J. Mus. Res. Cell Motil.* 4:529, 1983). Steps and pauses were observed consistently during release and stretch. Repeatability of the stepping pattern was moderate. Step size was typically 1% of initial sarcomere length. The character of the steps was similar to that observed earlier in larger preparations. Thus, stepwise shortening is a feature of the single myofibrillar sarcomere.

Since the bending of cilia may also occur in steps (Baba, *Nature* 282:717, 1979), the phenomenon may be a general feature of biological motility. How any theory invoking stochastic processes (such as the cross-bridge theory) can explain such discrete, synchronized events is not immediately obvious.

**T-Pos276**    **INTERCONNECTIONS BETWEEN FILAMENTS IN THE I-BAND OF SKELETAL MUSCLE.** P.H.W.W. Baatsen, K. Trombitás and G.H. Pollack, Center for Bioengineering, University of Washington WD-12, Seattle WA 98195.

I-bands of stretched intact frog sartorius muscle contain – besides filaments – structures of variable appearance. Some of these structures appear to interconnect adjacent filaments, whereas others may not be bound to filaments at all. Although most of them seem to be distributed randomly throughout the I-band, some seem to line up laterally. We wished to test whether these structures interact strongly or weakly with I-band filaments. Diffusion out of the filament lattice upon removal of the sarcolemma (skinning) was taken as a criterion for weak interaction. Specimens were prepared for electron microscopy by freeze-fracture and/or chemical fixation followed by thin sectioning. In the skinned preparations the structures with variable size and shape had disappeared. However, in some places adjacent filaments appeared to be interconnected by rodlike structures. The diffusible particles thus displayed a weak interaction with I-band filaments. This suggests a non-structural role for them – possibly they are enzymes. The rodlike interconnections have a much more uniform shape than the structures observed in I-bands of intact muscle specimens. In this case a structural role seems possible. Since it is well documented that glycolytic enzymes can form complexes (Stephan *et al.* (1986), *Biochim. Biophys. Acta* 873, 127-135) and bind to actin filaments *in vitro* (e.g. Masters, C. (1984), *J. Cell Biol.* 99 (1), 222-225) they are likely candidates for these interconnections. However, troponin could also play a role.

We have also investigated fish and glycerinated insect muscle, which have more regular I-band lattices than frog muscle. Glycerination is regarded as similar to mechanical skinning in permeabilizing the muscle, so we expected the weakly bound structures to have diffused out. It appeared that the I-bands of glycerinated insect muscle showed more interconnections between adjacent filaments than in skinned frog muscle. These data point toward a possible role for interconnections in stabilizing the lattice, giving rise to more regularity. In addition, when connecting filaments are revealed by breaking actin filaments off at the Z-line (Trombitás and Tigy-Sebes (1984), *Nature* 309, 168-170), they show many projections along their entire length. Perhaps these projections form interconnections in insect muscle. Preliminary results on preparations of the very regular intact fish muscle show many projections from and interconnections between adjacent I-band filaments. These seem to be spaced more regularly than in intact frog muscle. It remains to be tested by skinning whether these structures are weakly or strongly bound.

T-Pos277 A RELATIONSHIP BETWEEN MAMMALIAN SPERM DIMENSIONS, METABOLISM, AND MOTILITY. R.A. Cardullo and J.M. Baltz\*, Worcester Foundation for Experimental Biology, Shrewsbury, MA & \*Dept. of Physiology and Biophysics, LHRRB, Harvard Medical School, Boston, MA.

The mammalian spermatozoon is characterized by a long flagellum partially surrounded by a region of densely packed mitochondria known as the midpiece. Recently, data was compiled by Cummins and Woodall (J. Reprod. Fert. 75, 1985) on the linear dimensions of sperm from over 284 different species of mammals. We have taken this data and shown that there is a positive correlation between midpiece length ( $l_{mp}$ ) and total flagellum length ( $l_f$ ) in the form of the nonlinear function:  $l_{mp} \propto l_f^{3/2}$ . Hence, the larger the sperm, the greater the fraction of its flagellum occupied by the midpiece. If dynein consumption of ATP is constant among species, then the total ATP production of the midpiece should increase linearly with the flagellum. Indeed, we found that unlike midpiece length, the midpiece volume increases linearly with total tail length. In addition, we found that the rate of ATP production by aerobic metabolism, along with the empirical linear relationship between midpiece volume and flagellum length, accurately predicts both the values of the flagellar beat frequencies and that beat frequency decreases with increasing sperm length. These results indicate that there is a clear relationship between the metabolic turnover of ATP and flagellar beat frequency in mammalian sperm. Further, these data suggest that the metabolic turnover of ATP by a mammalian sperm flagellum can be determined solely by measuring waveform parameters. (Supported by NIH T32-HD07312 to RAC.)

T-Pos278 PRESSURE EFFECTS ON THE MITOCHONDRIAL ADENOSINE TRIPHOSPHATASE. Jerson L. Silva, Horacio Guimaraes-Motta and George Dreyfus. Depto de Bioquimica ICB/CCS, Universidade Federal do Rio de Janeiro, Brazil & Instituto de Fisiologia Celular, Universidade Nacional Autonoma de Mexico.

The effects of hydrostatic pressure on three different preparations of mitochondrial  $H^+$ -ATPase were investigated by studies of the hydrolytic activity, of the spectral shift and quantum yield of the intrinsic fluorescence and of filtration chromatography. Either the membrane bound or the detergent solubilized forms of the mitochondrial  $F_0-F_1$  complex were reversibly inactivated in the pressure range of 600-800 bars. Soluble  $F_1$ -ATPase was inactivated in the same pressure range but no recovery of activity was found after return to atmospheric pressure. Pressure-inactivation of soluble  $F_1$ -ATPase was facilitated decreasing the protein concentration, indicating that dissociation is probably the main event. Soluble  $F_1$ -ATPase in the presence of 30% glycerol becomes inactivated by pressure in a reversible fashion, recovering the original activity either if the assay is performed aqueous or glycerol containing buffer. Fluorescence studies under pressure revealed a red shift in the spectral distribution of the emission of tyrosine fluorescence of soluble  $F_1$ -ATPase. A decrease in the quantum yield of intrinsic fluorescence was also observed upon subjection to pressure. The fluorescence intensity decreased monotonically as a function of pressure when the sample was in an aqueous medium whereas presented a biphasic behavior in a 30% glycerol medium. Gel filtration studies demonstrated that the hydrodynamic properties of the  $F_1$ -ATPase are preserved if the enzyme is subjected to pressure in the presence of glycerol but they are modified when the same procedure is performed in an aqueous medium. It can be concluded that pressure dissociation of soluble ATPase is followed by reassociation to an inactive enzyme with altered hydrodynamic radius. Supported by CNPq, FINEP, OEA and CONACyt.

T-Pos279 ISOLATION OF A 53 kDa PROTEIN FROM MITOCHONDRIA WHICH MAY HAVE A ROLE IN MEDIATING  $K^+$  TRANSPORT. Joyce J. Diwan, Teresa Haley, Edward Kaftan, Saroj Joshi, and D. Rao Sanadi, Biology Department, Rensselaer Polytechnic Institute, Troy, NY 12180-3590, and Department of Cell Physiology, Boston Biomedical Research Institute, Boston, MA 02114.

A 53 kDa protein has been isolated from rat liver submitochondrial particles (SMP) by affinity chromatography on quinine, an inhibitor of mitochondrial  $K^+$  transport. SMP in a pH 7.5 medium including 2% triton X-100 are applied to columns of epoxy activated Sepharose 6B (Pharmacia), previously reacted with quinine. After washing with a pH 7 medium including 2% triton & 100 mM NaCl, elution e.g. with a pH 6.2 medium including 1% cholate and 500 mM KCl yields mainly a protein estimated by SDS PAGE to be about 53 kDa MW. For western blot analysis, this protein was further purified by preparative SDS PAGE. Using antibodies prepared against beef heart  $F_1$  ATPase, it was found that the 53 kDa protein does not bind antibodies which recognize the similarly sized alpha and beta subunits of beef heart  $F_1$  and appropriately sized proteins in rat liver SMP. Column eluates (about 2 mg protein), concentrated by ultrafiltration, were combined with alectin (45 mg) in 200 mM octyl glucoside, and dialyzed against 5 mM Tris  $P_i$  plus 25 mM KCl. The resulting vesicles, concentrated by ultracentrifugation, were diluted into a similar medium containing only 9  $\mu M$   $K^+$ . A monovalent cation electrode has recorded a more rapid  $K^+$  loss from vesicles prepared with the 53 kDa protein than from vesicles lacking protein.  $K^+$  efflux from vesicles made with the 53 kDa protein is accelerated by 1  $\mu M$  CCCP. The data are consistent with catalysis of  $K^+$  transport by the 53 kDa protein. (Supported by USPHS Grant GM-20726).

**T-Pos280** AN UBIQUINONE DERIVATIVE THAT INHIBITS MITOCHONDRIAL CYTOCHROME *b-c*<sub>1</sub> COMPLEX BUT ACTIVATES CHLOROPLAST CYTOCHROME *b*<sub>6-f</sub> COMPLEX. Yu, C. A., Gu, L.-Q. and Yu, L. Department of Biochemistry, OAES, Oklahoma State University, Stillwater, OK 74078.

An ubiquinone derivative, 3-chloro-5-hydroxyl-2-methyl-6-decyl-1,4-benzoquinone (CHMDB), which inhibits mitochondrial and photosynthetic bacterial cytochrome *b-c*<sub>1</sub> complexes (*b-c*<sub>1</sub> complex) and activates chloroplast cytochrome *b*<sub>6-f</sub> complex (*b*<sub>6-f</sub> complex), has been synthesized and characterized. Spectral properties of CHMDB are similar to those of Q<sub>2</sub>. Em of CHMDB is about 50 mV lower than that of Q<sub>2</sub>.

When the *b-c*<sub>1</sub> complex is treated with varying concentrations of CHMDB and assayed with a constant concentration of substrate (Q<sub>2</sub>H<sub>2</sub>), a 50% inhibition is observed when two mole CHMDB per mole enzyme is used. The degree of inhibition is depending upon the concentration of substrate used. At a given concentration of CHMDB, a relatively lower degree of inhibition is observed when a lower (Q<sub>2</sub>H<sub>2</sub>) concentration is used, suggesting a possible existence of different forms of ubiquinol-cytochrome *c* reductase with different affinity of Q.

In contrast to the inhibition observed with the *b-c*<sub>1</sub> complex, CHMDB shows a four-fold activation on the plastoquinol-plastocyanin reductase activity of chloroplast *b*<sub>6-f</sub> complex, and the degree of the activation is independent of concentration of plastoquinol (PQ<sub>2</sub>H<sub>2</sub>) used. When Q<sub>2</sub>H<sub>2</sub> was used as a substrate for *b*<sub>6-f</sub> complex assayed no activation or inhibition was observed. CHMDB restores the DBMIB altered epr spectra of ISP in both the *b-c*<sub>1</sub> and *b*<sub>6-f</sub> complexes. In the case of *b*<sub>6-f</sub> complex, CHMDB also restores the DBMIB inhibited activity. The reduced form CHMDB is oxidizable by the *b*<sub>6-f</sub> complex at a rate higher than that of PQ<sub>2</sub>H<sub>2</sub>. 2-chloro-5-hydroxyl-3-methyl-6-decyl-1,4-benzoquinone, an isomer of CHMDB, shows similar activation effect to *b*<sub>6-f</sub> complex but shows no inhibitory effect to *b-c*<sub>1</sub> complex. These results suggest that the quinol oxidizing site in these two complexes is different, and thus the reaction mechanism in these two complexes may not be identical. (Supported in part by grants from NIH and USDA).

**T-Pos281** ARGININE-328 OF THE β-SUBUNIT OF THE MITOCHONDRIAL ATPase IN YEAST IS ESSENTIAL FOR PROTEIN STABILITY. David M. Mueller, University of Health Sciences, The Chicago Medical School, Department of Biochemistry and Structure, North Chicago, IL., 60064.

The mitochondrial ATPase is rapidly inactivated by the arginine selective reagents phenylglyoxal and butanedione. Recently, the major reacting arginine has been reported in the chloroplast enzyme (Viale, A.M. and Vallejos, R.H., *J. Biol.Chem.* 260, 4958-4962, 1985) and it corresponds to Arg-328 of the yeast enzyme. This arginine residue was thus concluded to be in the active site and was possibly involved in the binding of the nucleotides. To test this hypothesis, site directed mutagenesis of the yeast enzyme has been used to alter Arg-328 to Lys-328 and Ala-328. The modified gene was placed into a yeast strain, DMY111, which was deleted of a major portion of the wild type gene coding for the β-subunit of the ATPase including the portion coding for Arg-328. There was little observable difference on the rate of growth on a nonfermentable carbon source of the mutant strains as compared to the wild type strain transformed with the wild type gene. Thus, the mutations did not sufficiently impair mitochondrial function to affect the rate of growth. Enzyme kinetic analysis has been performed on the mutant and wild type enzymes. The chloroform released enzymes with Ala-328 and Lys-328 are extremely unstable, but can be stabilized with glycerol. The rate of enzymatic decay follows first order kinetics with half-lives of 1.1 and 4.0 min. for the Ala-328 and the Lys-328 mutants in 10% and 5% glycerol, respectively. The wild type enzyme is stable even in the absence of glycerol. Kinetic analysis of both ATPase and GTPase has been determined. The wild type enzyme has two observable Kms and Vmaxs for ATPase which are 0.056mM<sup>-1</sup> and 67 units/min./mg. and 0.1 mM<sup>-1</sup> and 100 units/min./mg. The mutant enzymes demonstrate a single site with values of 0.121 mM<sup>-1</sup> and 45 units/min./mg. and 0.100 mM<sup>-1</sup> and 23 units/min./mg., for the Ala-328 and Lys-328 mutants respectively. GTPase activity of the mutant enzymes showed little difference on the Km or the Vmax values as compared to the wild type enzyme. In contrast to the predicted results, the mutant enzymes are more sensitive to the reagent phenylglyoxal. These results indicate that Arg-328 is important for protein stability, but not involved in substrate binding or catalysis. Supported by ACS and BRSG.

**T-Pos282** A NEW HIGH VOLTAGE REDOX TRANSITION FOR CYTOCHROME a<sub>3</sub>. Gurmel S. Sidhu and Richard W. Hendler, Laboratory of Cell Biology, NHLBI, National Institutes of Health, Bethesda, MD 20892.

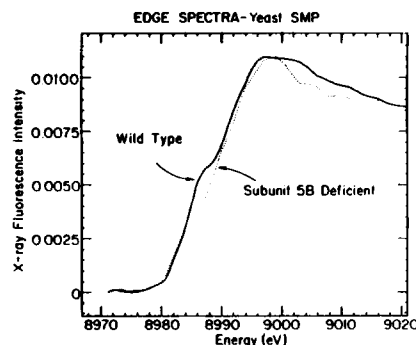
In previous studies with isolated beef heart cytochrome oxidase (Hendler et al., *Biophys. J.* 49: 717 (1987)) we have reported that cytochrome a<sub>3</sub> was reduced and cytochrome a was oxidized at 450 mV (vs S.H.E.). As the voltage of the medium was lowered to ~200 mV, cytochrome a<sub>3</sub> became oxidized as cytochrome a became reduced. At voltages below 200 mV, cytochrome a<sub>3</sub> became re-reduced with an Em near 180 mV. These results suggest that cytochrome a<sub>3</sub> has (at least) two redox potentials, one with E<sub>m</sub> > 450 mV and one at ~180 mV. We now present more direct proof for the high E<sub>m</sub> transition. Using cyano complexes of iron, tungsten, and molybdenum as mediators and a working platinum electrode for the coulometric addition and removal of electrons, we have been able to extend the range of controlled medium voltages to the 450 to 900 mV (vs S.H.E.) range. When resting (oxidized) enzyme is introduced into a medium with the voltage fixed at any voltage from 450 to 750 mV, cytochrome a<sub>3</sub> becomes reduced. The oxidation of this reduced high potential species of cytochrome a<sub>3</sub> occurs in the voltage region 750 to 800 mV. The reduced form of the high potential cytochrome a<sub>3</sub> does not show any ability to bind CO. These results indicate a high degree of redox cooperativity such that a third redox center controls the relative redox potential of cytochrome a<sub>3</sub> vs cytochrome a.

**T-Pos283** REDOX-INDUCED ELECTRONIC STRUCTURAL CHANGE AT  $Cu_A^{++}$  IN CYTOCHROME c OXIDASE AS PROBED BY ELECTRON NUCLEAR DOUBLE RESONANCE (ENDOR). C. P. Scholes, C. Fan, R. Dorr, and J. F. Bank, Department of Physics, SUNY at Albany, Albany, NY 12222.

This work showed a specific electronic change at the cysteine ligand(s) of  $Cu_A^{++}$  as brought on by reduction of other metals within cytochrome c oxidase, notably cytochrome a. The change manifested itself as a modification in the magnetic hyperfine coupling to the  $\beta$ -protons on the  $\beta$ -carbons adjacent to cysteine sulfur in the  $Cu_A^{++}$  coordination sphere. Their ENDOR signals had previously been assigned to the cysteine  $\beta$ -protons through ENDOR study of selectively deuterated yeast oxidase [Stevens et al. (1982) J. Biol. Chem. 257, 12106]. In the present study the ENDOR signals of the  $Cu_A^{++}$  center were compared from the following forms of cytochrome c oxidase; resting ( $a_3^{++} \cdot Cu_A^{++} \cdot a_3^{++} \cdot Cu_B^{++}$ ); mixed-valence, 2-electron reduced, CO-ligated oxidase ( $a_3^{++} \cdot Cu_A^{++} \cdot a_3^{++} \cdot CO \cdot Cu_B^{++}$ ); and a more completely reduced mixed-valence, CO-ligated oxidase prepared under potentiometric monitoring. In agreement with previous studies [Brudvig et al. (1984) J. Biol. Chem. 259, 11001] on 3-electron reduced oxidase, these latter more fully reduced forms showed cytochrome a preferentially reduced with respect to  $Cu_A$  so that the majority of paramagnetic  $Cu_A^{++}$  centers had reduced cytochrome a neighbors. The ENDOR-resolved splitting of the  $\beta$ -proton hyperfine features decreased from about 3.8 MHz in the first two more oxidized forms to 3.2 MHz in the more fully reduced forms. Thus we have shown that the electronic structure of the  $Cu_A^{++}$  center specifically monitored by hyperfine couplings to cysteine protons changes in response to reduction of cytochrome a. This structural change may correlate with anticooperative redox interactions reported between cytochrome a and  $Cu_A$ . (This work supported by NIH Grant No. GM 35103.)

**T-Pos284** EDGE STRUCTURES OF GENETICALLY ALTERED CYTOCHROME OXIDASES. Powers, L., Chance, B. & Poyton, R.O. Biochem.Biophys, U. of P, Phila., PA & AT&T Bell Labs, Murray Hill, NJ, U Colo., CO

Edge and EXAFS of beef heart mitochondria and SMP at 100-300  $\mu$ M Cu concentrations have been obtained for the copper components (1,2). Mutant cytochrome oxidases of *S. cerevisiae* (3) at 30-100  $\mu$ M Cu give the edge spectra shown (Fig. 1). The traces for the wild and mutant oxidases show an altered mid-edge feature and a high signal to noise ratio as obtained by enhanced X-ray detection systems (note the lack of fluctuations in the below edge portion). Thus X-ray absorption measurements at physiological concentrations of membrane proteins are feasible; the problems of cytochrome oxidase purification and alteration are obviated, allowing the following of structure changes of membrane bound cytochrome oxidase due to alterations of nuclear coded subunits (3,4).



(1) Powers, et al. (1986) Biophys.J. 49:96; (2) Powers, et al. (1987) J.Biol.Chem. 7:3160-3164; (3) Chance, B. et al. these proceedings; (4) Patterson, E. et al in Cytochrome Systems, Molecular Biology & Bioenergetics (Papa, S.ed) Plenum,1987. Supported in part by NIH Grants HL31909, GM31992

**T-Pos285** SUBUNIT CONTROL OF CYTOCHROME OXIDASE STRUCTURE AND ACTIVITY. Chance, B., Powers, L. Poyton, R.O. Waterland, R. Dept. Biochem/Biophys., Univ.of Penna, ISFS,UCSC, Phila.PA & MC&DB, Univ.Colorado, Boulder, CO; and AT&T Bell Labs, Murray Hill, NJ

Whilst catalytic functions are carried out by a minimal number of subunits, non-catalytic subunits exert an important regulatory role on membrane proteins, both in cytochrome oxidase (1) and in the oxygen evolving complex of photosynthesis (2). Our data for 4 altered forms of cytochrome oxidase of *S. cerevisiae* indicate that the subunit alterations influence the cytochrome c oxidase activity and the structure of the copper site (see also Powers, et al., this volume).

StrainA	Genotype	Cytochrome Content (uM/g wet weight)				Cytochrome-c Oxidase T.N.(sec <sup>-1</sup> )	$\lambda$ Max (nm)		$O_2$ reaction (initial phase)		Mid-edge feature (eV)
		c	c <sub>1</sub>	b	aa <sub>3</sub>		a <sub>3</sub> <sup>2+</sup> CO (aa <sub>3</sub> ) <sup>2+</sup>	a <sub>3</sub> <sup>2+</sup> CO (aa <sub>3</sub> ) <sup>2+</sup>	t <sub>1/2</sub> (min)	Temp(°C)	
JM43	COx5a+,COx5b+	65.0	65.9	56.0	15.3	65	592	610	5	-95	8889
GD5b	COx5a+,COx5b-	71.0	75.6	53.2	12.2	69	593	611	15	-95	8985
GD5a	COx5a-,COx5b+	75.4	70.0	53.5	4.6	108	-	-	-	-	-
GD5ab	COx5a-,COx5b-	70.1	73.7	59.9	0	0	-	-	-	-	-
RP3	COx5a-,COx5b+R	72.0	70.1	63.6	10.9	207	592	610	1.5	-105	-

(1) Patterson, E. et al in Cytochrome Systems Molecular Biology & Bioenergetics (Papa,S. ed), Plenum Publ.(1987). (2) Andersson, B. & Akerband, H-E. in Electron Transfer Mechanism and Oxygen Evolution (Barber, J.ed) 1987. Supported in part by NIH Grants HL 31909 and GM 31992.

**T-Pos286** THE INTERACTION BETWEEN METHYLAMINE DEHYDROGENASE AND AMICYANIN FROM PARACOCCLUS DENITRIFICANS. Kevin A. Gray\*, David B. Knaff\*, Mazhar Husain† and Víctor L. Davidson†. \*Department of Chemistry and Biochemistry, Texas Tech University, Lubbock, TX 79409, †Molecular Biology Division, Veterans Administration Hospital, San Francisco, CA 94121, and Department of Biochemistry and Biophysics, University of California, San Francisco, CA 94143.

When grown on methylamine, Paracoccus denitrificans induces the synthesis of a methylamine dehydrogenase (MADH) containing a covalently bound pyrroloquinoline quinone (PQQ). This enzyme is an oligomeric protein comprised of two 47-kDa subunits and two 15 kDa subunits. One PQQ prosthetic group is bound to each of the small subunits. A Type I blue copper protein, amicyanin, as well as two c-type cytochromes are also synthesized in the presence of methylamine. Kinetic experiments have shown that the electron transfer pathway is from the MADH to the amicyanin and then to one of the c-type cytochromes (probably cytochrome c-551). Previously we have measured the oxidation-reduction potentials for all the proteins involved in this pathway. We present here evidence for the formation of an electrostatically stabilized complex between MADH and amicyanin and have calculated dissociation constants ( $K_d$ ) for the oxidized and reduced forms of amicyanin. The effects of complex formation on the redox properties of the proteins will also be discussed. This work was supported by grants from NIH (HL-16251), NSF (PCM-8408564) and the Robert A. Welch Foundation (D-710).

**T-Pos287** MITOCHONDRIAL CONVERSION OF ESTERIFIED FURA-2 AND INDO-1 TO CALCIUM-SENSITIVE FORMS. K.K. Gunter, D. Restrepo, T.E. Gunter, V.K. Sharma, D.J. Williford, and S.-S. Sheu. Dept. of Biophysics and of Pharmacology, Univ. of Rochester, Rochester, NY 14642

Rat liver mitochondria convert the acetoxymethyl ester forms of fura-2 and indo-1 into calcium dependent forms of these indicators. The excitation spectrum of the calcium-dependent conversion product of fura-2AM is identical to that of the pentacarboxylic acid form of fura-2 (fura-2FA). Conversion of fura-2AM reaches a plateau in 12-15 min at 39°C and in a slightly longer time at 21°C. Conversion of indo-1AM takes considerably longer to reach a plateau level (40-50 min at 35°C and 90-100 min at 21°C). While the calcium-indicator dissociation constant ( $K_d$ ) of both fura-2FA and indo-1FA may be shown by a systematic study to decrease significantly as pH increases from 6.2 to 7.2, only a small further decrease of  $K_d$  is observed in the pH region important following mitochondrial calcium sequestration (pH 7.2 to 8.7). Only a small increase of  $K_d$  of fura-2FA and of indo-1FA is observed as ionic strength is increased from 0.1 to 0.2 M. These results suggest that it might be possible to measure intramitochondrial free calcium using one of these indicators inside the matrix. Indeed, utilizing fluorescence digital imaging microscopy, intense fluorescence was seen from a similarly treated mitochondrial preparation. Results of measurements of intramitochondrial free calcium with fura-2 suggest levels lower than those observed using the "null-point titration technique." Possible reasons for this disagreement will be discussed. A rough estimate of the mitochondrial contribution to the fura-2FA fluorescence of hepatocytes, at 360 nm excitation, following incubation of these cells in fura-2AM is around 4 percent. Supported by GM35550.

**T-Pos288** On the use of fluorescent aminoacridine probes to kinetically characterize proton pumping activity of the membrane-bound bacterial ATPase. Rita Casadio, Dept. of Biology, University of Bologna, Via Irnerio 42; I-40126 Bologna, Italy.

The use of fluorescent amines to detect  $\Delta pH$  across vesicular membranes, acidic inside, is based on the relation between the extent of  $\Delta pH$  and the quenching of fluorescence ( $Q$ ), following the equilibrium redistribution of the dye between the inner ( $V_i$ ) and external ( $V_e$ ) volumes, at the  $\Delta pH$  onset, as described by the equation:  $\Delta pH = \log Q / (100 - Q) + \log V_i / V_e$ .  $Q$  is thereof calibrated in terms of  $\Delta pH$  units by imposing across the membrane  $\Delta pH$ s of known extent, by means of acid to base transitions. In chromatophores from photosynthetic bacteria, at 25°C and 0.1 M ionic strength,  $\Delta pH$  is linearly related to  $\log Q / (100 - Q)$  with the expected slope of one, and the expected dependence on osmolarity, when 10  $\mu M$  9-aminoacridine (9AA) and 9-amino-6-chloro-2-methoxyacridine (ACMA) are utilized as  $\Delta pH$  probes. The range of linearity depends on the different probe: up to 2.2-2.5 and 1.5-1.8  $\Delta pH$  units for 9AA and ACMA, respectively. The half time of ACMA response to  $\Delta pH$  onset is, however, 5-6 times faster than that of 9AA (150 and 500 ms, respectively, at the above experimental conditions). These results indicate that ACMA is a more suited probe than 9AA to monitor and time resolve  $\Delta pH$  of low extent (0.2-1.5 pH), as those coupled to the oligomycin-sensitive ATPase activity in the dark, and produced by addition of different MgATP concentrations, in the presence of valinomycin. Kinetic analyses indicate for  $H^+$  pumping a  $V_{max}^+$  of 0.2-0.3 pH  $s^{-1}$  and a  $K_m$  of 0.15 mM MgATP, coincident with that of the hydrolytic activity.

**T-Pos289** PROTON CONDUCTANCE CAUSED BY LONG-CHAIN FATTY ACIDS IN PHOSPHOLIPID BILAYER MEMBRANES. John Gutknecht, Physiology Dept., Duke University, and Duke Marine Lab., Beaufort, NC 28516.

Mechanisms of proton conductance ( $G_H$ ) were investigated in planar bilayer membranes containing long-chain fatty acids (lauric, myristic, palmitic, oleic or phytanic). Membranes were formed from diphtanoyl phosphatidylcholine (25 mg/ml) in decane plus chlorodecane (usually 30% v/v). Fatty acids were added either to the aqueous phase or to the membrane-forming lipid solution. Proton conductance was calculated from the steady-state total conductance and the  $H^+$  diffusion potential produced by a transmembrane pH gradient. All fatty acids caused  $G_H$  to increase in proportion to the first power of the fatty acid concentration. The  $G_H$  induced by fatty acids was inhibited by phloretin, serum albumin, glycerol and low pH.  $G_H$  was increased by chlorodecane, and the voltage dependence of  $G_H$  was superlinear. The results suggest that fatty acids behave as simple ( $A^-$  type) proton carriers. The membrane:water partition coefficient ( $K$ ) was estimated by determining the membrane and aqueous fatty acid concentrations which gave identical values of  $G_H$ . The  $K_D$  for palmitic acid was about  $10^7$ , 5-fold higher than  $K$  for myristic acid. The  $A^-$  "flip-flop" rate was estimated from the value of  $G_H$  and the fatty acid concentration in the membrane, assuming that  $A^-$  translocation is the rate limiting step in  $H^+$  transport. For myristate, palmitate and phytanate the flip-flop rate was about  $10^{-4} \text{ sec}^{-1}$ , slower than classical weak acid uncouplers by a factor of  $10^5$ . Although long-chain fatty acids are inefficient  $H^+$  carriers, they may cause significant biological  $H^+$  conductance when present in high membrane concentrations, e.g., in ischemia, hormonally induced lipolysis, diabetic lipidemia, or Refsum's (phytanic acid storage) disease. (Supported by NIH grant GM 28844.)

**T-Pos290**  $Ca^{2+}$  UPTAKE BY PHOSPHATIDYLCHOLINE (PC)/PHOSPHATIDYLETHANOLAMINE (PE)/CARDIOLIPIN (CL) LIPOSOMES. Mary Beth Kester and Patricia M. Sokolove, Department of Pharmacology & Experimental Therapeutics, University of Maryland Medical School, Baltimore, MD 21201.

A brief report of  $Ca^{2+}$  uptake by PC liposomes containing 20% CL has recently appeared [Smaal et al. (1987) *Biochim. Biophys. Acta* 897:191]. In eukaryotic cells, CL is found exclusively in the inner mitochondrial membrane, which contains in addition almost equimolar amounts of PC and PE.  $Ca^{2+}$  uptake was therefore examined in liposomes composed of all three lipids. Liposomes (PC/PE/CL, 2:2:1, mole/mole) containing 3 mM Arsenazo III were formed by repeated extrusion through 0.1  $\mu\text{m}$  polycarbonate filters. The procedure of Smaal et al. [*Biochim. Biophys. Acta* 816:418] was adapted to permit determination of the time course of both  $Ca^{2+}$  entry and dye release with the following results: (1)  $Ca^{2+}$  entry was a slow, sustained process occurring over a period of 60 min or more. (2) The rate of  $Ca^{2+}$  uptake was heavily dependent on both temperature and  $Ca^{2+}$  uptake, increasing sharply as the temperature was raised above 25°C or the  $Ca^{2+}$  concentration above 2 mM. (3) Arsenazo III efflux was similarly dependent on temperature and  $Ca^{2+}$  concentration, except that both curves were shifted towards higher parameter values. Conditions could therefore be identified under which  $Ca^{2+}$  uptake occurred in the absence of dye efflux. This contrasts with the reported behavior of PC/CL liposomes in which  $Ca^{2+}$  uptake and dye efflux were linked. [Supported by NIH (HL32615), an American Cancer Society Junior Faculty Research Award (#JFRA-109) and the Graduate School, Univ. of MD, Baltimore.]

**T-Pos291** UPTAKE OF CATIONIC ANTICANCER DRUGS AND POLYAMINES BY MAMMALIAN MITOCHONDRIA.

R. BAWA and J. J. DIWAN, Dept. of Biology, Rensselaer Polytechnic Institute, Troy, New York 12180.

The cationic anticancer drugs methylglyoxal-bis(guanylhydrazone) (MGBG) and daunomycin (a structural analog of adriamycin), and the polyamine spermidine, adsorb to anionic membrane sites of isolated rat-liver mitochondria. Selective lysis of the outer membrane with the detergent digitonin (0.1mg/mg protein) causes a rapid jump in uptake of MGBG or spermidine, followed by slower progressive uptake, indicating transport across the inner membrane into the matrix [Diwan et al, 1987, *Biochem. Pharm.* in press]. Such findings suggest that the outer membrane is a permeability barrier to the organic cations, contrary to common belief. Recent studies also indicate that following outer membrane lysis there is a potentiation of the inhibitory effects of organic cations on respiration [Manella et al, 1986, *BBA*, 848:312]. Uptakes of radioisotope labeled MGBG, spermidine and daunomycin were measured using the silicone sampling technique. Both the initial surface adsorption and the transport of spermidine into the mitochondrial matrix in digitonin treated and untreated mitochondria, at 5mM  $Mg^{++}$ , is significantly diminished by the presence of equimolar MGBG (5mM) in the medium. Equimolar spermidine (5mM) included in the medium does not significantly affect the uptake of MGBG. These results may indicate different affinities of these structurally similar cations for anionic sites on the membranes and transport mechanism(s) of the inner membrane. Studies of daunomycin uptake confirm that daunomycin rapidly binds to mitochondria via both ionic and nonionic interactions. Even at 25mM  $Mg^{++}$ , added to diminish ionic interactions, the amount of adsorbed daunomycin is so much as to prevent determination of whether there is an increment of uptake upon outer membrane lysis. [Supported by NIH Grant-20726].

**T-Pos292** AN AUSTRALIAN HALOBACTERIUM CONTAINS A NOVEL LIGHT-DRIVEN PROTON PUMP: ARCHAERHODOPSIN  
Yasuo Mukohata, Yasuo Sugiyama, Kunio Ihara and Manabu Yoshida  
Department of Biology, Faculty of Science, Osaka University, Toyonaka 560 Japan

A bacterial strain was isolated from extreme halophiles collected in Western Australia. The reddish orange rods looked like *Halobacterium halobium* RjmR in which we discovered the second bacterial rhodopsin in 1977 (BBRC 78, 237-243) and named it as halorhodopsin (ABB 206, 72-76). This Australian bacterium, however, does not contain either bacteriorhodopsin or halorhodopsin, but does contain a novel proton pump rhodopsin that is distinct from bacteriorhodopsin.

The bacterium has only non-saponifiable lipids in the membrane, is pigmented by bacterioruberin, and grows optimally in 3-4 M NaCl, even in the presence of 100 µg/ml penicillin G. Thus it is now classified in *Halobacterium* sp. aus-1. ATP in the cells reversibly increased in the light under N<sub>2</sub>. The pH of suspensions of the cells and their sonicated vesicles changed upon actinic illumination. The pH change (and the concomittant membrane potential change) was diminished by CCCP. The "claret" membrane was isolated and reconstituted into liposomes, which then pumped protons into the proteo-liposomes in the light, even in a Na<sub>2</sub>SO<sub>4</sub> solution where halorhodopsin can not function. A protein of 26 kDa was purified from the claret membrane and was shown to be a retinal protein ( $\lambda_{\max} \approx 560$  nm in 0.5% C<sub>12</sub>E<sub>9</sub>). Limited proteolysis products of this bacterial rhodopsin differed from those of bacteriorhodopsin. The N-terminus is Thr but not pyro-Glu (bacteriorhodopsin) or Ala (halorhodopsin). The amino acid sequence shows homologies upto 50% to bacteriorhodopsin and 30% to halorhodopsin. The novel proton pump rhodopsin of the Australian halobacterium is named ARCHAERHODOPSIN.

**T-Pos293** INVESTIGATION OF SENSORY RHODOPSIN PHOTOCHEMISTRY AND THE BEHAVIORAL RESPONSES OF *H. halobium* TO LIGHT STIMULI. Steven A. Sundberg, Walther Stoeckenius, and Roberto Bogomolni, Cardiovascular Research Inst. and Dept. of Biochemistry and Biophysics, UCSF, San Francisco, CA.

Sensory rhodopsin-I (SR-I) and -II (SR-II) are retinal pigments thought to mediate the phototactic behavior of *Halobacterium halobium*. Spectroscopic and behavioral studies using a retinal analogue are being carried out with the goals of (1) testing the correlations between SR-I spectral properties and the behavior, and (2) developing a kinetic analysis of the behavior in the hope of suggesting possible signaling mechanisms. Membrane vesicles prepared from the retinal-deficient strain Flx3RSS were reconstituted with either all-trans retinal or 3,4-didehydroretinal (retinal<sub>2</sub>). The SR-I apoprotein binds retinal<sub>2</sub> and forms an analogue pigment having an absorbance spectrum which is red-shifted ( $\lambda_{\max} = 620 \pm 4$ nm) relative to that of the native pigment ( $\lambda_{\max} = 592 \pm 2$ nm), as previously reported (Spudich, et al., 1986, Biophys. J. 49:479-483). Lineshape analysis of the spectra, using an assumed linear relation between bandwidth and absorbance maximum, indicates that these samples also contain substantial quantities of SR-II. The estimated absorbance maximum of the SR-II analogue pigment is also red-shifted ( $\lambda_{\max} = 520 \pm 7$ nm) relative to the native form ( $\lambda_{\max} = 481 \pm 4$ nm). Flash-photolysis studies indicate that the SR-I analogue pigment undergoes a photochemical reaction cycle which is slower than that of native SR-I ( $t_{1/2} \sim 800$  msec at room temperature) by a factor of 2 - 3, and generates an S-like intermediate that is red-shifted by approximately 20nm. In cells, retinal<sub>2</sub> reconstitutes behavioral responses to both reversal-inducing and reversal-suppressing stimuli, with altered kinetics in some cases. Results will be presented and discussed in terms of the goals outlined above. Supported by NIH and NSF grants.

**T-Pos294** STRUCTURE OF THE RETINAL CHROMOPHORE IN THE hR<sub>L</sub> INTERMEDIATE OF HALORHODOPSIN FROM RESONANCE RAMAN SPECTROSCOPY. Stephen P. A. Fodor and Richard A. Mathies, Department of Chemistry, University of California, Berkeley, California 94720; and Roberto A. Bogomolni, Cardiovascular Research Institute, University of California, San Francisco, California 94143.

We have obtained time-resolved resonance Raman spectra of the hR<sub>L</sub> intermediate in the light-driven chloride ion pump, halorhodopsin. hR<sub>L</sub> exhibits lines in the fingerprint region at 1164, 1188, and 1198 cm<sup>-1</sup>. These frequencies and intensities are very similar to those seen in bacteriorhodopsin's L<sub>550</sub> intermediate, which is known to have a 13-cis structure. This indicates that an all-trans → 13-cis isomerization occurs in the halorhodopsin photocycle. Furthermore, the "normal frequency" of the 1164 cm<sup>-1</sup> band which is assigned as the C<sub>14</sub>-C<sub>15</sub> stretch indicates hR<sub>L</sub> contains a 14-s-trans chromophore and suggests that only 14-s-trans structures are involved in the chloride pumping cycle. The insensitivity of the C-C stretching mode frequencies to N-deuteration shows that the Schiff base configuration is anti. The 1644 cm<sup>-1</sup> Schiff base stretching mode in hR<sub>L</sub> shifts to 1620 cm<sup>-1</sup> in D<sub>2</sub>O. The 24 cm<sup>-1</sup> shift indicates that the Schiff base proton is more strongly hydrogen-bonded in hR<sub>L</sub> than in hR<sub>578</sub> where the D<sub>2</sub>O shift is only 12 cm<sup>-1</sup>. Furthermore, the D<sub>2</sub>O-induced shift in hR<sub>L</sub> is the same as that observed in L<sub>550</sub>, suggesting that the perturbation responsible for the decrease in hydrogen bonding in hR<sub>578</sub> has been removed in hR<sub>L</sub>. If the weak hydrogen bonding of the Schiff base in hR<sub>578</sub> is due to some direct or indirect interaction with chloride, then the stronger hydrogen bond in hR<sub>L</sub> suggests that this interaction has been lost.

**T-Pos295** STRUCTURE AND ORIENTATION OF HALORHODOPSIN IN THE MEMBRANE: A PROTEOLYTIC DIGESTION STUDY, Brigitte Schobert, Janos K. Lanyi, Department of Physiology and Biophysics, University of California, Irvine, CA 92717; Dieter Oesterhelt, Max Planck Institute for Biochemistry, D-8033 Martinsried, FRG.

Halorhodopsin (HR), the light-driven chloride pump in halobacteria, was digested with different proteolytic enzymes. Carboxypeptidase A removed 14 amino acids from the C-terminal tail of detergent solubilized HR, producing a fragment of 25.2 kDa. Membrane associated HR could be digested as well, but not in right-side-out sealed cell envelope vesicles. From this result we conclude that the orientation of halorhodopsin in the cytoplasmic membrane is such that the C-terminal tail faces the cytoplasmic side. Tryptic digestion resulted in the removal of the same C-terminal segment, but also in the production of two more cleavage products (molecular mass 20.9 and 16.8 kDa, respectively). The other cleavage sites were determined by amino acid sequencing of the newly produced N-termini, and they turned out to be within interhelical loops in an earlier proposed structural model derived for HR (Blanck and Oesterhelt, EMBO J. 6, 265-273, 1987). Incubation with chymotrypsin and thermolysin yielded different sites of attack, but also in regions which were proposed to be accessible on the surface of the protein. Since three of six proposed interhelical loop segments could be degraded enzymatically, these results support the proposed structural model for HR.

**T-Pos296** PURIFICATION AND CHARACTERIZATION OF BACTERIORHODOPSIN.

L.J.W. Miercke, P.E. Ross\*, R.M. Stroud, and E.A. Dratz\*, Department of Biochemistry & Biophysics University of California, San Francisco, California, 94143-0448 and \*Department of Chemistry, Montana State University, Bozeman, Montana 59717.

Bacteriorhodopsin (BR) essentially free of native lipids has been prepared in a highly stable state. Purple membrane (PM) (40-50 mg BR) was solubilized in Triton X-100 and then purified by size exclusion chromatography using CHAPSO detergent at pH5. Phospholipid/BR molar ratios of the BR fractions range from 0.4 to 0.05 corresponding to 94-99% phospholipid removal. Purified BR has an absorbance ratio (A280/A548) of 1.5-1.6 in the dark-adapted state which is the highest BR/protein ratio reported to date. The purified BR in CHAPSO shows maximum stability in the pH range 5.0-5.5; less than 10% loss occurs over 7 months when stored at 4°C, pH5, in the dark. Isoelectric focusing resolved delipidated and non-delipidated samples into 10 bands. Both components of the principal doublet with pI's of 5.20 and 5.24 have absorption maxima characteristic of solubilized BR at 550 nm. Minor bands include a quartet in the range of pI 5.5 to 5.6 and doublets centered at pI 4.9 and 5.0. BR in Triton X-100 or nonylglucoside, delipidated BR in CHAPSO, and BR in intact PM all have a 13-cis to all-trans dark-adapted ratio of 2:1 as shown by organic extraction and HPLC. SDS-PAGE profiles of native PM and solubilized BR from many but not all of our *H. halobium* JW-3 cultures show two higher molecular weight bands in addition to BR. These bands may be incompletely processed forms of the precursor protein.

**T-Pos297** CARBOXYLMETHYLATED MEMBRANE PROTEINS IN HALOBACTERIUM HALOBIUM CHEMO- AND PHOTOTAXIS: A POSSIBLE METHYL-ACCEPTING RETINYLIDENE PROTEIN. C.A.Hasselbacher, E.N.Spudich, J.L. Spudich. Dept. of Structural Biology, A. Einstein College of Medicine, Bronx, N.Y. 10461.

Membrane proteins of *H. halobium* were examined by SDS-PAGE after *in vivo* labeling with [<sup>3</sup>H]-methyl-methionine in the presence of puromycin, following procedures known to label carboxylmethylated chemotaxis proteins in eubacteria (e.g. *E. coli*). Autoradiography reveals 9 bands with M<sub>r</sub> from 65,000-150,000 in pho<sup>+</sup>che<sup>+</sup> strains. Analysis of pho<sup>-</sup> mutants isolated previously (1) shows 7 of the bands are missing in one class of pho<sup>-</sup>che<sup>-</sup> mutants which are defective in adaptation. The parent methylation pattern is restored in strains selected for reversion to the parent phenotype.

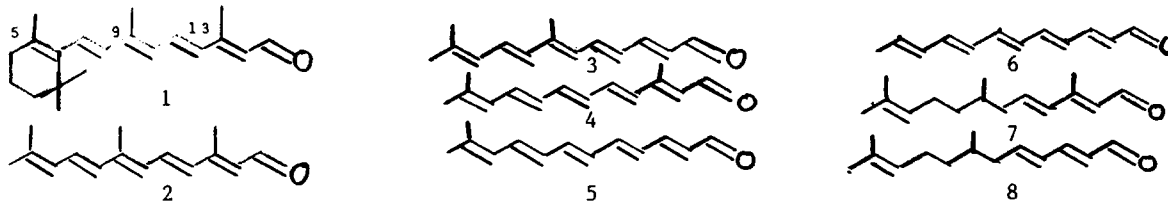
Several observations suggest that one of the 7 methyl-labeled bands is also a retinylidene protein. Two phototaxis receptors (SR-I and SR-II) which use retinal as their chromophore have been identified. Radiolabeling membranes with [<sup>3</sup>H]retinal produces 4 main bands, two of which are at 25,000 and 23,000 and correlate with SR-I and SR-II respectively (2). A mutant with normal chemotaxis but no phototaxis sensitivity has been characterized. This mutant lacks both SR-I and SR-II photoreactions, the 23,000 and 25,000 retinal-labeled bands, as well as a third band at 94,000. In addition, the mutant is missing one of the methyl-labeled bands, which runs at the same position in the gel as the 94,000 retinal-labeled band. Both the methyl and retinal labeling at 94,000 are enhanced in a strain with increased amounts of at least one of the known phototaxis receptors (SR-I). Abbreviations: SR-I & SR-II, sensory rhodopsins I & II; pho<sup>+</sup>, phototactic; che<sup>+</sup>, chemotactic.

(1) Sundberg, S.A., Bogomolni, R.A., Spudich, J.L. (1985) J. Bacteriol. 164, 282-287.

(2) Spudich, E.N., Sundberg, S.A., Manor, D., Spudich, J.L. (1986) Proteins 1, 239-246.

**T-Pos298 Bacteriorhodopsin Pigments with Polyene Aldehydes** - V. Mani, G. Christensen and R. Crouch - Medical University of South Carolina - Charleston, SC 29425

The role of retinal 1 in the proton pumping function of bacteriorhodopsin is still unknown. To determine the role of certain structural features of 1 in formation and function, a series of polyene aldehydes (2-8) have been synthesized, purified and characterized as acyclic models. The polyenes are the same length as the retinal side chain plus the ring double bond and the methyl groups correspond to the 5,9, and 13 positions on retinal. These analogues form pigments with the apoprotein of bacteriorhodopsin. Methyl groups on the polyenes stabilize the pigments but do not significantly affect the absorption maximum, the methyl group at the "9" position of retinal being particularly key for stability. Saturation of two of the double bonds did not prevent pigment formation but the  $\lambda_{\max}$  was blue shifted. All the pigments were somewhat unstable to the presence of hydroxylamine or all-trans retinal, indicating that binding is not as tight as with the native chromophore. (Supported by NIH grant EY03949)



**T-Pos299 MECHANISTIC STUDIES WITH MODELS FOR THE BACTERIORHODOPSIN-CATALYZED DARK CIS-TRANS ISOMERIZATION OF RETINAL.** Stanley Seltzer, Chemistry Department, Brookhaven National Laboratory, Upton, New York 11973.

Nonphotolytic cis-trans isomerization of bound retinal in bacteriorhodopsin during its photocycle and bicycle pedal double cis-trans isomerization of retinal while the pigment is in its dark-adapted state, are reactions which are most likely catalyzed by the host protein. Current studies are directed towards testing the hypothesis that this catalysis results from the interaction of the protonated retinal Schiff base with a negatively charged amino acid side chain acting both as a counteranion and as a nucleophile. We have proposed aspartate-212 for this role.

MNDO molecular orbital calculations predict that the barriers to bicycle pedal double cis-trans isomerization and to ordinary single cis-trans isomerization would be lowered by about 35 and 26 kcal/mol, respectively, if a negatively charged ion were to move from the region around the positively charged Schiff base nitrogen where it could serve as a counteranion, to the vicinity of retinal's C13 atom where it could interact with the polyene in nucleophilic or electrostatic catalysis. If instead the counteranion were to move from the positively charged nitrogen to "infinity", the barriers to double and ordinary cis-trans isomerization would be reduced by only 26 and 22 kcal/mole, respectively.

Kinetic studies of catalyzed retinal cis-trans isomerization by model compounds support the theoretical predictions. The first of a family of model compounds, each having a secondary amine to form a positively charged Schiff base with retinal, and a pendant carboxyalkyl group to provide a negatively charged nucleophile, has been synthesized and studied. The isomerization kinetics that these Schiff base zwitterions exhibit will be discussed. Supported by the Department of Energy.

**T-Pos300 TWO-PHOTON SPECTROSCOPY OF BACTERIORHODOPSIN**

Chian-Fan Zhang, Mark B. Masthay, G. Alan Schick, Cora M. Einterz, Henry M. Knapp, and Robert R. Birge, Department of Chemistry, Carnegie-Mellon University, Pittsburgh, PA. 15213

The room-temperature two-photon double-resonance spectrum of bacteriorhodopsin was collected with the goal of locating the low-lying  ${}^1A_g^{*-}$   $\pi\pi^*$  state in the protein bound chromophore. The relative ordering of the low-lying two-photon allowed, covalent  ${}^1A_g^{*-}$  state and the one-photon allowed, ionic  ${}^1B_U^{*+}$  state is indicative of the total charge within the protein binding site and of the extent of protonation on the Schiff base chromophore. Furthermore the sensitivity of energy splitting between these two states to small changes in counterion location provides a unique probe of the local counterion environment in the vicinity of the chromophore. Our results show a large two-photon allowed  ${}^1B_U^{*+}$  band at the one-photon absorption region, and a  ${}^1A_g^{*-}$  band appears as a shoulder near 475 nm. The fact that the  ${}^1B_U^{*+}$  state is more two-photon allowed than the  ${}^1A_g^{*-}$  state implies that the binding site in bacteriorhodopsin is much more ionic in character than is the case for rhodopsin. The Franck-Condon maximum of  ${}^1A_g^{*-}$  state is approximately  $3400\text{ cm}^{-1}$  above that of the  ${}^1B_U^{*+}$  state, which confirms that the chromophore has a protonated Schiff base. More experimental studies are in progress to specify more accurately the location of the  ${}^1A_g^{*-}$  state and to achieve definitive assignments for the low-lying two-photon allowed excited states.

**T-Pos301** INTERACTION OF PROTEIN RESIDUES WITH THE RETINAL PROTONATED SCHIFF BASE OF BACTERIORHODOPSIN IN PURPLE MEMBRANE; ANALYSIS BY UV, VISIBLE AND RESONANCE RAMAN SPECTRA IN THE WEAK ALKALINE pH REGION.

Akio Maeda (Department of Biophysics, Faculty of Science, Kyoto University, Kyoto, 606 Japan)  
Masashi Nakagawa, Takashi Ogura & Teizo Kitagawa (Institute for Molecular Science, Okazaki National Research Institutes, Okazaki, 444 Japan)

Changes in the visible and UV absorption spectra, the resonance Raman spectra and the photoreactions in the weak alkaline pH region were measured for bacteriorhodopsin and its lysine-modified forms in order to reveal the residues surrounding the chromophore retinal Schiff base. Small increases of absorbance around 610 nm were observed in parallel with the appearance of structured features at 297 and 286 nm, which could be mimicked by the pH difference spectrum of tryptophan but not of tyrosine. These features were weakened when bR was extensively acetylated but not when methylated. The alkali-induced red shift in the visible region was observable only for bacteriorhodopsin with the all-trans chromophore and abolished by extensive acetylation or methylation. Instead, these yielded the blue shift of the visible absorption band to 470 nm upon alkalization. Raman spectrum of the blue shifted species indicates that the Schiff base is protonated and the C=N stretching frequency in either H<sub>2</sub>O or D<sub>2</sub>O is lower than that of native bR. It is proposed that a lysine residue of pK<sub>a</sub>=9.2 and possibly a carboxylic acid residue are present in the neighborhood of tryptophan residues. These may also be located at a place to affect the spectral properties of the all-trans but not of the 13-cis chromophore.

**T-Pos302** PHOTOCHEMISTRY OF METHYLATED AND PERMETHYLATED BACTERIORHODOPSIN AND RHODOPSIN.

R. Govindjee†, Zs. Dancshazy†, T.G. Ebrey†, C. Longstaff‡ and R.R. Rando‡ Department of Physiology and Biophysics† University of Illinois, Urbana, IL 61801 and Departments of Biological Chemistry and Molecular Pharmacology‡ Harvard Medical School, Boston, MA 02115.

Methylation of the non-active site lysines of bacteriorhodopsin (BR), permethylated BR, allows the complete photocycle to proceed with the formation of M412 and proton release/uptake. The absorption spectrum is similar to that of native BR with normal light/dark adaptation. However, additional monomethylation of the active site lysine causes a red shift of the absorption spectrum from 568 nm (in light-adapted BR) to 630 nm, and light/dark adaptation is not observed. Flash spectroscopy shows that the photocycle of methylated BR stops at the L550 photointermediate. The photointermediate M412 does not form, and no proton release/uptake is observed.

Similarly the photochemistry of methylated rhodopsin proceeds only up to the formation of a species analogous to the Meta-I photointermediate of rhodopsin. The Meta-I to Meta-II transition is not observed.

The Schiff base is deprotonated in the Meta-II and M412 states of rhodopsin and bacteriorhodopsin respectively. In methylated rhodopsin and bacteriorhodopsin, no deprotonation can take place due to the methylation of the active site lysine. Thus, deprotonation of the Schiff base is obligate to the Meta-I to Meta-II transition in rhodopsin, and the L to M transition and proton pumping in bacteriorhodopsin.

**T-Pos303** DIFFERENCE SPECTRA OF THE LATE INTERMEDIATES OF THE BACTERIORHODOPSIN PHOTOCYCLE.

Zs. Dancshazy, R. Govindjee and T.G. Ebrey, Department of Physiology and Biophysics, University of Illinois, Urbana, IL 61801

There are inconclusive kinetic indications that the M intermediate of the bacteriorhodopsin (BR) photocycle actually consists of more than one species. We will present evidence for distinct M forms having different spectra. We measured the flash induced difference absorbance spectra of purple membrane vs. time (using a Diode Array Spectrophotometer; 300-700 nm) and established the distinct difference spectra for Mfast (Mf), Mslow (Ms) and R. The main distinguishing features of the 3 difference spectra at pH=10.5 and 5°C (apparently little or no O660 is formed under these conditions) are as follows: Mf:  $\Delta A_{max}=414$  nm, a shoulder at 436 nm, no absorbance at 350 nm,  $\Delta A_{min}=565$  nm;  $\Delta A_{414}/\Delta A_{565}=0.9$ . Ms:  $\Delta A_{max}=414$  nm, a shoulder at 386 nm,  $\Delta A_{min}=580$  nm;  $\Delta A_{414}/\Delta A_{580}=0.6$ . R:  $\Delta A_{max}=336-350$  nm (double peak), smaller peaks at 386 and 414 nm;  $\Delta A_{min}=586-590$  nm;  $\Delta A_{350}/\Delta A_{585}=0.2$ . At pH 10.5, 5°C the t<sub>1/2</sub> of Mf, Ms and R and the relative weights of BR570 recovered with these rates are: 1 sec (50%), 3-5 sec (25%) and 35 sec (25%) respectively. These spectral features can also be seen at pH=7, -16°C, and at pH=9-10.5, 20°C. The difference spectrum of R has several similarities with the difference spectrum between the dark adapted and light adapted BR. It suggests that R possibly has a reprotonated, but not reisomerized Schiff base and chromophore.

**T-Pos304 TRYPTOPHAN PERTURBATIONS DURING THE BACTERIORHODOPSIN PHOTOCYCLE DETECTED BY FTIR DIFFERENCE SPECTROSCOPY** P.D. Roepe, D. Gray, E.M.M. Van den Berg, C. Winkel, J. Lugtenburg, J. Herzfeld and K.J. Rothschild Dept. of Physics, Boston University, Boston, MA (P.D.R., D.G., K.J.R.), Dept. of Biochemistry, Roche Institute of Molecular Biology, Nutley, NJ, (P.D.R.), Dept. of Chemistry, Brandeis University, Waltham, MA (J.H.), Dept. of Chemistry, University of Leiden, Leiden, The Netherlands (E.M.M.VdB., C.W., J.L.)

Recent UV difference measurements of the bacteriorhodopsin (bR) photocycle have suggested that one or more tryptophans are perturbed during formation of the K<sub>630</sub> and M<sub>412</sub> intermediates (Rothschild *et al.*, *Proc. Natl. Acad. Sci.* 89, 347 (1986), Roepe *et al.* *Biochemistry*, *in press*, Sabes *et al.*, *Photochem. & Photobiophys.* 8, 97 (1984)). Low temperature Fourier transform infrared (FTIR) difference spectroscopy combined with selective isotopic labeling of tryptophan residues (<sup>2</sup>H<sub>5</sub>-trp) has now been used to study tryptophan alterations in the BR<sub>570</sub>→K<sub>630</sub>, BR<sub>570</sub>→L<sub>550</sub> and BR<sub>570</sub>→M<sub>412</sub> transitions. A pair of peaks at 741 (negative) and 745 (positive) cm<sup>-1</sup> are found in the BR<sub>570</sub>→K<sub>630</sub> difference spectrum which disappear in the analogous spectrum for bR-[<sup>2</sup>H<sub>5</sub>trp]. These bands are near the expected frequency for an indolyl ring breathing mode and are thus assignable to a tryptophan(s) which undergoes a change in its local environment during this step of the photocycle. The appearance of additional peaks assignable to tryptophan at the L<sub>550</sub> and M<sub>412</sub> stage indicates that further tryptophan alterations occur at these stages of the photocycle. These results will be compared with FTIR spectra of tryptophan model compounds. *This work was supported by grants from the NSF to K.J.R., the NIH to J.H., and the ZWO to J.L. P.D. Roepe is supported by a Jane Coffin Childs postdoctoral fellowship for medical research.*

**T-Pos305 LIGHT-INDUCED STRUCTURAL CHANGES IN BACTERIORHODOPSIN DURING THE BR-568 TO M-411 TRANSITION DETECTED BY NEUTRON DIFFRACTION.**

N.A. Dencher, D. Dresselhaus, G. Zaccai\* and G. Büldt.

Dept. Physics/Biophysics, Freie Universität, Arnimallee 14, D-1000 Berlin 33, FRG.

\*Inst. Laue-Langevin, B.P. 156 X, F-38042 Grenoble, France.

Investigation of the structure-function relationship is of importance for the elucidation of the transmembrane transport mechanisms of membrane pumps at the molecular level. In the case of bacteriorhodopsin (BR) in the purple membrane (PM) of *Halobacterium halobium*, the occurrence and extent of conformational changes in BR during the light-induced vectorial H<sup>+</sup>-translocation across the PM is controversial. We have therefore performed neutron diffraction experiments on oriented PM samples containing BR exclusively in the ground state BR-568 and in the M-411 intermediate of the photocycle. The M-state was trapped under various conditions at low temperature (about -40°C) and diffraction patterns were recorded at -180°C. The results show that during the BR-568 to M-411 transition

1. conformational changes of the protein localized both in the vicinity of the retinal ring portion and the Schiff's base are observed.
2. no changes in the quality of the hexagonal in-plane lattice and its dimensions occur between the two states at the same temperature.
3. the lamellar spacing of the PM stack reversibly increases by 3.7 Å. The contribution of the possible different hydration of the membrane in the M-state will be explored by H<sub>2</sub>O/D<sub>2</sub>O exchange.

**T-Pos306 Infrared Studies of the Late Steps in the Bacteriorhodopsin Photocycle Investigation of the O Form and The Two M Forms at High pH.**

Pál Ormos, David Braunstein, Mi Kyung Hong, Shuo-Liang Lin, Joseph Vittitow, Departments of Physics and Biophysics, University of Illinois, Urbana, IL 61801.

FTIR spectra of bR suspensions were taken in the temperature range 275K-320K at normal and high pH. By continuous illumination a photoequilibrium of M, O and bR was produced. From spectra taken at different temperatures the O/bR difference spectrum could be extracted. In experiments at high pH the spectra of two M forms were separated. The conclusions are: 1) The IR spectra of M and O markedly differ in the carboxylic region - in addition to obvious differences in the retinal spectra. 2) The slow M form seen at pH 9.4 has an IR spectrum different from the one at pH 6.5 in the carboxylic region. This region of the spectrum of the slow M is identical to that of O. 3) At high pH bR has two independent photocycles: one through the "normal" M and O, and one through the slow M.

## T-Pos307 HIGH RESOLUTION SOLID STATE NMR OF BLUE MEMBRANE

H.J.M. de Groot\*, S.O. Smith\*, J. Courtin<sup>‡</sup>, E. van den Berg<sup>‡</sup>, C. Winkel<sup>‡</sup>, J. Lugtenburg<sup>‡</sup>, J. Herzfeld<sup>#</sup> and R.G. Griffin\* \*Francis Bitter National Magnet Laboratory, M.I.T., Cambridge, MA 02139, <sup>‡</sup>Gorlaeus Laboratoria der Rijksuniversiteit te Leiden, 2300 RA Leiden, The Netherlands, and <sup>#</sup>Department of Chemistry, Brandeis University, Waltham, MA 02254

Blue membrane samples containing bacteriorhodopsin with an absorption maximum at  $\lambda_{\text{max}} > 600$  nm ( $\text{bR}_{600}$ ) were obtained by deionizing purple membrane suspensions. This purple membrane was regenerated with 5-<sup>13</sup>C, 12-<sup>13</sup>C, 14-<sup>13</sup>C or 15-<sup>13</sup>C retinal. The  $\text{bR}_{600}$  was investigated at temperatures between 170 K and 300 K using high-resolution solid state NMR techniques. Two components are observed in the 12-, 14- and 15-<sup>13</sup>C labeled  $\text{bR}_{600}$  spectra. The chemical shift difference between these components is larger for the 12 and 14 than for the 15 label, thus indicating the presence of 13-cis and all-trans retinal, as in purple dark-adapted bacteriorhodopsin ( $\text{bR}_{558}$ ). However, considerable differences between  $\text{bR}_{600}$  and  $\text{bR}_{558}$  are observed. The spectra of  $\text{bR}_{600}$  show inhomogeneous broadening which indicates irregular distortions of the protein system. Surprisingly, the largest chemical shift difference is observed for the 5-<sup>13</sup>C resonance, which is downfield shifted by ~5 ppm, whereas the 12, 14 and 15 are upfield shifted by only ~2 ppm. This indicates that at least a large part of the redshift in  $\text{bR}_{600}$  may be due to an increased polarization by the negative charge close to the  $\beta$ -ionone ring of the retinylidene chromophore as opposed to protonation effects at the Schiff base end.

## T-Pos308 THE ROLE OF LYSINE IN THE BACTERIORHODOPSIN PHOTOCYCLE Earl L. McMaster\*, Aaron Lewis\*, and Henry L. Crespi+ \*Department of Applied Physics, Cornell University, Ithaca, New York 14853 +Chemistry Division, Argonne National Laboratory, Argonne, Illinois 60439

We have used low temperature FTIR difference spectroscopy to investigate the role of the retinylidene Lysine in the photocycle of light-adapted bacteriorhodopsin (BR). K/BR and M/BR FTIR difference spectra were taken of fully deuterated purple membrane (pm) and of deuterated pm containing selectively protonated Lysine. This allows assignment of some of the IR peaks in the difference spectra to Lysine vibrational modes. Upon deuteration of Lysine we observed a shift in the 1730-1750  $\text{cm}^{-1}$  bands assigned to the aspartic acid COOH mode as well as the expected shifts in the intrinsic Lysine modes. FTIR spectra of the protonated Schiff Base (SBH<sup>+</sup>) formed from all-trans-retinal with n-butyl-amine and n-butyl-d<sub>9</sub>-amine were used as model compounds for BR. Semiempirical molecular orbital calculations and normal mode analysis using the MNDO (modified neglect of diatomic overlap) program at the Cornell National Supercomputer Facility (CNSF) facilitated the assignment of the retinylidene Lysine vibrational modes as well as their interpretation in terms of conformational changes during the BR photocycle. A model depicting the retinylidene Lysine chromophore conformation at various stages in the BR proton pump cycle which is consistent with the spectral data will be presented.

## T-Pos309 THE ROLE OF BASE CATALYSIS IN BACTERIORHODOPSIN'S PHOTOCYCLE, Eric J. Cornavaca and T. Gregory Dewey, Department of Chemistry, University of Denver, Denver, Colorado 80208

We have studied the effects of several bases on the photocycle of bacteriorhodopsin. The photocycle kinetics were monitored using circular dichroism and absorption spectroscopy. Results showed that structurally different bases can trap bR in its M photocycle state. This allows the M state's C.D. spectra to be obtained at room temperature. This spectrum shows a single broad peak centered at the M's absorption maximum. The ability of different bases to trap the M intermediate suggests that a base-catalyzed reaction is involved in the deprotonation step of the bR photocycle. Previous results (Lanyi et al., Biochemistry, 1986, 25, 6706-6711) showed this is also the case with halorhodopsin. This serves to confirm that the deprotonation of the Schiff base in both illuminated hR and bR proceeds with a much lower pK<sub>a</sub> than the unilluminated pigments. The kinetics of the M decay are changed in the presence of these bases. Kinetics of these decays have been measured.

**T-Pos310** NONPROTON ION RELEASE BY BACTERIORHODOPSIN IS A COOPERATIVE EVENT.

T. Marinetti, Rockefeller University, 1230 York Ave., New York NY 10021

Conductivity transients exhibited by photoexcited purple membrane (PM) at pH 7 in 0.4 - 0.5 M NaCl are known to be caused by the release of ions other than H<sup>+</sup> (1). The light energy dependence of the transient amplitude relative to the conductivity change caused by heating from absorbed photons was measured. This provides a direct determination of the ratio of the optical cross section for nonproton ion release to that for light absorption and thus measures the number of bacteriorhodopsin (bR) molecules involved in ion release per photon absorbed. Analysis of the data using Poisson statistics shows that 3 to 4 bR molecules act in concert to generate the conductivity transient. The method features internal calibration: no independent measure of the actinic flash energy is required. Also, the result is insensitive to the signal amplitude at saturation. As a comparison, similar data at pH 4 and low ionic strength, where the signal is due to H<sup>+</sup> alone (2), show that the cross section is equal to that of a single bR molecule. The conclusion is that the changes in surface charge distribution which give rise to the nonproton ion release are cooperative: excitation of one bR evidently stimulates similar conformational changes in its neighbors in the PM.

(1) Marinetti, *Biophys. J.* 51:875 (1987)

(2) Marinetti and Mauzerall, *PNAS* 80:178 (1983)

This work supported by NIH grant GM 32955-03

**T-Pos311** LANTHANUM INHIBITION OF BACTERIORHODOPSIN PROTON PUMPING IN A PLANAR BILAYER. Marie Kenyon, Kenneth J. Rothschild and Bernard Chasan, Physics Department, Boston University, Boston MA, 02215

Bacteriorhodopsin (bR) incorporated into a planar bilayer by fusion of bR-asolectin vesicles exhibited steady state photocurrents of 15-20 pA in a direction indicating that protons were pumped out of the cis chamber, to which the vesicles were added. Dose response curves for lanthanum inhibition were obtained by adding LaCl<sub>3</sub> to the cis chamber at different values of pH. The concentration needed for half inhibition at pH 8 was .8 mM, and was found to increase steeply as pH was decreased. No inhibition was observed at pH 6.3 at a lanthanum concentration of 70 mM. These results are qualitatively consistent with lanthanum inhibition of the decay of the M412 intermediate state. Addition of LaCl<sub>3</sub> to the cis chamber results in an apparent reversal of the current direction due to preferential inhibition of bR oriented with C termini exposed to the cis chamber. Comparison of initial and reversed photocurrents indicates that 2/3 to 4/5 of the incorporated bR molecules are oriented in this direction. In support of this conclusion addition of lanthanum to the trans side only was found to increase the current by 30% as minority pumps were now turned off by the lanthanum. (Part of this research was supported by a grant from the NSF to KJR.)

**T-Pos312** PHOTOCURRENT MEASUREMENTS OF THE PURPLE MEMBRANE ORIENTED IN A POLYACRYLAMIDE GEL

S.Y. Liu and T.G. Ebrey, Department of Physiology and Biophysics, University of Illinois, Urbana, Illinois 61801

When illuminated, oriented purple membrane isolated from *Halobacterium halobium* gives a photoelectric effect. A photocurrent measuring system for purple membranes oriented and immobilized in the polyacrylamide gel was constructed and its frequency response was analyzed from DC to 100 MHz. The waveform of the photocurrent is very sensitive to the measuring system (including the gel's bathing solution, electrodes, and the ammeter) at both the low and high frequency ends. In the DC-1 kHz range (ms signals), the apparent lifetime of the photocurrent component is distorted if the electrode is not platinized and if the conductivity of the bathing solution is not low. In the 1 kHz to MHz range ( $\mu$ s signals), the frequency response is linear under most conditions. In MHz range (ns signals), the apparent lifetime of the photocurrent component will be distorted if the conductivity of the bathing solution is not high and if the input impedance of the ammeter is not low and constant throughout the frequency range. With our optimized measuring system, we could measure the photocurrent transients with lifetimes from 50 ms to 32 ns without distortion by the measuring system. Our measurement shows that there is no photocurrent component than can be correlated with the K-L optical intermediate transition.

**T-Pos313** THE EFFECT OF BLEACHING ON THE APPARENT TILT ANGLE OF THE ALPHA HELICAL SEGMENTS OF THE BACTERIORHODOPSIN OF THE PURPLE MEMBRANE.

J.E. Draheim, Dept. of Chemistry, Univ. of Toledo, Toledo, Ohio, N. Gibson, and J.Y. Cassim, Dept. of Microbiology, The Ohio State Univ., Columbus, Ohio.

An FTIR linear dichroic study has been performed on native and bleached purple membrane (PM) oriented films. At  $4\text{ cm}^{-1}$  resolution the horizontally polarized (ip-plane) spectrum of native PM exhibits amide peaks ca. 3304, 1659, and  $1546\text{ cm}^{-1}$  with the absorbance ratio of the 1546/1659 peaks ca. 1.03. The vertically polarized spectrum of native PM exhibits peaks ca. 3307, 1665, and  $1546\text{ cm}^{-1}$  with a 1546/1665 ratio ca. 0.74. Assuming a classic alpha I type of helix, the linear dichroism of the 3307 and  $1665\text{ cm}^{-1}$  bands indicates an apparent tilt angle for the polypeptide segments of  $33\text{--}29^\circ$ . The horizontally polarized spectrum of bleached PM exhibits peaks ca. 3301, 1659, and  $1545\text{ cm}^{-1}$  with a 1545/1659 ratio ca. 0.93. The vertically polarized spectrum of bleached PM exhibits peaks ca. 3304, 1663, and  $1545\text{ cm}^{-1}$  with a 1545/1663 ratio ca. 0.70. The linear dichroism of the 3304 and 1663 bands indicates an apparent tilt angle of  $40\text{--}37^\circ$  for the bleached PM. Thus upon bleaching there is a net change in the calculated tilt angle of  $8^\circ$ . This is considerably smaller than the calculated  $26^\circ$  change based upon previous CD experiments. It will be shown that this apparent paradox can be resolved assuming an alpha II type of helix for the protein of the PM.

**T-Pos314** CATIONS AFFECT THE PURPLE-TO-BLUE TRANSITION OF BACTERIORHODOPSIN IN PURPLE MEMBRANE VIA CHANGES IN SURFACE pH. I. Szundi and W. Stoeckenius, Cardiovasc. Res. Inst. and Dept. of Biochem. and Biophys., Univ. of California, San Francisco, CA 94143

The reversible red shift of the purple membrane (pm) absorption maximum from purple ( $\lambda_{\text{max}} = 568\text{ nm}$ ) to blue ( $\lambda_{\text{max}} = 605\text{ nm}$ ) is caused by either acidification or removal of metal cations. It becomes essentially independent on cation concentration, when most of the acidic lipids are removed or replaced by neutral lipids and the pK of the transition shifts to lower values (pH  $\sim 1.5$ ). We conclude that the cations affect the membrane color through their effect on the surface pH. Based on the differences in the effects of different acids on the purple-to-blue transition, we shall argue that the red shift is not due to protonation of a Schiff base counterion but to conformational changes in the protein molecule. The indirect effect of cations is explained by a surface model based on the known composition of pm, the dissociation constants of surface lipid and protein groups, and the influence of surface charges on the local ion concentration. Calculations of the surface pH at different electrolyte concentrations reproduce the experimentally observed sigmoidal titration curves for the blue-to-purple transition with mono- and divalent cations.

**T-Pos315** REGENERATION OF BLUE AND PURPLE MEMBRANES FROM DEIONIZED BLEACHED MEMBRANES OF HALOBACTERIUM HALOBIUM. Chung-Ho Chang<sup>1</sup>, Roy Jonas<sup>2</sup>, Ragni Govindjee<sup>2</sup>, and Thomas G. Ebrey<sup>2</sup>.

<sup>1</sup>Department of Cell Biology, Stanford University, Stanford, CA 94305, <sup>2</sup>Department of Physiology and Biophysics, University of Illinois, Urbana, IL 61801.

Bleached purple membrane normally binds  $\text{Ca}^{2+}$  and  $\text{Mg}^{2+}$ , which can be removed by the divalent cation chelator ethylenediaminetetraacetic acid (EDTA). Regeneration of pigments from EDTA-treated bleached membrane (apomembrane) and retinal leads to the formation of blue membrane at pH 4.8, and purple membrane at neutral pH. The pigments take much longer to regenerate than with un-deionized apoprotein. Adding back cations to the deionized apomembrane only partially speeds up the regeneration process. Like native purple membrane, the regenerated purple membrane also undergoes a photocycle and shows a light-induced proton release and uptake, although with much slower kinetics than the native species. Thus, cations control the kinetics of pigment regeneration, and also some aspects of the pigment's conformation which controls the photocycle kinetics. The removal and replacement of the cations is not completely reversible, suggesting the cations are not merely bound in the double layer.

**T-Pos316** STUDIES OF THE pH DEPENDENCE OF LIGHT-INDUCED ABSORBANCE CHANGES OF BACTERIORHODOPSIN IN PURPLE MEMBRANE. R. Lozier, J. Hofrichter, L. Murray, and E. Henry, Laboratory of Chemical Physics, NIDDK, and R. Shrager, Laboratory of Applied Studies, DCRT, NIH, Bethesda, MD 20892

Although the visible absorption spectrum of bacteriorhodopsin in aqueous suspensions of purple membrane is insensitive to pH over a broad range, the kinetics of its light-induced absorption changes are markedly pH dependent. Xie et al. (*Biophysical J.* 51:627, 1987) have recently reported evidence for seven kinetic intermediates in the bacteriorhodopsin photocycle at times ranging from 1  $\mu$ s to the completion of the cycle (about 50 ms) at pH 5, pH 7 and pH 9 and several temperatures. We are extending these studies in two directions. First, we have used singular value decomposition (Shrager, *Chemometrics and Intelligent Lab. Systems* 1:59, 1986) to analyze the combined data at the three pH values to obtain a consistent set of basis spectra. If it is hypothesized that only the relative concentrations (and not the absorption spectra) of the kinetic intermediates are pH-dependent, then the minimum number of distinct spectral species can be obtained from this analysis. The results clearly show the existence of at least five and perhaps as many as seven species. Second, we are collecting time resolved absorption spectra over a wider range of times (10 ns-100 ms) and across a finer grid of wavelengths and pH values and will analyze them using the SVD-based procedures. A more precise characterization of the pH dependence of the kinetic intermediates is a step toward a more complete description of the bacteriorhodopsin photocycle.

**T-Pos317** STRUCTURE-FUNCTION STUDIES OF BACTERIORHODOPSIN BY SITE-DIRECTED MUTAGENESIS.

Tatsushi Mogi, L. J. Stern, T. Marti, B. Chao, M. Hughes, and H. Gobind Khorana (Intr. by R. Swanson) From the Departments of Biology and Chemistry, M.I.T., Cambridge, MA 02139

In continuing previous studies, we have now individually replaced all aspartic acid residues, except for Asp-242, as follows: Asp-212 $\rightarrow$ Asn, Glu and Ala; Asp-85, 96 and 115 by Asn and Glu; Asp-36, 38, 102 and 104 by Asn each. Following results were obtained: 1) Asp212 $\rightarrow$ Asn and Glu showed red-shifted chromophores (584 and 560nm, respectively) and reduced proton pumping (11 and 5%, respectively). Severe photobleaching of Asp212 $\rightarrow$ Ala chromophore (538nm) was observed. Regeneration rates of all three mutants were much slower than that of the wild-type bR. 2) Asp-85 and 96 to Asn showed no detectable proton pumping, while Asp-85 and 96 to Glu showed about 50% pumping. Asp-85 $\rightarrow$ Asn showed a red-shifted chromophore (587nm) with a reduced rate of chromophore regeneration, while Asp-85 $\rightarrow$ Glu regenerated a red-shifted chromophore with a faster rate. 3) Asp-115 to Asn and Glu regenerated blue-shifted chromophores (537 and 541nm, respectively). Both these mutants pumped protons. 4) Asp-36, 38, 102 and 104 to Asn showed the wild type phenotypes.

We concluded that Asp-85 and 96, on the hydrophilic surface of the helix C, are directly involved in proton pumping mechanism by bR, and that none of the aspartic residues is the major cause of the opsin shift postulated by the point charge model. It is probable that Asp-85 and -212 interact with the protonated Schiff base. A tertiary structure model for bR will be discussed. (Supported by grants from N.I.H. and ONR)

**T-Pos318** NORMAL MODE ANALYSIS OF THE ANOMALOUS HYDROGEN OUT-OF-PLANE WAG VIBRATIONS OF BATHORHODOPSIN PROVIDES FURTHER EVIDENCE FOR PROTEIN PERTURBATIONS NEAR THE CENTER OF THE CHROMOPHORE. Ilona Palings and Richard A. Mathies, Chemistry Department, University of California, Berkeley, CA 94720; Johannes A. Pardoën, Albert Broek, Ellen van den Berg, Chris Winkel, Jacques Courtin and Johan Lugtenburg, Chemistry Department, Leiden University, 2300 RA Leiden, The Netherlands.

We have obtained resonance Raman spectra of  $34\text{ }^2\text{H}$ - and  $^{13}\text{C}$ -labeled bathorhodopsin derivatives and have assigned the hydrogen out-of-plane wag modes at 921, 875, 858, 850, and 838  $\text{cm}^{-1}$ . A normal mode analysis was performed in which 20 force constants were adjusted to fit 135 frequencies with an average error of  $\pm 2\text{ cm}^{-1}$ . Previously, three modes at 921, 875, and 853  $\text{cm}^{-1}$  were assigned to isolated 11H, 10H, and 14H wag vibrations. The 12H wag was found to be uncoupled from the 11H wag, but a specific assignment could not be made (Eyring et al., Biochem. 21, 384, 1982). The higher resolution spectra and much larger data set presented here have allowed us to confirm and refine these assignments. The 921  $\text{cm}^{-1}$  line is again assigned to an isolated 11H wag. The 875  $\text{cm}^{-1}$  line is assigned to the 10H wag mixed with the  $\text{HC}_7=\text{C}_8\text{H B}_g$  wag. The 858  $\text{cm}^{-1}$  line is assigned to predominantly the 12H wag. The 850  $\text{cm}^{-1}$  line is assigned to an isolated 14H wag, and the weak 838  $\text{cm}^{-1}$  line is assigned to the  $\text{HC}_7=\text{C}_8\text{H B}_g$  wag mixed with the 10H and 12H wags. The diagonal force constant for the 12H wag is significantly smaller than that of model compounds, and the 11H $\times$ 12H interaction constant is also anomalously small in bathorhodopsin. These perturbations indicate that there are chromophore-protein interactions near  $\text{C}_{12}$ , which may be involved in the energy storage mechanism. This is consistent with previously observed perturbations of the C-C stretch frequencies in bathorhodopsin (Palings et al., Biochem. 26, 2544, 1987).

**T-Pos319** SOLID-STATE NMR STUDIES ON THE MECHANISM OF THE OPSIN SHIFT IN RHODOPSIN S.O. Smith\*, J. Friedlander#, I. Palings#, J. Courtin&, H. de Groot\*, J. Lugtenburg&, R.A. Mathies# and R.G. Griffin\* (Intr. by R. Frankel) \*Francis Bitter National Magnet Laboratory, M.I.T., Cambridge, MA 02139, #Department of Chemistry, University of California, Berkeley, CA 94720, and &Department of Chemistry, Rijksuniversiteit te Leiden, 2300 RA Leiden, The Netherlands.

Solid-state  $^{13}\text{C}$ -NMR spectra have been obtained of bovine rhodopsin regenerated with retinal  $^{13}\text{C}$ -labeled at positions 6, 7, 8, 9, 10, 11, 12, 13, 15 and 20. These results extend our previous spectra of 5- $^{13}\text{C}$  and 14- $^{13}\text{C}$ -rhodopsin [Biochemistry (1987) 26: 1606]. The chemical shifts for  $^{13}\text{C}$ -5 through  $^{13}\text{C}$ -7,  $^{13}\text{C}$ -14 and  $^{13}\text{C}$ -15 correspond closely to the chemical shifts observed in the 11-cis protonated Schiff base model compound. These results argue that the factors regulating the absorption wavelength of bacteriorhodopsin, namely protein charges near the ionone ring (C-5...C-7), a 6-s-trans single bond, and a weak N-H bond, are not present in rhodopsin. Differences in chemical shift relative to the 11-cis PSB chloride salt are observed for positions 11, 12 and 13 with the largest difference (6.2 ppm) localized at position 13. The large shift at C-13 is also observed in isorhodopsin arguing that an unusual twist in the cis  $\text{C}_{11}=\text{C}_{12}$  bond in rhodopsin is not responsible for the opsin shift. The localized effect at C-13 supports previous models of rhodopsin that place a negative protein charge in the vicinity of C-13 as a mechanism for the opsin shift.

**T-Pos320** THE NATURE OF CHROMOPHORE PROTEIN LINKAGE IN THE U.V. ABSORBING VISUAL PIGMENT OF OWL FLY. P. Rath, C. Pande, H. Deng, R. Callender and J. Schwemer\*. Physics department, City College of New York, U.S.A.; \* Institut für Zoophysiology, Ruhr-Universität Bochum, F.R.G.

The U.V. absorbing (abs.max. 345 nm) visual pigment of the invertebrate, *Ascalaphus macaronius* (owl fly), contains the 11-cis isomer of retinal as its chromophore. This makes it an interesting exception to the other retinal containing visual pigments which have absorption maxima that are red-shifted relative to the absorption maximum of free retinal (abs. max. 380 nm) and retinal Schiff bases (abs. max. 360 nm). The red-shift in the absorption maxima of other retinal pigments results from the protonation of the Schiff base linkage between the chromophore and the protein, which is further modulated by other electrostatic chromophore protein interactions. Thus, a key question is whether the chromophore-protein linkage in the owl fly pigment is unprotonated.

Resonance Raman measurements performed to answer this, and other structural questions, clearly show that the chromophore is attached to the protein by a protonated Schiff base linkage in the stable photoproduct, acid metarhodopsin, of the owl fly visual pigment. Comparison of the fingerprint region in the owl fly acid metarhodopsin spectrum to that of acid meta species of another invertebrate, octopus, as well as to the bovine meta-I species, suggests that the owl fly metarhodopsin is also an all-trans retinal pigment. Our data also strongly suggest a protonated Schiff base linkage between the chromophore and the protein in owl fly rhodopsin.

These results suggest that a charged (protonated Schiff base) chromophore is essential to visual transduction and that the effect of absorbed light is to isomerize the 11-cis chromophore to all-trans. This is the same basic pattern shared by all pigments which have been studied to date. The mechanism responsible for the low absorption maximum in the case of owl fly visual pigment needs to be explored.

**T-Pos321** EXCITED STATE STRUCTURE AND ISOMERIZATION DYNAMICS OF THE RETINAL CHROMOPHORE IN RHODOPSIN FROM RESONANCE RAMAN INTENSITIES. Glen R. Loppnow and Richard A. Mathies, Chemistry Department, University of California, Berkeley, CA 94720.

Resonance Raman spectroscopy provides detailed information about excited-state structure and dynamics because the intensity of a vibrational line directly reflects the ground-to-excited state geometry change along that normal coordinate. To study the isomerization dynamics of 11-*cis* retinal in the visual pigment rhodopsin, we have measured its resonance Raman intensities at excitation wavelengths ranging from 457 to 647 nm. A Franck-Condon analysis of the absorption spectrum and resonance Raman excitation profiles has been performed. This has enabled us to determine the ground-to-excited state geometry changes along 25 normal coordinates. Six intense low-frequency Raman lines are observed in the 50-500  $\text{cm}^{-1}$  region whose intensities provide mode-specific information about the excited-state torsional deformations that lead to isomerization. The dominant contribution to the absorption width in rhodopsin arises from Franck-Condon progressions in high-frequency ethylenic normal modes. The diffuseness of the absorption spectrum comes from progressions in low-frequency torsional modes, fast electronic excited-state relaxation, and inhomogeneous site distribution effects. The Raman cross sections of rhodopsin are unusually weak because the excited-state wavepacket distorts rapidly ( $\sim 35$  fs) and permanently away from the Franck-Condon geometry along skeletal stretching and torsional coordinates. The red-edge slope of the absorption spectrum is shown to be inversely proportional to the magnitude of the inhomogeneous linewidth. This leads to a molecular interpretation for the observed increase of the absorption red-edge slope in cone visual pigments as the absorption maximum increases. A model is proposed which correlates the inhomogeneous width with the magnitude of the opsin shift.

**T-Pos322** BLEACHING AND REGENERATION OF OCTOPUS RHODOPSIN IN MICROVILLAR MEMBRANES

Y. Koutalos\*, T. Ebrey\*, K. Odashima†, K. Konno†, H. Ok†, N. Shimizu†, F. Derguini†, K. Nakanishi†

\*University of Illinois, Department of Physiology and Biophysics, Urbana, IL 61801

†Columbia University, Department of Chemistry, New York, New York

The chromophore of octopus rhodopsin is 11-*cis* retinal, the same as in most vertebrate rhodopsins. In contrast to the vertebrates, the final photoproduct of this rhodopsin, metarhodopsin, is stable and its chromophore is all-*trans*. The natural chromophore was removed and the opsin was regenerated in situ with the 11-*cis*, all-*trans*, 9-*cis* and 13-*cis* isomers. By titrating the octopus opsin with 11-*cis* retinal a rhodopsin extinction coefficient of  $27,000 \text{ M}^{-1} \text{ cm}^{-1}$  at 475 nm was obtained. In order to study the color regulation in rhodopsin and metarhodopsin the 11-*cis* and all-*trans* chromophores of the dihydro series were used for regeneration.

CHROMOPHORE	SBH <sup>†</sup> max nm	PIGMENT max nm	OPSIN SHIFT $\text{cm}^{-1}$	CHROMOPHORE	SBH <sup>†</sup> max nm	PIGMENT max nm	OPSIN SHIFT $\text{cm}^{-1}$
11- <i>cis</i>	440	475	1,540	all- <i>trans</i>	445	510	2,860
5,6-dih, 11- <i>cis</i>	433	464	1,700	5,6-dih, 11- <i>trans</i>	430	471	2,020
7,8-dih, 11- <i>cis</i>	392	416	1,470	7,8-dih, 11- <i>trans</i>	392	433	2,420
9,10-dih, 11- <i>cis</i>	322	330	750	9,10-dih, 11- <i>trans</i>	322	<330	<750
9- <i>cis</i>	440	460	1,000	13- <i>cis</i>	445	502	2,550

**T-Pos323** TIME-RESOLVED SPECTRAL AND KINETIC MEASUREMENTS OF VISUAL PIGMENTS: EVIDENCE FOR, AND IMPLICATIONS OF, TWO FORMS OF BATHORHODOPSIN, C.M. Einterz, J.W. Lewis, S.J. Hug and D.S. Kliger

Results of spectral and kinetic measurements after photolysis of rhodopsin and isorhodopsin indicate that two forms of bathorhodopsin (batho) are produced from each of these pigments. The estimated lifetimes for the decay of the batho products from rhodopsin, bathoR<sub>1</sub> and bathoR<sub>2</sub>, to lumirhodopsin (lumi) are 170±20 ns and 36±15ns, respectively. The lifetimes of the batho products from isorhodopsin, bathoI<sub>1</sub> and bathoI<sub>2</sub>, are 195±20 ns and 25±20ns. The difference spectra for the decays of bathoR<sub>1</sub> to lumiR<sub>1</sub> and of bathoR<sub>2</sub> to lumiR<sub>2</sub> are identical within experimental error to the spectra for the decays of bathoI<sub>1</sub> to lumiI<sub>1</sub>, and of bathoI<sub>2</sub> to lumiI<sub>2</sub>, respectively. The results are consistent not only with the production of two batho products after photolysis of rhodopsin, but also with the formation of identical intermediates from rhodopsin and isorhodopsin. Photolysis with several different actinic wavelengths indicates that neither batho product is a photoproduct of the other. In order to gain insight into the mechanism of formation of the two batho products, similar measurements have been performed on visual pigment analogs in which opsin was regenerated with synthetic chromophores. Preliminary results of measurements on the time scale corresponding to the decay of lumirhodopsin are also presented to help elucidate the pathways of decay of the intermediates after excitation of rhodopsin.

**T-Pos324 DIFFUSION OF DYE MOLECULES IN THE CYTOPLASM OF ROD OUTER SEGMENTS.** S. Yoshikami, K.R. Spring, & W.A. Hagins. Lab. of Chemical Physics, NIDDK, and Lab. of Kidney and Electrolyte Metabolism, NHLBI, NIH, Bethesda, MD 20892.

Rod outer segment structure and the response speed and light sensitivity of the dark current define certain features of the excitatory mechanism controlling the plasma membrane conductance of the outer segment. Is the active cytoplasmic volume for the intracellular transmitter(s) restricted to the space adjoining the plasma membrane, or does it include the interdisk water? The answer determines the amount of transmitter that must be created or removed during photon responses.

6-carboxyfluorescein (CF) was loaded into isolated rods from bleached live frog retinas by patch electrode injection or by hydrolytic transfer of CF diacetate. The dye fluorescence was recorded by image-intensified video microscopy. When injected from a patch pipette with an i.d. of  $1.5 \mu\text{m}$ , CF equilibrated throughout the length of a  $70 \mu\text{m}$  outer segment in 5 m. When a cell preloaded with CF was lysed with a high-voltage current pulse from a pipette tip at one end of the outer segment, the interdisk spaces nearby dumped 90 % of their CF within 100 ms. to create a luminous local cloud of dye. Distant regions of the o.s. emptied much more slowly and striking longitudinal dye concentration gradients developed. The apparent longitudinal diffusion of CF was about  $10^{-7} \text{cm}^2 \text{s}^{-1}$ . The active transmitter volume is thus the entire outer segment cytoplasm. Loading of CF from patch pipettes is markedly restricted by diffusion at the pipette tips.

**T-Pos325 HEAT TRANSIENTS DURING PHOTOTRANSDUCTION IN FROG RETINAL RODS STUDIED BY PYROELECTRIC CALORIMETRY.** W.A.Hagins, P.D.Ross, and S.Yoshikami. Labs. of Chemical Physics & Molecular Biology, NIDDK, NIH, Bethesda, MD 20892

Using pyroelectric poly(vinylidene 1,1-difluoride) films [Tasaki, *BJ*, 50, 285(1986)], heat evolution and transretinal (PIII) electrical responses have been recorded simultaneously from live frog retinas whose synapses have been blocked with glutamate.  $6 \mu\text{s}$  560 nm light flashes caused four distinct heat responses:

$q_p$ :  $\sim 1$  ms duration, size equivalent to 70% of photon energy absorbed by rhodopsin, independent of retinal metabolic state.

$q_3$ : Heat burst raising retinal temperature 20-30  $\mu\text{K}$  in 200 ms. Saturated by  $5 \times 10^6$  photons absorbed/rod. Recovery after 10-30 s dependent on rod metabolic state but independent of PIII.

$r_1$ : Slow continuous cooling of 3-5  $\mu\text{K s}^{-1}$  seen only while a large dark current was being suppressed by a flash causing 200-5000 photoisomerizations/rod.

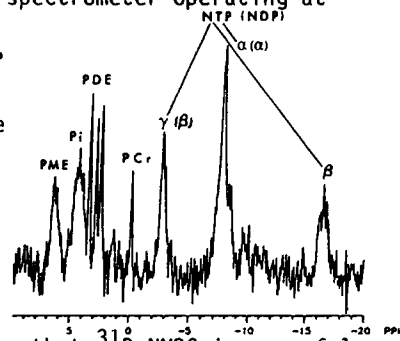
$q_1$ : 1 - 2  $\mu\text{K}$  temperature rise almost paralleling the 100-200 ms time course of shutdown of the dark current. Light adaptation similar to that of PIII. IBMX slows PIII and  $q_1$  differently without affecting the total  $q_1$  heat. 20 mM  $\text{Ca}^{++}$  and 50  $\mu\text{M}$  ouabain suppress PIII without affecting  $q_1$ . Thus  $q_1$  resembles the heat to be expected from hydrolysis of 1-2  $\mu\text{M}$  cGMP in outer segment cytoplasm during transduction but is tenfold smaller than that predicted from responses of membrane patches to applied cGMP.

**T-Pos326  $^{31}\text{P}$  NMR SPECTROSCOPY OF LIVING TOAD RETINAE**

D. V. Apte, Y. Koutalos, D. K. McFarlane, M. J. Dawson, T. G. Ebrey

Department of Physiology and Biophysics, University of Illinois, Urbana, IL 61801

Phosphorus-31 nuclear magnetic resonance spectra were obtained from living toad retinae and toad retinal extracts on a General Electric/Nicolet GN300 wide bore spectrometer operating at 121.48 MHz. All experiments were performed at 4.0°C. Based on the pH dependence of the chemical shift of the inorganic phosphate peak, the intracellular pH of toad retinae was determined to be about 7.2. Several phosphorus metabolites were identified from the spectra of whole retinae (Figure); phosphocreatine (PCr), nucleotide di- and triphosphates (NDP and NTP, respectively), phosphodiester (PDE), phosphomonoesters (PME), and inorganic phosphate (Pi). In contrast to chemical analysis techniques which measure the total metabolite concentrations, phosphorus-31 nuclear magnetic resonance spectroscopy ( $^{31}\text{P}$  NMRS) measures only mobile pools of phosphorus metabolites. An estimate of the relative concentrations of several metabolites was obtained. Titrations of adenosine triphosphate solutions with magnesium were done to determine the MgATP/ATP ratio in whole retinae; this was found to be at least 75%. This study shows that  $^{31}\text{P}$  NMRS is a useful, noninvasive tool for studying the intracellular pH and  $\text{Mg}^{++}$  concentration in retinae and that it may be used to effectively study the metabolism of retinae.



**T-Pos327** SYNTHETIC PEPTIDES TO  $G_{\alpha}$  COMPETE WITH G-PROTEIN FOR INTERACTION WITH LIGHT-ACTIVATED RHODOPSIN AND MONOCLONAL ANTIBODY 4A. H. E. Hamm, D. Deretic, P. A. Hargrave, A. Arendt, J. H. McDowell, B. Koenig and K. P. Hofmann. Dept. Physiol. Biophys., Univ. Ill. Coll. Med. Chicago, Dept. Ophthalmol. Univ. Fla. Gainesville, Inst. Biophys. Strahlenbiol. Univ. Freiburg, FRG.

Mab 4A inhibits G-protein interaction with ROS membranes and with rhodopsin (Hamm et al., *J. Biol. Chem.*, 1987). The Mab 4A binding site on  $G_{\alpha}$  was mapped to  $G_{\alpha}$ -311-328 by tryptic fragment analysis (Deretic and Hamm, *J. Biol. Chem.*, 1987). Thus this region of  $G_{\alpha}$  may be close to or a part of the rhodopsin binding site. To further characterize the functional role of this region of  $G_{\alpha}$ , we have made synthetic peptides corresponding to the Mab 4A antigenic site and have measured the effect of these peptides on G-protein interaction with Mab 4A and rhodopsin. Synthetic peptide  $G_{\alpha}$ -311-328 was an effective competitor for antibody 4A binding, measured by a competition enzyme-linked immunosorbant assay (ELISA), confirming the 4A antigenic site deduced from tryptic mapping studies.

Peptides were derived from this parent peptide to further define the antigenic site. Peptide 311-323 was almost as effective at blocking antibody binding, while 316-328 was 10x less effective. Peptides 311-319 and 320-328 had no effect on Mab 4A binding to G-protein. The effect of these synthetic peptides on light-activated G-protein binding to rhodopsin was measured spectroscopically by the stabilizing effect of G-protein on metarhodopsin II (extra meta II). Peptide 311-328 completely blocked extra meta II, while 311-323 and 316-328 blocked partially with similar potency. Peptides 311-319 and 320-328 had no effect on extra meta II. Thus it appears that  $G_{\alpha}$ -311-328 is involved in interaction with light-activated rhodopsin. The amino acids involved in this site are being investigated by single amino acid substitutions of the parent synthetic peptide.

**T-Pos328 REGULATION OF BOVINE ROD OUTER SEGMENT GUANYLATE CYCLASE BY  $Ca^{2+}$**

Karl-Wilhelm Koch and Lubert Stryer, Dept. of Cell Biology Stanford University School of Medicine, Stanford CA94305

We are studying the guanylate cyclase of retinal rod outer segments, a key enzyme in visual transduction. Suspensions of isolated bovine rod outer segments were incubated with an assay buffer containing [ $\alpha$ - $^{32}P$ ]GTP as a substrate for the guanylate cyclase. The formation of [ $\alpha$ - $^{32}P$ ]cGMP was measured by separating the nucleotides on a TLC sheet and counting the [ $\alpha$ - $^{32}P$ ]cGMP spot. Corrections for the hydrolysis of cGMP were made by measuring the recovery of added [ $^3H$ ]cGMP. The basal activity of guanylate cyclase in bovine rod outer segments was estimated to be 1-2 nmol/min/mg rhodopsin and showed the already known dependence on the cofactors  $Mg^{2+}$  and  $Mn^{2+}$ . Is the guanylate cyclase feedback regulated by  $Ca^{2+}$ ? The concentration of  $Ca^{2+}$  in a photoreceptor cell is known to drop following closure of the cGMP-activated cation channel after a light pulse. We measured the guanylate cyclase activity as a function of the concentration of free  $Ca^{2+}$ -concentration. Different ratios of a  $Ca^{2+}$ /EGTA buffer system were used and the free  $Ca^{2+}$ -concentration was determined using the  $Ca^{2+}$ -indicator fura-2. Guanylate cyclase activity increased between 10 and 20-fold when [ $Ca^{2+}$ ] was decreased from 200 nM to 50 nM. The effect was much steeper than reported for toad rod outer segments (Pepe et al. 1986 FEBS Lett. 203, 73-76). The Hill coefficient for activation by lowering [ $Ca^{2+}$ ] was 3.5 in our experiments. This highly cooperative effect of  $Ca^{2+}$  is mediated by a soluble component, which can be removed by washing and added back to restore calcium regulation.

**T-Pos329 EFFECT OF TRIPHOSPHATE NUCLEOTIDES ON THE RESPONSE OF DETACHED ROD OUTER SEGMENTS TO LOW EXTERNAL CALCIUM.** G. Rispoli, W.A. Sather and P.B. Detwiler. Dept. of Physiology & Biophysics, Univ. of Washington, Seattle, WA

Lamb, Matthews and Torre (*J. Physiol.* 369:34P, 1985) have reported that a sudden reduction in external Ca causes a small, rapid increase in dark current followed by a large, slow increase. The rapid increase is attributed to an external effect of low Ca on the light-regulated channel while the slow increase is thought to be due to an internal effect on the biochemical events controlling dark levels of cGMP. We recorded the change in whole-cell current in response to a rapid decrease in external Ca (1 mM to 1  $\mu$ M) from detached gecko ROS using patch pipets filled with standard internal solution containing 10 mM BAPTA and either 5 mM ATP and 1 mM GTP or 50  $\mu$ M cGMP and no triphosphate nucleotides. We found that triphosphate nucleotides were required for the large slow but not the small rapid increase in dark current. Since detached outer segments contain guanylate cyclase and synthesize cGMP when supplied with triphosphate nucleotide precursors (Sather & Detwiler, PNAS in press) this result suggests that reduced Ca activates guanylate cyclase.

Low external Ca has also been shown to increase the Ca permeability of the light-regulated channel (Hodgkin, McNaughton & Nunn, *J. Physiol.* 358:447, 1985). We find that increased Ca permeability only occurs in the presence of triphosphate nucleotides, suggesting that cGMP levels control the Ca permeability of the light-regulated channel.

These results provide information about the mechanism responsible for the reciprocal relationship between intracellular Ca and cGMP. A fall in [ $Ca$ ]<sub>in</sub> activates guanylate cyclase causing an increase in [cGMP], which in turn results in an increase in the Ca permeability of the light-regulated channel and a rise in [ $Ca$ ]<sub>in</sub>.

T-Pos330 CONCENTRATIONS OF IONS MEASURED AS A FUNCTION OF POSITION ALONG FROG RETINAL ROD OUTER SEGMENTS. Margaret C. Foster & W. A. Hagins, Lab. of Chemical Physics, NIDDK, National Institutes of Health, Bethesda, Md. 20892.

A concentration gradient of free calcium along retinal rod outer segments has been proposed to account for differences of kinetics of light responses when photons are absorbed at the tip or at the base of the rods (J.L. Schnapf, *J. Physiol.* (1983) 343, 147-159). Sodium and voltage gradients due to the dark current would give rise to gradients of free calcium if calcium is in equilibrium with sodium-calcium exchange. Using electron microprobe analysis we have found that gradients of Na, Cl, and K along frog retinal rod outer segments are small, such that the free calcium concentration in equilibrium with the sodium-calcium exchanger changes by less than 20% from tip to base in rods incubated in 0.01 mM  $\text{Ca}^{++}$  and by less than a factor of about 2 in rods incubated in 1 mM  $\text{Ca}^{++}$  Ringer's. Frog retinal samples were incubated in the dark or in saturating light to stop the dark current. Ringers used in different experiments had 1, 0.1, and 0.01 mM Ca, and in mM: 105 NaCl, 20 or 40 NaSc-EDTA, 2.5 KCl, 0.5  $\text{MgSO}_4$ , 0.5 Na phosphate, 11 dextrose, and 10 HEPES (pH 7). Samples were washed in a salt-free solution (in mM: 200 betaine, 20 Cr-EDTA, Tris base to pH 7) for 0 to 20 seconds before freezing. After samples were freeze-dried and carbon-coated, a 10 keV electron beam was scanned in 2 by 2 micron rasters at intervals of 5 to 10 microns along rod outer segments, and X-ray spectra were analyzed by the peak-to-local background method. Ionic concentrations were measured vs. position in about 50 rods under various conditions. Concentration differences of Na and K between tip and base of dark adapted rods were less than 5 to 10 mM. In dark adapted rods incubated in 0.01 to 1 mM Ca Ringer's, free cytoplasmic calcium concentrations calculated to be in equilibrium with sodium-calcium exchange (3 Na/1 Ca) were 1 to 10 micromolar.

T-Pos331 NA-CA EXCHANGE IN BOVINE ROD OUTER SEGMENTS REQUIRES POTASSIUM. Paul P.M. Schnetkamp, Robert T. Szerencsei, Debesh K. Basu (Intr. by M.P. Walsh); Department of Medical Biochemistry, University of Calgary, Calgary, Alberta, Canada, T2N 4N1.

We have used arsenazo III as a  $\text{Ca}^{2+}$ -indicating dye, neutral red binding as a measure for  $\text{Na}^+$  currents (Schnetkamp, 1985, *J. Membrane Biol.* 88, 249), and atomic absorption as a measure for  $\text{Ca}^{2+}$  and  $\text{K}^+$  to study the cation fluxes associated with Na-Ca exchange in intact isolated bovine rod outer segments. Depletion of intracellular  $\text{K}^+$  by addition of gramicidin or by Cs-K exchange caused a more than five fold reduction in the rate of  $\text{Na}_o$ -stimulated  $\text{Ca}^{2+}$  release. Addition of  $\text{K}^+$  reactivates Na-Ca exchange with a half-maximal activation by 1-3 mM  $\text{K}^+$ .  $\text{K}^+$  could be replaced by  $\text{NH}_4^+$  and  $\text{Rb}^+$ , but not by  $\text{Li}^+$  or  $\text{Na}^+$ . In a similar manner,  $\text{Ca}_o$ -activated  $\text{Na}^+$  release required external  $\text{K}^+$ . In the case of  $\text{Na}_o$ -activated  $\text{Ca}^{2+}$  release, we observed that  $\text{Ca}^{2+}$  release was accompanied by an equimolar amount of  $\text{K}^+$  release.  $\text{Sr}_o$ -activated  $\text{Ca}^{2+}$  release was measured as indicator for electro-neutral Ca-Ca exchange; it did not require the presence of either internal or external  $\text{K}^+$ . These results could suggest that Na-Ca exchange in bovine rod outer segments reflects a  $3\text{Na}-(1\text{Ca}+\text{K})$  exchange. The Ca-Ca exchange mode can operate perhaps as either Ca-Ca exchange or as  $(\text{Ca}+\text{K})-(\text{Ca}+\text{K})$  exchange. In the latter case Ca-Ca exchange would be accompanied by an exchange of  $\text{K}^+$  or those monovalent cations that can substitute for  $\text{K}^+$  in activating Na-Ca exchange (e.g. Rb and  $\text{NH}_4$ ). In accordance with this we observed a  $\text{Ca}_o$ -dependent Rb- and  $\text{NH}_4$ -activated  $\text{K}^+$  release from intact bovine rod outer segments. Alternatively, the observed  $\text{K}^+$  fluxes may reflect a distinct  $\text{K}^+$  transport system that acts as an electrical shunt for electrogenic Na-Ca exchange. (Supported by The Alberta Heritage Foundation for Medical Research and MRC grant MA-10013).

T-Pos332 PARTIAL PURIFICATION OF THE Na/Ca EXCHANGER FROM BOVINE ROD OUTER SEGMENTS  
D.A. Nicoll and M.L. Applebury, Purdue University W. Lafayette IN and University of Chicago, Chicago IL

In the rod outer segment (ROS) Ca modulates the properties of at least two of the proteins involved in signal transduction: the light dependent channel and the guanylcyclase. The Na/Ca exchanger is one of the primary regulators of Ca in the outer segment. To be able to better understand the role of the exchanger in ROS, this protein has been partially purified. ConA-sepharose binds to rhodopsin, the major contaminating protein, but not to the Na/Ca exchanger, resulting in a 6-fold enrichment of exchanger activity. Exchanger activity does not bind to WGA-agarose and can be eluted with the competing sugar, GlcNAc, yielding a 2.5-fold enrichment of activity. The exchanger can be bound to and eluted from an anion exchange resin, DEAE-sepharose. Use of these three chromatographic resins provides a significant purification of the Na/Ca exchanger, thereby allowing studies of this protein in the absence of interfering ion fluxes and the controlled study of possible regulatory substances on its activity.

**T-Pos333 EFFECT OF CALCIUM ON LIGHT ADAPTATION IN DETACHED GECKO ROD OUTER SEGMENTS.** W.A. Sather, G. Rispoli and P.B. Detwiler, Dept. Physiol. & Biophys. Univ. of Washington, Seattle, WA.

Whole-cell responses to flashes and steps of light were recorded from detached ROS bathed in normal Ringer (1 mM Ca) using patch pipets filled with a standard internal solution containing 5 mM ATP, 1 mM GTP and either 10 mM BAPTA, 0 added Ca (control) or 1 to 10 mM added Ca. Mean dark current decreased with increasing Ca: -121 pA (BAPTA), -68 pA (control) and -23 pA (10 mM Ca). Absolute flash sensitivity was highest with control solution (1.5 pA/Rh\*) and was reduced with either BAPTA (30%↓) or high Ca (>60%↓). Response kinetics were accelerated 20-50% with 10 mM Ca. Flash responses recorded with BAPTA were slowed relative to control (t<sub>peak</sub> increased 2.4-fold; t<sub>1/2</sub> for recovery increased 4-fold).

The waveform of the step response was similar for control and high Ca solutions; the initial peak of the response declined rapidly to a stable plateau. With BAPTA the peak of the step response declined more slowly to a fluctuating plateau. In all solutions there were two phases to the recovery of step responses: a rapid phase followed by a slow phase, which, for brighter steps, lasted several minutes. With control or high Ca solutions the initial phase accounted for ~50% of the recovery. With BAPTA the slow phase of recovery was preceded by an initial phase that transiently undershot the baseline dark current. With all solutions, steady background illumination decreased flash sensitivity and accelerated response kinetics. In the presence of BAPTA, however, dim to moderate step intensities were less effective in initiating adaptation. The background intensity that reduced flash sensitivity by half was ~11 Rh\*/sec in control or 1 mM Ca vs 26 Rh\*/sec in BAPTA; the intensity that reduced sensitivity to 1/4 was the same in all solutions. These results suggest that the [Ca] of the dialysis solution has a greater effect on the characteristics of the flash response than on the properties of light adaptation. This may indicate that the transduction machinery is more sensitive to transient changes in Ca<sub>in</sub> than to steady state Ca<sub>in</sub>.

**T-Pos334 ION CHANNELS IN LIGHT-ADAPTED TIGER SALAMANDER CONE PHOTORECEPTORS.** Steven A. Barnes & Bertil Hille. Physiology & Biophysics, Univ. of Washington School of Medicine, Seattle, WA 98195.

Once light is transduced into photocurrent at the outer segment, the voltage response of rods and cones is shaped by voltage- and Ca-sensitive channels. Five channel types have been described in rods (Bader et al., 1982, *J. Physiol.* 331) but cone channels have remained largely uncharacterized with the exception of a hyperpolarization-activated cation channel similar to I<sub>h</sub> in rods (Attwell et al., 1982, *J. Physiol.* 328) and GABA<sub>A</sub> and glutamate-sensitive channels (Tachibana & Kaneko, 1987, *ARVO Abstr.*; Kaneko & Tachibana, 1984, *PNAS* 81). Here in enzymatically-isolated, light-adapted cones voltage-clamped with the whole-cell tight-seal technique, we characterize the light insensitive currents, including I<sub>h</sub>, activated by hyperpolarization beyond -50 mV (τ = 520 msec at -60 mV, 24°C), an L-type Ca current activated positive to -40 mV, and Ca-sensitive K and Cl currents. Both Ca-sensitive channel types showed complex activation and deactivation kinetics which were sensitive to the concentration of EGTA or BAPTA in the pipette. We saw no voltage-sensitive Na channel.

Since cones receive inhibitory feedback we looked for responses to a variety of neurotransmitter candidates. 100 μM GABA elicited currents reversing at E<sub>Cl</sub> and 100 μM glutamate elicited currents reversing near 0 mV. With 100 μM GTP and leupeptin in the pipet neither adenosine, adrenalin, ACh, dopamine, GABA, nor glutamate affected I<sub>h</sub>. However, in 2 of 8 cells 100 μM GABA and in 2 of 6 cells 100 μM adenosine caused a reversible, near total reduction of the Ca-sensitive Cl current. This current, often stable for up to 1 hr, also vanished within 2 min when 100 μM GTP<sub>γ</sub>S was included in the pipet solution. Supported by NIH grant NS08174 and NRSA fellowship NS07097.

**T-Pos335 VOLTAGE-DEPENDENCY OF GATING OF CYCLIC GMP-ACTIVATED ION CHANNELS IN BOVINE ROD OUTER SEGMENTS AND BLOCK BY L-CIS DILTIAZEM.** Fred N. Quandt, Grant D. Nicol<sup>+</sup>, and Paul P. M. Schnetkamp. Lions Sight Centre, University of Calgary, Fac. of Med., Calgary, Alberta, Canada T2N 4N1; and <sup>+</sup>Lab. Molec. Biol. Univ. Wisconsin, Madison, WI 53706.

The electrical properties of cGMP activated channels found in bovine rod outer segments were examined using patch clamp techniques applied to membranes excised in the inside-out configuration. Intact rod outer segments were purified from bovine retinas by sucrose-ficoll gradient centrifugation. Symmetric 150 mM NaCl solutions, free of divalent cations were utilized. The current-voltage curve in the presence of 30 μM cGMP showed outward rectification at potentials positive to +10 mV. Current at +50 mV (0.09 nA) was typically twice the amplitude of that at -50 mV. The rectification appeared to be due to an increase in the opening rate with depolarization. First, the outward current increased following a voltage jump from -60 to +60 mV with a time constant of 7 msec in the presence 60 μM cGMP. The time constant decreased as the concentration of cGMP was increased. Second, the extent of outward rectification was also reduced as the concentration of cGMP was increased. Third, the single channel conductance was independent of the membrane potential. The conductance of a single channel, measured in the presence of 1 μM cGMP, was 6 pS. Block of cGMP-activated channels by 10 μM diltiazem was also found to be voltage and time dependent. Block increased as the membrane was depolarized since the current-voltage curve became inward rectifying in the presence of the drug. The time constant for the onset of block was 12 msec at +60 mV and increased at less depolarized potentials. Supported by the MRC (Canada).

**T-Pos336** TETRODOTOXIN MODIFIES THE RESPONSES OF DRONE PHOTORECEPTORS TO SMALL DECREMENTS IN LIGHT INTENSITY. Jonathan A. Coles and Gisela Schneider-Picard, Geneva University, Département d'Oto-neuro-ophtalmologie, Laboratoire d'Ophtalmologie expérimentale, 22 rue Alcide-Jentzer, CH-1211 Genève 4, Switzerland.

Photoreceptor cells of the honeybee drone have a TTX-sensitive, voltage-dependent Na conductance (Baumann (1968) *J. Gen. Physiol.* 52: 855). But the cells do not normally produce spikes in response to moderate (less than twofold) changes in light intensity. Does this Na conductance have a function? We measured intracellular potentials with respect to the bath in photoreceptors in superfused slices of drone retina. To mimic a physiological stimulus, we applied steady background lights that produced steady (but noisy) depolarizations of 5-22 mV and presented 9% decrements lasting 100 ms that produced mean responses of -0.5 to -1 mV. Application of tetrodotoxin ( $10^{-7}$  -  $10^{-6}$  M) reduces the voltage noise during steady illumination (Ferraro et al. (1983) *Biophys. Struct. Mech.* 10: 129). We report that it also reduced the rate of change of voltage at the onset of the response to the decrement, and in some cases, the amplitude. Light opens a class of Na channels of no known sensitivity to TTX. Following the idea of Bass and Moore (1970, *Biophys. J.* 10: 1) we suggest that local current flow in a restricted extracellular space near these channels can cause local changes in transmembrane potential large enough to modulate the TTX-sensitive, voltage-dependent channels.

JAC has a Career Development Award from the Cloëtta Foundation. Supported by USPHS EY3504 and SNSF 3.066.

**T-Pos337** DIFFERENTIAL SCANNING DENSITY AND COMPRESSIBILITY MEASUREMENTS OF THE THERMAL DENATURATION OF LYSOZYME AND DNA. Don Eden, Ling X. Shen and Yun-Xing Wang, Dept. of Chemistry and Biochemistry, San Francisco State Univ., San Francisco, CA 94132.

We have developed a temperature scanning instrument to study structural changes in biopolymers. We measured the density and sound velocity of dilute solutions and from these quantities we calculated the adiabatic compressibility of the solution using the Laplace equation. Experiments with lysozyme (<5mg/mL) in a pH 2.0 glycine buffer have been performed over a temperature range of 15 to 73 C. The apparent specific volume of lysozyme increases by .018 cm<sup>3</sup>/gm in roughly a linear fashion over this temperature range. The thermal expansion coefficient, which is 2.8x10<sup>-4</sup>cm<sup>3</sup>/gm K below the transition at 50 C, increases by 20% above it. The overall increase in specific volume is in contradiction with the results of Velicelebi and Sturtevant (*Biochemistry* **18**, 1180 (1979)) in the same buffer. The partial specific compressibility of lysozyme, which is in good agreement with previous measurements at 25 C, also increases with increasing temperature. However, there is no pronounced change at the denaturation temperature. A correlation between the specific compressibility and volume that had been observed previously in a variety of protein solutions is observed in our samples. Measurements have also been performed on nucleosomal and sonicated DNA between 25 and 80 C in neutral pH 1mM NaPi buffers for concentrations < 3 mg/mL. In accord with the work of Chapman and Sturtevant (*Biopolymers* **7**, 527 (1969)), the specific volume increases with temperature. However, we observe a distinct decrease in the thermal expansion coefficient near T<sub>m</sub> and a subsequent increase to approximately the value before the transition. The apparent specific compressibility of the DNA has a weak, positive temperature dependence below T<sub>m</sub>, but increases rapidly at temperatures starting just below it.

**T-Pos338** USE OF RHODAMINE 123 AS A PROBE OF CELL VIABILITY IN *IN VITRO* TOXICOLOGICAL STUDIES. Robert M. Lachowicz\*, Robert G. Van Buskirk\*, Maria J. Perotto\* and James A. Dix\*, Departments of \*Chemistry and \*Biology, State University of New York, Binghamton, NY 13901

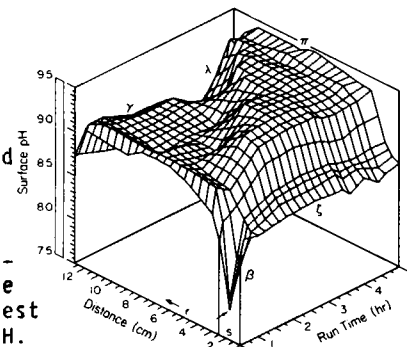
Rhodamine 123 is a fluorescent dye that is taken up by mitochondria of viable cells in a variety of cell types. Disruption of cellular mitochondrial function results in dissipation of rhodamine fluorescence from mitochondria. We have evaluated the use of rhodamine as a probe for the toxic effects of mercury on the Madin-Darby Canine Kidney (MDCK) cell line. Cells were grown to 50% confluency on plastic cell culture dishes in Gey's buffer and loaded by incubation with 10 ug/ml rhodamine. No toxic effects of rhodamine were seen by morphology as visualized by phase contrast microscopy. Treatment of MDCK cells with the nephrotoxin, mercuric chloride, at 10 μM resulted in a time-dependent loss of localized rhodamine fluorescence (half-time, 40 min); the fluorescence from control cells was unchanged. When MDCK cells were grown on Millipore CM filter supports, they exhibited a phenotype more similar to epithelial cells than MDCK cells grown on plastic culture dishes. Labelling of cells grown on CM filter supports with rhodamine resulted in long-term stability of rhodamine uptake, and treatment of these cells with mercuric chloride gave results similar to those obtained with cells grown on plastic. Our results demonstrate the potential of cell culture on Millipore CM membranes coupled with rhodamine fluorescence as a reliable assay for both short-term and long-term toxicological effects. Supported by the American Heart Association, Upstate New York Affiliate, and Millipore Corporation.

**T-Pos339** ZERO-LENGTH CROSSLINKING PROCEDURE WITH THE USE OF ACTIVE ESTERS. Z. Grabarek and J. Gergely, Dept. of Muscle Res., Boston Biomed. Research Inst.; Depts. of Neurology, and Biol. Chem. and Mol. Pharmacol., Harvard Medical School, and Dept. of Neurol., Mass. General Hosp., Boston MA

In order to study protein-protein interactions in a multicomponent system such as the regulated thin filament of muscle we have employed a two-step crosslinking procedure involving formation of an active ester. One component of a complex is incubated with 1-ethyl-3-(3-(dimethyl-amino)propyl)-carbodiimide (EDC) in the presence of N-hydroxysuccinimide (NHS) (15 min, 22°C, 2mM EDC, 5mM NHS, pH 6.0). The reaction is stopped by addition of β-mercaptoethanol and the other components of the complex are added. The crosslinking occurs during a 1-2 hour incubation at 22°C. In the absence of an amino group the N-succinimidyl derivative hydrolyzes and the COOH groups are recovered. The extent of modification with NHS can be monitored by following the increase in absorbance at 260 nm upon fast removal of the excess of the reagents. When troponin C was activated with EDC-NHS under the above conditions up to three NHS groups were incorporated per molecule and the hydrolysis proceeded with an apparent first order rate constant k=0.015 min<sup>-1</sup>. The decrease of the initially high yield of crosslinking with troponin T or troponin I paralleled the decomposition of the NHS-derivative. Our method has several advantages over a one step procedure: i) since only one component of the complex is activated our method eliminates complications arising from crosslinking between several proteins of a multicomponent complex; ii) it enables crosslink formation under various conditions including the presence of DTT and EDTA; iii) can provide information about distribution of charged groups at the interaction interface. (Supported by grants from NIH: HL-05949, HL-07266, and MDA)

**T-Pos340** PROTEIN SIEVING ON SDS-PAGE: EVIDENCE THAT THE APPARENT SDS-PROTEIN MOLECULAR SIZE VARIES WITH pH. Gary G. Giulian and James M. Graham, Department of Physiology, University of Wisconsin - Madison, Madison, WI 53706.

Under standard SDS conditions it is assumed that relative protein sieving is primarily a function of %T. As one decreases the random mesh network (pore size) of acrylamide polymer by increasing the amount of acrylamide monomer (%T), the relative migration rate ( $R_f$ ) of a protein will decrease. This phenomenon is demonstrated in the Ferguson relationship, plotted as %T vs.  $R_f$ , with the slope of the line ( $-K_r$ ) proportional to the "shape" of the protein molecule. Under the conditions of SDS-PAGE, most proteins assume a uniform charge density, migrating only on the basis of unfolded or rigid rod size proportional to log molecular weight. We have measured the pH on gels and assembled composite surface pH profiles (see Figure) where  $\beta$ ,  $\gamma$ ,  $\lambda$ ,  $\pi$  and  $\zeta$  refer to the Jovin (Biochemistry 12:871, 1973) multiphasic buffer theory and  $r, s$ ; the resolving and stacking gel regions. There is a complex profile of pH during a gel run with proteins sieving along the the " $\pi$  plateau". When one varies pH in the  $\pi$  plateau region on SDS gels at constant %T it is possible to dramatically affect relative protein migration. Assuming there is a constant polymer "pore size" and a uniform SDS charge density then our results would suggest that SDS-protein molecular size is affected by pH. Supported by NIH.



**T-Pos341** ISOELECTRIC FOCUSING WITHOUT CARRIER AMPHOLYTES. A. D. Hausfeld, Dept. of Biochemistry, Mount Sinai School of Medicine, One Gustave L. Levy Place, New York, NY 10029.

Isoelectric focusing for preparative isolation of proteins would be more useful if pH gradients could be obtained without carrier ampholytes. For high resolution, these ampholytes must be an ill-defined and costly mixture of many species that are subsequently difficult to remove; proteins contaminated with ampholytes may be difficult to characterize further by methods such as amino acid sequencing, X-ray diffraction, and *in vivo* assays. Further, the carrier ampholyte gradient is unstable due to a well known cathode drift; this is troublesome in alkaline pH ranges precluding high resolution focusing of certain basic proteins. A method has been developed for providing a stable pH gradient with a  $\Delta$  pH of 0.2 to 0.7 in simple buffers. The gradient is set up in a flat bed of gel (Sephadex G-75) supported by a cation selective membrane; below the membrane is a buffer conduit of cross-section that varies positionally from cathode to anode. This configuration provides a gel bed of constant cross-section with a positionally varying electric field strength. A constraint is thus imposed on the buffer anions in the gel bed resulting in an anion concentration gradient, with no constraint on neutral or cation species. Hence, the anion gradient gives rise to a pH gradient through a Henderson-Hasselbach type of relation. Gradients of pH have been set up centered about pH 5.0, pH 7.5, and pH 9.0, with sodium acetate, Tris HCl, and sodium glycine buffers respectively. Protein focusing has been demonstrated with pea lectins, horse and sperm whale myoglobins, and ribonuclease in the above respective pH ranges.

**T-Pos342** ENZYME IMMUNOCHROMATOGRAPHY: A NOVEL NON-INSTRUMENTED METHOD TO QUANTITATE C-REACTIVE PROTEIN (CRP). Richard F. Parrish, Richard Rodgers and David J. Litman (Intr. by.. Thomas M. Li). SYVA COMPANY, PALO ALTO, CA 94303

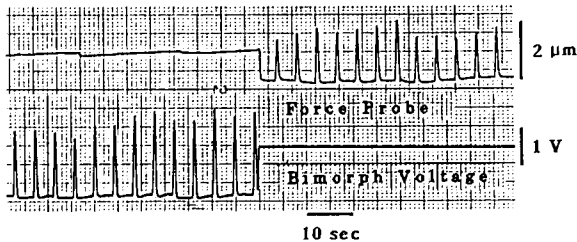
Enzyme immunoassay is an immunoassay technique that combines some of the properties of heterogeneous immunocapillary migration with homogeneous enzyme channelling immunoassay. A simple two step protocol is utilized. An aliquot of serum containing CRP is added to an enzyme reagent containing glucose oxidase and a horseradish peroxidase (HRP)-CRP conjugate. One end of a paper test strip to which anti-CRP immunoglobulin has been immobilized is placed into the test solution and the liquid components are drawn up the strip by capillary action. In the absence of free CRP, the HRP-CRP conjugate, which is present at low concentrations (as a tracer) is bound near the bottom of the test strip. When free CRP is present in the sample, competition for the available antibody binding sites allows the HRP-CRP conjugate to migrate further up the test strip. The test strip is then fully immersed in a developer solution that contains glucose and a chromogenic HRP substrate. Color develops only where the HRP-CRP conjugate has been bound by the antibody. The height of the colored area is proportional to the concentration of free CRP. Unlike other quantitative enzyme immunoassays that measure the rate of product formation or measure product after a fixed time interval, this protocol is essentially independent of enzymatic activity, temperature and length of incubation time. This technique has been used to quantitate CRP within the range of 0.6 to 20 mg/dl, with within run and between run CV's of 6.5% and 8.1% respectively. The assay can be performed with CRP present in buffer, serum, plasma and whole blood

**T-Pos343** APPARENT SEDIMENTATION AND DIFFUSION COEFFICIENTS: NOVEL EXPERIMENTAL INDICES OF MACROMOLECULAR ASSOCIATION AND HETEROGENEITY. Ronald C. Chatelier and Allen P. Minton, Laboratory of Biochemical Pharmacology, National Institute of Diabetes and Digestive and Kidney Diseases, National Institutes of Health, Bethesda, Maryland 20892

The apparent sedimentation and diffusion coefficients are defined as functions of the rate of migration and shape of the trailing boundary of macromolecular solute(s) sedimenting at high  $g$ -force in an analytical ultracentrifuge. These quantities are readily measured as functions of time, concentration, and angular velocity. For a single homogeneous solute sedimenting in dilute solution, the apparent values of the coefficients reduce to their true values. Three cases are treated by numerical solution of the Lamm equation: (1) a single macrosolute, (2) a mixture of macrosolutes, and (3) a self-associating macrosolute. The time dependence of the apparent coefficients may be used to rapidly distinguish case 1 from cases 2 and 3. The concentration dependence of the apparent coefficients may be used to distinguish case 3 from cases 1 and 2. Finally, when case 3 pertains, the dependence of the apparent coefficients upon angular velocity can, under favorable conditions, provide information about the rate constants for association and dissociation.

**T-Pos344** MEASUREMENTS OF ISOMETRIC FORCE OF SINGLE HEART CELLS USING A CLOSED LOOP SERVO-CONTROL SYSTEM. Ching-Hsing Luo and Leslie Tung, Department of Biomedical Engineering, Johns Hopkins University, Baltimore, MD 21205 (Intr. by P. Maloney)

We have previously measured the contractile force of single frog ventricular heart cells by monitoring the displacement of the tip of a glass fiber-optic, cantilever beam force probe (Tung, *Biophys J* 51:1111, 1987). By designing the compliance of the probe to be about  $15\text{--}20\ \mu\text{m}/\mu\text{N}$ , the cell length shortens by only 1-2% during the twitch contraction. We have now mounted the probe onto a linear positioning device (piezoelectric bimorph crystal) so that the tip displacement can be reduced further using a feedback control circuit (noise filter, frequency compensation and high gain amplifier). The effective stiffness of the probe has been increased about 60-fold, and the frequency response of the closed loop system is flat between 0.1 and 40 Hz. Shown below is a dual channel recording of probe position and compensation voltage applied to the bimorph. In open loop mode (right hand side) the bimorph voltage is constant, and the force probe moves with a displacement proportional to force. In closed loop mode (left hand side) the force probe is held at constant position (for frequencies greater than 0.1 Hz), and the bimorph voltage is now proportional to force. The shape of the twitch is unchanged between modes, suggesting that the open loop mode is adequate to measure isometric force. The closed loop mode, however, can also be used for control of cell length.



**T-Pos345** THE DISTRIBUTION OF FLOURESCENT LABELED MYOSIN LIGHT CHAIN IN CULTURED NEONATAL RAT HEART CELLS AS SHOWN BY CONFOCAL TANDEM SCANNING LIGHT MICROSCOPY AND THREE DIMENSIONAL RECONSTRUCTION TECHNIQUES. H.K. Hagler, P. Dunnmon, R.R. Reynolds and K. Chien, The Departments of Pathology and Internal Medicine, The University of Texas Health Science Center at Dallas. (Intr. by L.M. Buja)

Cultured neonatal rat myocardial cells develop organized sarcomeres in a time dependent manner. The present study was designed to examine the time course of the assembly of the contractile elements by indirect immunofluorescence with myosin light chain antisera. After plating for 24 hours, myocardial cells were fixed and stained at 6, 12, 36, and 60 hours and the structural reorganization of the cells was examined in a Tracor-Northern Tandem Scanning Microscope with a 490 nm bandpass excitation filter and a mercury illuminator. An intensified video camera was used to collect the fluorescent images produced with a 530 nm emission filter. A T-N 8500 image analyzer was used to frame average images of optical sections taken through the Z axis of the cells and three dimensional images were reconstructed using analygraphs or stereo viewing of the primary stereo pairs generated by the system. At 6 hours, the contractile elements of the isolated cells were disorganized and displayed random orientation within the myocytes. After 12 hours in culture, there were occasional areas of the cells which developed characteristic striations of organized sarcomeres. The percentage of cells with organized contractile elements continued to increase until all cells displayed sarcomeric units at 60 hours. This study documents the utility of this three dimensional reconstruction technique to examine the assembly of myosin into organized contractile units in cultured myocardial cells.

**T-Pos346** ACOUSTIC MICROSCOPY OF NEUROBLASTOMA CELLS ADHERING TO SILICON SUBSTRATA

M. Grattarola, M. Tedesco, A. Cambiaso, F. Conzi, G. Cerofolini(\*), L. Meda(\*)

Biophysical and Electronic Engineering Department, Via all'Opera Pia 11a 16145 Genoa Italy

(\*) SGS Microelettronica SpA, Agrate, Italy

The quite new technique of reflection scanning acoustic microscopy is utilized for viewing cultured living cells growing on silicon wafers.

Neuroblastoma cells are let to grow on silicon wafers covered with  $\text{Si}_3\text{N}_4$ . An ELSAM (Leitz) acoustic microscope, connected with an AT personal computer (IBM), is used. The cells are imaged by means of ultrasonic waves in the range 0.8 - 2 GHz, with a resulting space resolution comparable with the optical one. The culture medium is used as a coupling medium between cell and acoustic lens. The coupling medium can be warmed up to 37°C. Under these experimental conditions the cells can be viewed for several minutes in a quasi-physiological state. The identification of adhesion regions in moving cells is discussed. Rings of alternate intensity in the cell images, originated from acoustic interference fringes, are utilized for gaining information about cell morphology.

This work is a part of a long-range project, dealing with the functional coupling of living cells with integrated circuits (Progetto Finalizzato CNR- MADESS- contract # 86. 029601/115. 11820)

**T-Pos347** ANALYSIS OF PHOTOACOUSTIC WAVEFORMS USING FLUORESCENT DECAY ANALYSIS TECHNIQUES.

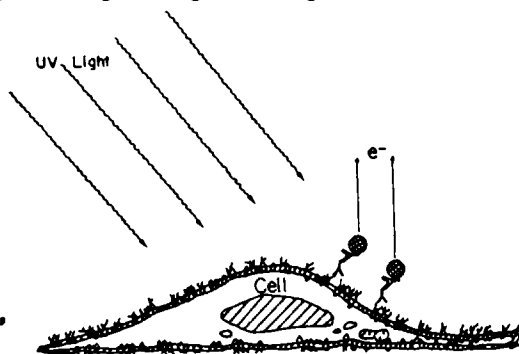
Jeanne E. Rudzki, Louis J. Libertini, and Enoch W. Small, Department of Biochemistry and Biophysics, Oregon State University, Corvallis, Oregon 97331.

Time-resolved photoacoustic calorimetry measures the heat released by photoexcited molecules as they relax back to the ground state. The technique is thus complementary to fluorescence spectroscopy in that it provides information on an alternate, non-luminescent channel for the decay of excited states. In the pulsed-laser, time-resolved experiment utilizing a piezo-electric transducer detector, the photo-induced enthalpic changes of a system, as well as the kinetics of those changes, may be determined simultaneously [Rudzki *et al.* (1985) *J. Am. Chem. Soc.* 107, 7849-7854]. To maximize the information extractable from photoacoustic waveforms, it is necessary to develop deconvolution and data analysis methods analogous to those used in time-domain, fluorescence decay spectroscopy. We have explored the use of two techniques, iterative non-linear least squares and the method of moments, to analyze computer-simulated photoacoustic waveforms. As with fluorescence data analysis, the photoacoustic data require the deconvolution of the instrumental impulse response function from the decay functions of interest to yield amplitude and lifetime values. Some important differences between fluorescence decay and photoacoustic waveform analysis exist, however. For example, the pre-exponential amplitude factors recovered from photoacoustic waveforms give enthalpic information, and a very wide range of lifetime values (from nsec to msec) must be recoverable by photoacoustic waveform analysis. The adaptability of fluorescence decay analysis methods to photoacoustic data will be explored.

Supported by NIH grants GM 10889 (JER), GM 25663 (EWS), and NSF grant DMB-8707705 (JER).

**T-Pos348** PROGRESS IN PHOTOELECTRON IMAGING. O.H. Griffith, G.B. Birrell, D.L. Habliston and K.K. Hedberg. Institute of Molecular Biology, University of Oregon, Eugene, Oregon 97403.

The photoelectric effect explained by Einstein in 1905 can be utilized to obtain high resolution images of cells (1). This approach, photoelectron microscopy (PEM), is the electron optical analog of fluorescence microscopy. Specimens subjected to uv light photoemit electrons (see diagram). These low energy electrons are accelerated and then imaged by an optics system resembling that of a transmission electron microscope. Recent advances in instrumentation and methodology have made this approach practical in biophysics and cell biology. Images to be illustrated include cytoskeletal elements of cultured cells, cell surfaces and DNA. Theory predicts a resolution of 5nm using present optics, and the possibility of attaining 1nm-2nm with corrected optics. Advantages include high sensitivity to topographical detail, a new source of contrast, surface selectivity and less sample damage. Supported by PHS grant no. CA 11695.



1. O.H. Griffith and G.F. Rempfer, *Adv. in Optical and Elect. Micros.* 10, 269.

**T-Pos349** IMAGING BIOPOLYMERS USING SCANNING TUNNELING MICROSCOPY IN SOLUTION. L.A. Nagahara, S.M. Lindsay, B.J. Barris, T.G. Thundat and U. Knipping. Department of Physics, Arizona State University, Tempe, AZ 85287.

We describe a technique for obtaining images of biopolymers on various metal surfaces submerged in buffer solutions using a scanning tunneling microscope (STM). We appear to be able to deposit and strip the biopolymers from the metal surface by electroplating. Current-distance ( $I_t$ -s) measurements indicate that elastic deformation of the adsorbate contributes to contrast in the STM image. Images of DNA and cytochrome-c adsorbate patches have been obtained. The DNA patches sometimes show liquid-crystalline order.

**T-Pos350** SCANNING TUNNELING MICROSCOPY (STM) FOR BIOMOLECULAR IMAGING AND INTERACTIONS, M Voelker, D He, E Dereniak, Optical Sciences Ctr, S Bell, Lunar Planetary Lab, R McCuskey, Dept. Anatomy, C Schneiker, S Hameroff, Dept. Anesthesiology, Univ. of Ariz., Tucson, Arizona 85724

Scanning tunneling microscopy (STM) uses computer controlled piezoceramic actuators to scan an atomically sharp needle tip over a surface. Voltage applied between tip and conductive surface yields tunneling current when tip to substrate distance is several angstroms. A current-sensing feedback loop enables scanning at constant distance, current, or voltage, leading to mapping of surface topography with atomic resolution. STM can operate in ionic solution, image atomic surface lattices, monitor dynamics, do atomic spectroscopy, etching, and single atom deposition. Biological applications of STM have been hampered by non-conductivity of biomolecules and poor localization and stability of biomolecular targets by "near-sighted" STM. Nevertheless, STM imaging of biomolecules has been reported by "shadowing" with conductive metals (Travaglini, Gross, and Rohrer, 1987) and atomic force microscopy (AFM) in which van der Waals forces move a lever mounted on, and whose motion is detected by, an STM tip. Because STM has such profound potential benefits for biomolecular studies (i.e. nondestructive imaging of receptor conformational dynamics), we have built an STM system with specific biomolecular applicability and initiated studies on a highly conductive, fibrous biopolymer: collagen. Our STM system is mountable on an inverted optical microscope for coarse approach and imaging and is adaptable for AFM. A wide scanning mode enables STM imaging within an area of one square micron selected down to an area of 100 square nanometers. Electronic design enables fast framing (approximately 10 frames per second) in real time. Fast Fourier transforms using coherent optical data processing lead to optimal imaging. STM observations of collagen will be presented.

**T-Pos351** CHARACTERIZATION OF HUMAN OCULAR LENS MECHANICAL PROPERTIES. Christopher A. Cook\*, Jane F. Koretz\*, \*Center for Biophysics and Biology Department, #Physics Department, Rensselaer Polytechnic Institute, Troy, NY 12180-3590. (Intr. by R. H. Parsons).

The mechanical properties of the human ocular lens are characterized using a novel modeling technique and elastometer. The elastometer incorporates the lens directly to provide the restoring force for driven, harmonic oscillations; the magnitudes and relative phase of the oscillatory amplitude and force displaced through the lens give a viscoelastic (complex) spring constant. Similar treatment of standard and lenticular shapes of a well characterized material (e.g., polyacrylamide) enables formation of an analogy with which the nonlinear deformation of the lens is corrected. With consideration of dynamical shape changes (i.e., contact area, volume, etc.), accurate values for the Young's modulus and Poisson's ratio are obtained as a function of frequency (rate of deformation) from the corrected constant. Variations in these parameters with frequency are indications of the relative contributions of lens structures to the accommodative process. Current data indicate a modulus in the range of 4 to 8 psi for lens tissues. These structures appear to exhibit a viscoelastic nature. An asymptotic increase of measured nucleus moduli with frequency has been noted. This increase also appears superposed on curves of  $Y$  vs. frequency for the entire lens. Increase in nucleus density with age conjoined with the apparent superpositioning of nucleus mechanical properties on the lens structure may offer an explanation of accommodative loss with age. These data then form the basis for the modelling of accommodation and accommodative loss. Supported by NIH grants EY02195 and EY04146.

**T-Pos352** RHEOLOGY OF ATELLOCOLLAGEN DISPERSIONS. V. Glushko and C. Karp, Yardley, PA 19067.

Dispersions consisting of intact or reassociated type I collagen fibrils are utilized in a variety of biomedical applications. In addition to being used directly as gels or coatings for prosthetic implants, a broad range of bioactive factors can be incorporated into the fibrils, which then function as a delivery vehicle. The biophysical behavior of dispersed native collagen fibrils in suspension is complex; furthermore it can be affected by additives and the treatments to which the collagen is exposed to. Type I atellocollagen purified from bovine Achilles tendon (P1531) was reconstituted in 15 mM phosphate buffer with the aid of a PT45 Polytron homogenizer. The dispersions were equilibrated for at least 24 hr prior to collecting any measurements with a Brookfield DV-II Digital Viscometer fitted with LV Spindles. The dispersions were stable except at or near the isoelectric point, where the collagen fibrils aggregated into loose flocculants that interfered with viscometric measurements. In the pH range of 5.5 to 8.5, collagen dispersions exhibited non-Newtonian, pseudoplastic, thixotropic behavior. At 20 degrees C, 6.5 pH, a 3.33 mg/ml dispersion dropped in viscosity from 35.4 P to 50 cP as the shear rate was increased from 0.64/s to 12.7/s; this effect was less pronounced at lower concentrations. At the higher shear rates, the viscosity decayed by 10 to 20% with time, requiring from 2 to 15 minutes to come to equilibrium. Glycerol and PEG tended to increase viscosity whereas SDS and related surface active agents significantly lowered the apparent viscosity. By proper adjustment of collagen content, temperature, pH, ionic strength, and by using certain additives, the rheological properties of atellocollagen dispersions can be optimized for use as biocompatible coatings, drug delivery vehicles and soft tissue analogs.

**T-Pos353** IMPROVED COLLECTION, ISOLATION, AND ANALYSIS OF HUMAN URINARY PROTEINS, P. Baxter-Rahmoeller<sup>1</sup>, S. Smith<sup>2</sup>, M. Molinaro<sup>1</sup>, and H. Mizukami<sup>1</sup>. <sup>1</sup>Division of Regulatory Biology and Biophysics, Department of Biological Sciences, Wayne State University, Detroit, Michigan, 48202 and <sup>2</sup>Enzymes of America, Inc., Utica, Michigan, 48087

It is known that there are approximately 40,000 different proteins in human urine, but the concentration of each protein is usually very low. Thus, collecting and purifying any specific urinary protein in large quantities has been difficult. We present a new method to simplify and maximize recovery of these trace proteins.

In the original patented method of Enzymes of America, the urinary proteins were allowed to bind to a cation exchange resin (IRC-50, pH 6.0), placed inside a portable toilet. The resin was washed with high salt and basic proteins were extracted. Our new method places an anion exchange resin (IRA-400, pH 6.0) on top of the cation resin to capture the acidic proteins ("double deck"). The double deck system was tested in our laboratory by applying a known volume of urine to an IRA-400 column, flowing directly into an IRC-50, column of equal bed volumes. The columns were washed with 10mM NaCl and then independently eluted with high salt buffers. The eluents were analyzed by HPLC with a DEAE column. The protein concentrations were determined by the BCA protein assay (Pierce). More than 60% of the proteins were bound to the IRA-400 resin and analysis by HPLC revealed that albumin was the major constituent. The cationic resin bound about 10% of the proteins and showed nine major peaks in the HPLC. The remaining proteins were lost. For example, the urinary urokinase concentration ranges from 5-9 IU/ml. We were able to extract more than 50% of the enzyme. (supported by IPPRI grant for W.S.U. and Enzymes of America, Inc.)

**T-Pos354** TRANSFER-FUNCTION CORRECTION OF THERMOPILE OUTPUT USING AN IBM AT COMPUTER AND AN IN-LINE MICROWATT POWER METER. LA Muller, RK Wright, GP Gianetti, TP Haviland and NR Alpert. Univ of Vermont, Burlington, Vermont 05405

Thermopiles offer a convenient means of measuring heat output from active tissue on a millisecond time-scale. Use of a small digital computer to correct the thermopile output for conduction delay and heat loss (deconvolution) is greatly hindered because the long-lasting (minutes) nature of the thermopile output signal resulting from heat stored in the tissue and thermopile results in memory overload when ms sampling intervals are used. Rather than incurring the band-width reducing effect of record truncation with a "window-filter" we have developed an alternative solution of "periodizing" the data so that its total duration need be no longer than the duration of exo/endo-thermic activity in the tissue (e.g. 1-5 sec). Either repetitive activation of the tissue or artificial periodization of the single activation response by additively accumulating its entire duration into a single 1-5 second "period" is used. Deconvolution is achieved by the transfer function method using standard, fast Fourier transform computational methods. Further, we have developed an apparatus and method of on-line absolute calibration of the corrected output which eliminates the need to make any prior measurements of the thermal or electrical properties of the tissue, adhering bathing solution, or thermopile/amplifier system. Calibration is achieved during the experimental run by recording the output in response to artificial heating of the tissue with a burst (3 ms) of 1 MHz sinewave current while simultaneously measuring the instantaneous power dissipated using an in-line, analog microwattimeter. Corrected, 5 sec long records with approximately 200 Hz band width are obtained using an IBM-AT computer. Supported by PHS P01-HL28001-06/P1.

**T-Pos355** ALLOMETRIC DESCRIPTION OF HEART WEIGHT AFTER MAJOR GAIN OR LOSS FROM "IDEAL" BODY WEIGHT. Richard P. Spencer. Department of Nuclear Medicine, University of Connecticut Health Center, Farmington, CT 06032

After significant gain or loss of body weight from "ideal," we can inquire as to cardiac weight and any accompanying functional alterations. There are now data in the literature that permit an analysis that provides a partial answer. Gottdiener and coworkers (*Circulation* 58:425, 1978) gave information on both body weight and left heart ventricular mass (estimated ultrasonographically) in 11 patients with anorexia nervosa and a mean body weight of 30 kg. In adults, the allometric equation gives heart weight (H) as a function of body weight (B):  $H = a \cdot B^{(exp P)}$ . Using the accepted P value of 0.95, and the reported left ventricular mass of 93.9 grams, the equation is:  $H = (3.71)B^{.95}$ . After body weight had been regained to 39.5 kg (32% above the low point), the allometric prediction of left ventricular weight was 122.1 grams. The value found by Gottdiener et al was 120.6 grams. The allometric relationship appears to hold during weight regain. At the other extreme, we examine cardiac weight in the morbidly obese. Using autopsy data of Warnes et al (*Am. J. Cardiol.* 54:1087, 1984), the allometric equation did not produce a close description of cardiac weight in morbidly obese men ( $r=0.51$ ) or women ( $r=0.48$ ). We define excess cardiac weight (E) as the difference between the actual (A) and the allometric prediction (H):  $E = A - H$ . In the 10 morbidly obese patients with heart and body weight data available, 8 out of 10 had actual weight exceed that predicted (by from 11 to 524 grams). The difference was likely due to adipose tissue. In 2 cases, heart weight was less than that expected allometrically, & 1 died of congestive failure. Thus, there may be prognostic significance. (Supported by USPHS CA 17802 from the National Cancer Institute).

**T-Pos356** PROPERTIES OF THE STEADY-STATE MEMBRANE POTENTIAL. David R.L. Scriven and Aubrey Blumsohn, Physiology Dept., Witwatersrand Univ. Med. Sch., Johannesburg, South Africa.

When a cell is at steady-state, the transmembrane flux of water, charge and each ionic species is zero. Analytic equations describing the steady-state membrane potential (1,2) cannot legitimately be used to predict the response of the steady-state to a perturbation since the internal ion concentrations are treated as independent variables. We have used a cell model to investigate the effect of changing the Na-K pump density on the steady-state of an excitable cell. The model incorporates voltage-dependent Na and K fluxes, a concentration dependent Na-K pump, a passive Cl current, and a Na-K-Cl coport. The transmembrane ionic fluxes, water flux and membrane potential are represented by a series of non-linear equations. All of the system variables (internal ion concentrations, cell volume and membrane potential) are interdependent. The steady-state solution was determined by solving the system equations numerically for the five unknowns ( $N_{a_i}$ ,  $K_i$ ,  $Cl_i$ ,  $E_m$ , Volume).

With physiological values for the system parameters, we have found that the steady-state potential (SSP) is only weakly dependent on the pump density, with a variation of less than a millivolt for a ten-fold change in pump density. Moreover, the SSP may exhibit a paradoxical depolarization when the pump density is increased. The behavior of the SSP may therefore be counter-intuitive.

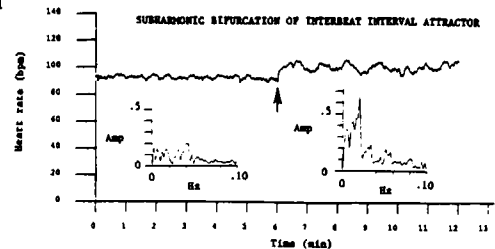
1. Mullins L. & Noda K., *J. Gen. Physiol.*, 47: 117-132, 1963.
2. Jacob R. et al., *J. Gen. Physiol.*, 83: 47-56, 1984.

**T-Pos357** DESCRIPTION OF A NONEQUILIBRIUM BINDING SYSTEM AND METHODS FOR ANALYSIS OF BINDING DATA Jeffrey P. Bond and Angelo C. Notides (Intr. by S. Rackovsky), Dept. of Biophysics, University of Rochester School of Medicine and Dentistry, Rochester, NY 14642

In living systems, ligands bind to proteins which are continuously synthesized and degraded. These systems may be described by equilibrium binding models only under special conditions. Since these conditions are not satisfied for all systems (e.g. steroid hormone-receptor systems), we developed an elementary model for the binding of a ligand to identical and independent binding sites when protein synthesis and degradation occur. We found equations for the bound ligand concentration and for the total protein concentration as a function of the free ligand concentration and time. We found an approximation to the total protein concentration which permits an accurate prediction of the response of the model system to changes in the free ligand concentration using parameters easily determined experimentally. The steady state results show that the data can be analyzed using methods analogous to the methods used for analyzing equilibrium binding data, and we describe how to interpret the binding data. These results show that experiments can be performed which determine whether the elementary model is applicable, and if so, determine the binding parameters. When complexities exist, the results permit decisions regarding the types of additional components and interactions that exist.

**T-Pos358** NONLINEAR DYNAMICS, PERIODIC ATTRACTORS, AND BIFURCATION BEHAVIOR IN SUDDEN CARDIAC DEATH SYNDROMES. A.L. Goldberger, D.R. Rigney, Department of Medicine, Beth Israel Hospital and Harvard Medical School, Boston, MA 02215

Healthy subjects in sinus rhythm show considerable beat-to-beat heartrate variability, represented by a broadband spectrum with a  $1/f$ -like distribution. We have proposed that fractal neurohumoral control mechanisms underly these physiologic fluctuations. We postulated that disruption of this nonlinear regulatory system in patients at high risk of sudden death would lead to a loss of normal heartrate variability, with bifurcations to periodic regimes in the interbeat interval phase space. We performed time series and Fourier analysis of sinus rhythm dynamics from the ambulatory ECG records of 16 patients with sustained ventricular tachyarrhythmias during the recording (Sudden Death Database) and from 14 patients with severe congestive heart failure (High Risk Database). 12 of 16 patients in the first group and all 14 patients in the second showed unusually narrowband spectra due to overall loss of heartrate variability or to low frequency (.01-.04 Hz) oscillations in sinus rate. These oscillations started and stopped abruptly. One example of a subharmonic bifurcation (Fig) was observed. We conclude that sudden cardiac death syndromes are associated with periodic interbeat interval dynamics and bifurcation behavior consistent with perturbations of the stable fractal control mechanisms regulating healthy heartrate dynamics.



**T-Pos359**

A DECONVOLUTION MODEL TO DESCRIBE HORMONE SECRETORY RATES

Susan G. Frasier, Johannes D. Veldhuis and Michael L. Johnson

Department of Pharmacology, School of Medicine, University of Virginia, Charlottesville, VA 22908

We propose a deconvolution model to describe endogenous hormone release *in vivo*. Measured hormone concentrations reflect a secretory input "cumulation" function combined with a metabolic clearance "elimination" mechanism. The cumulation function, representing a hormone secretory burst, can be described by a Gaussian distribution of instantaneous molecular secretory rates, which are centered with some finite and determinable standard deviation about a particular moment in time. The elimination mechanism is described by a mono- or biexponential clearance function. The resultant convolution integral is then solved by iterative nonlinear least-squares parameter estimation which utilizes the independent hormone concentration measurements with their concomitant experimental variances.

Time series experiments with luteinizing hormone, follicle-stimulating hormone, growth hormone, prolactin, thyrotroponin and adrenocorticotrophic hormone can all be described effectively by this deconvolution model. Therefore, we conclude that the observed fluctuating pattern of hormone concentration in the plasma can be accounted for by distinct, random bursts of hormone release, separated by intervals of inactivity.

**T-Pos360** MULTI-DIMENSIONAL NUMERICAL SOLUTIONS FOR ELECTROSTATIC INTERACTION OF CHARGED MOLECULES WITH LIPID MEMBRANES AND ION CHANNELS. J.E. Schnitzer and C.C. Lambrakis; Yale Univ. School of Medicine, Dept. of Cell Biol.; New Haven, Ct.

Recently, many attempts have been made to realistically model the interaction of charged molecules with lipid membranes and/or ion channels. We have first started with a continuum approach in 1-dimension utilizing a modified Poisson-Boltzmann equation describing the charge-potential relation throughout a lipid bilayer membrane. This nonlinear P-B equation is solved numerically via finite difference equations and includes hydration, ion-size, and ionogenic effects, continuous dielectric variation occurring within the polar region of the membrane, entropy-induced exclusion based on the specific atomic structure of the lipid, and a continuous smeared charge within the lipid polar region. This continuum analysis is extended further to 2-dimensions so that the electrostatic potential profile for ion channels with various charge and dielectric distributions within a variable pore diameter: Furthermore, exact numerical solutions were derived for the electrostatic potential profile when an ion of discrete size and charge is placed within the lipid membrane or within the ion channel. These numerical solutions converge so that additional electrostatic considerations such as polarization and dipole-interaction effects may be added easily. Numerical solutions for a combine continuum-discrete charge approach in 3-dimensions is currently being optimized. In addition, the electrostatic potential profiles will be used to derive position dependent energy profiles within the ion channel and membrane. After reaching a better understanding of the limitation of these different approaches by comparison, they need to be specifically applied to various ion channels where the necessary structural details are available for prediction of energy profiles and ultimately ion conductances.

**T-Pos361** SIMULATION OF KINETICALLY CONTROLLED ELUTION CHARACTERISTICS EXHIBITED BY MACROMOLECULAR INTERACTIONS DURING SIZE-EXCLUSION HPLC. F.J. Stevens, Division of Biological & Medical Research, Argonne National Laboratory, Argonne, IL 60439.

Size-exclusion chromatography is a convenient method to demonstrate interaction between macromolecules. Relative to a synthetic chromatogram constructed by the arithmetic summation of elution profiles exhibited by two molecular species chromatographed individually, the elution profile of the mixture will be shifted to earlier elution times as determined by the affinity and stoichiometry of interaction. We have previously developed an iterative computer simulation of small-zone size-exclusion interaction chromatography. As in other analyses of mass transport phenomena involving sedimentation, electrophoresis, or chromatography, the simulation assumed instantaneous equilibration. However, for contemporary HPLC technology with complete run times on the order of a few minutes, this assumption is not valid for interactions of moderate or high affinity. Therefore, the simulation has been modified to incorporate the determining aspects of forward and reverse rate constants on observed chromatographic behavior. The modification includes calculation of the time-dependent incomplete equilibration during each interaction cycle and determination of the appropriate constituent velocity distributions effected by partial intermixing of free and complexed pools. The constituent velocity distributions are based on stochastic representations of association and dissociation rate constants. The algorithm is programmed in vectorized Fortran and is executed on a Cray 2 (Livermore National Laboratory). (Work supported by the U.S. Dept. of Energy under contract W-31-109-ENG-38).

**T-Pos362** COMPARISON OF SYNCYTIAL RESPONSES IN 1, 2 AND 3 DIMENSIONAL NUMERICAL MODELS. N. G. Publicover, Department of Physiology, University of Nevada School of Medicine, Reno, Nevada 89557.

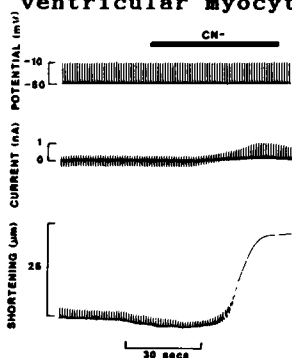
Finite-element techniques were used to develop a numerical model of the spread of current and generation of membrane potential in multi-dimensional syncytia. Electrical parameters were selected based on intracellular recordings from gastrointestinal smooth muscle. Voltage responses to steps of current injected into a single cell were simulated to characterize the passive electrical waveforms which govern conduction. In the first series of simulations, large arrays were utilized to exclude the effects of boundaries. As the number of dimensions increase: (i) the amplitudes of voltage responses decrease due to decreased input resistance; (ii) maximum, steady-state responses are reached in shorter times; and (iii) currents spread from the site of injection over shorter distances. In 1, 2 and 3 dimensional syncytia, the temporal waveform at the site of current injection is a function of the membrane time constant. In a second series of simulations, smaller arrays were utilized to include the effects of tissue boundaries. The input resistance, temporal waveform and spatial spread are unique functions of tissue geometry. A continuum of spatial and temporal waveforms are generated which are intermediate between the responses of large syncytia. Results of numerical simulations demonstrate the basic waveforms which govern conduction in 1, 2 and 3 dimensions. They provide an opportunity for the quantitative analysis of responses in multi-dimensional syncytial tissues. (Supported by NIH grant DK34406.)

**T-Pos363** ASSUMPTION OF ALTERED HYDRODYNAMICS QUANTITATIVELY EXPLAINS THE SIEVING OF SOLID SPHERES IN AGAROSE GELS. Gary A. Griess, Elena T. Moreno, Shirley J. Hayes and Philip Serwer. The U. of Texas Health Science Center, San Antonio, TX 78284-7760.

For electrophoresis of solid spheres in agarose gels, semilogarithmic plots of electrophoretic mobility ( $\mu$ ) as function of agarose percentage ( $A$ ) are linear (slope  $=-K_R$ ) at the lower  $A$  values, an observation explainable by the assumption that sieving is steric. However, as  $A$  increases the apparent  $K_R$  increases (convex curvature). This and other observations put stress on explanations based on the assumption that sieving is steric. Therefore, equations based on the assumption that sieving is hydrodynamic have been tested for accuracy in explaining the data. Assuming that particles migrate in cylindrical tubes of radius,  $P_E$ , equal to the average radius of a gel's pore, then from ref. 1:  $\mu = \mu_0' (1 - 2.104[R/P_E] + 2.09 [R/P_E]^3 - 0.95[R/P_E]^5)$ ;  $R$  is a particle's radius and  $\mu_0'$  is  $\mu$  extrapolated to an  $A$  of 0. For 13 nm  $< R < 150$  nm, values of  $P_E$  calculated from  $\mu/\mu_0'$  are independent of  $R \pm 5\%$ . The values of  $P_E$  determined are in reasonable agreement with values of  $P_E$  determined by assuming that  $P_E$  is the  $R$  of the largest particle that enters the gel during electrophoresis; these latter values of  $P_E$  have previously been obtained.<sup>2</sup> Thus, the assumption of hydrodynamic sieving provides a self-consistent explanation of  $\mu$  vs.  $A$  plots with convex curvature. To test the previously described<sup>3</sup> conclusion that borate ions present during gelation and electrophoresis increase the sieving (and, therefore, decrease the  $P_E$ ) of agarose gels, values of  $P_E$  in Tris-borate were compared to those in Tris-acetate buffers. This conclusion was confirmed. Supported by NIH (GM24365 and AI22568) and NSF (DMB-87-01379). 1. Bacon, L.R. (1936). *J. Franklin Inst.* **221**, 251-273. 2. Serwer, P. and Hayes, S.J. (1986). *Anal. Biochem.* **158**, 72-78. 3. Peats, S., Nochumson, S. and Kirkpatrick, F.H. (1986). *Biophys. J.* **49**, 91a (abstract).

**T-Pos364** A DECLINE IN ACTION POTENTIAL DURATION UNDERLIES DISAPPEARANCE OF THE TWITCH IN SINGLE RAT VENTRICULAR MYOCYTES EXPOSED TO METABOLIC BLOCKADE C.G. Nichols, G.L. Smith\* & W.J. Lederer. Department of Physiology, University of Maryland School of Medicine, Baltimore, MD 21201, U.S.A., and \*Department of Physiology, University College, Gower Street, London WC1E 6BT.

Using the whole cell clamp technique, we have observed a decline in action potential duration that paralleled a decline of the twitch in isolated rat ventricular myocytes exposed to 2 mM cyanide (CN) in the presence of 10 mM 2-deoxyglucose (DOG). The twitch always disappeared completely before a contracture developed ( $n=9$ ). Under voltage-clamp we observed an increase in  $K^+$  conductance ( $> 20 \times$  control) that occurred 1 - 2 minutes before contracture. Under these conditions we were not able to adequately control membrane potential. The increase in current was reduced by replacing  $K^+$  with 140 mM N-methyl glucammonium and including 2 mM tolbutamide in the patch pipette. Step depolarisation then elicited a twitch which was maintained on exposure to CN and DOG (Fig. 1) until a substantial contracture had developed ( $70 \pm 3\%$  of control when contracture shortening had reached 10% of maximal;  $n=8$ ). These results provide evidence that the abolition of the twitch on exposure to metabolic blockade results from a shortening of the action potential due to an increase in  $K^+$  conductance.



**T-Pos365** A FRACTAL VASCULAR NETWORK EXPLAINS REGIONAL FLOW HETEROGENEITY

J.H.G.M. van Beek, J.B. Bassingthwaite, and R.B. King. Center for Bioengineering, University of Washington, Seattle, WA 98195.

Regional myocardial blood flows range over six-fold in the normally functioning heart. In anesthetized sheep and rabbits and in awake baboons, the flow distributions have relative dispersions ( $RD = SD/mean$ ) that closely follow a fractal relationship with respect to the mass,  $m$ , grams, of the pieces into which the heart is divided:

$$RD(m) = RD(m=1) \cdot m^{1-D}$$

where the fractal dimension  $D$  is about 1.14, the coefficients of regression of approximately 0.99 in sheep and baboons, and 0.98 in rabbits. The values of  $RD(m=1)$  varied considerably from animal to animal; in the awake baboons the range was 0.15 to 0.30. The distributions were relatively stable over time. A possible explanation is that the vascular tree is described by a fractal recursion. A purely deterministic dichotomous branching with a specified asymmetry at the branch points fits the data. Alternatively, symmetrical branching with Gaussian variation in daughter radii provides a similarly good description. Neither recursion reduces to the equation above but both are good predictors of the data.

(Supported by NIH grants HL19139 and HL38736.)

**T-Pos366** HYDROGEN BOND DYNAMICS IN BIOLOGICAL INFORMATION PROCESSING. Michael Conrad, Departments of Computer Science and Biological Sciences, Wayne State University, Detroit, MI 48202

Electronic digital and analog computers use the flow of electrons to process information. In biological systems, by contrast, mobile hydrogen bonds (protons) are the main charge carriers. Free and bound water comprise a vast network of mobile hydrogen bonds, and this network interpenetrates with hydrogen bond chains associated with proteins and nucleic acids. Here we review a model of coherent hydrogen bond dynamics that allows for a highly dynamic, global form of biological information processing. The chief feature of the model (Conrad, M., *Biop. J.* 49, 274a, 1986 and *Biop. J.* 51, 94a, 1987) is that the effective mass of a small fraction of protons at the water-membrane interface is sufficiently reduced for degeneration (spreading out of the wave function) to occur. Bose-Einstein statistics can thus apply to proton pairs. Propagating electronic oscillations induced in the side groups of the membrane by the motion of degenerated protons in the adjacent layer of bound water are responsible for the pairing. The situation may be pictured as local pools of "supermobile" protons linked into a coherent global network by connecting channels. The rigid aspect of this network allows for lock-key type fitting to widely distributed patterns of signals impinging on the cell membrane, while its dynamic order allows for the coordination of cellular events, that are widely separated in space and time.

**T-Pos367** GRAND CANONICAL MONTE CARLO CALCULATIONS OF THERMODYNAMIC COEFFICIENTS AND RADIAL DISTRIBUTIONS OF COUNTERIONS FOR DNA OLIGOMER-SALT SOLUTIONS. M.C. Olmsted, C.F. Anderson and M.T. Record, Jr., Departments of Chemistry and Biochemistry, University of Wisconsin, Madison, WI 53706.

Monte Carlo (MC) simulations based on the grand canonical ensemble are being used to calculate thermodynamic coefficients and radial and axial small ion distributions for a cell model representation containing a NaDNA oligomer and NaCl. The model used in the majority of the simulations represents the oligomer as an impenetrable cylinder with 16 axial point charges uniformly spaced 1.7 Å apart. The small ions are modeled as hard spheres of 3 Å diameter. The preferential interaction coefficient,  $\Gamma$ , which may be interpreted in terms of the number of Na<sup>+</sup> ions thermodynamically bound per phosphate ( $1+2\Gamma$ ), has been calculated for a range of  $C_u$  between 0.73 and 1.70 mmol dm<sup>-3</sup> and a range of  $C_3$  between 1.0 and 13.45 mmol dm<sup>-3</sup>.  $\Gamma$  is found to be independent of  $a_3$ . The average  $\Gamma$  over the range of  $a_3$  investigated is  $-0.309 \pm 0.006$ , which corresponds to  $0.38 \pm 0.01$  Na<sup>+</sup> ions thermodynamically bound per phosphate. This value of  $\Gamma$  indicates that an oligomer of 16 phosphates is behaving thermodynamically in a manner that is intermediate between ideal and polyelectrolyte behavior.

The small ion distributions are computed for NaCl concentrations ranging from a 25 percent excess to a sixfold excess over DNA phosphates. The radial distributions are broken into four regions of four phosphates each, where the first region contains the four central phosphates, the second contains the two phosphates on either side of this region, and so on. These distributions reveal a dramatic end effect. Concentrations in the central region range from 2.3 to 2.7 times those in the end regions. The strong presence of an end effect again illustrates the nonpolyelectrolyte behavior of an oligomer of 16 phosphates.

**T-Pos368** NUMERICAL SOLUTIONS OF THE NERNST-PLANCK AND POISSON SYSTEM OF EQUATIONS FOR ELECTRODIFFUSION. Oscar J. Riveros, Thomas L. Croxton, and William McD. Armstrong. Dept. of Physiology and Biophysics, Indiana Univ. School of Medicine, Indianapolis, IN 46223.

Approximate solutions of the Nernst-Planck and Poisson system of equations under conditions of zero current were used by Planck to estimate junction potentials and by Goldman to calculate membrane potentials. These solutions assumed fixed values of ion concentrations at the planar boundaries of an interfacial region of thickness  $L$ . The Planck and Goldman theories are valid in the limits  $L \rightarrow \infty$  or  $L \rightarrow 0$ , respectively. The ranges over which these theories are useful have not been rigorously determined. We have obtained exact numerical solutions to this system of equations for arbitrary values of  $L$ . To accomplish this, two different approaches were required. For relatively smaller  $L$ , we iterated the steady-state equation  $dJ_i/dt=0$  where  $J_i$ , the flux of ions of type  $i$ , was given by the Nernst-Planck equation. For relatively larger  $L$ , we integrated  $\partial c_i/\partial t$  over time, where  $c_i$  is the local concentration of ions of type  $i$ . The continuity equation was used to relate  $\partial c_i/\partial t$  to  $J_i$ . In both approaches the electric field within the interface was obtained by numerical integration of the Poisson equation. Its value at one boundary was calculated using the Nernst-Planck equation and the condition of zero current. In the overlapping regions, the two approaches yielded identical results. The results indicate that for a dilutional junction the Planck approximation is valid for values of  $L > 10\kappa_0^{-1}$ , where  $1/\kappa_0$  is the Debye length of the more dilute solution. The Goldman approximation is valid for  $L < 0.1\kappa_1^{-1}$  where  $1/\kappa_1$  is the Debye length of the more concentrated solution. Supported by USPHS grants DK 12715, DK 36575 and DK 07554.

**T-Pos369** CALCULATION OF UPTAKE RATE CONSTANTS IN LIVING CELLS FROM DIGITAL IMAGING FLUORESCENCE MICROSCOPY DATA. Zeljko Jeričević, Brent Wiese, Laura Rice, Reynold Homan, Joseph Bryan and Louis C. Smith. Baylor College of Medicine and the Methodist Hospital, Houston, TX 77030.

Digital imaging fluorescence microscopy provides information about the spatial distribution of fluorescent probes in cells and has the potential to give information about active and passive mass transport processes in living and dead cells. In fixed cells, the uptake rate of fluorescent compounds can be calculated directly from a series of images sampled as a function of time during the uptake process. Using this data, we calculate a rate constant for every spatially defined pixel using a nonlinear least squares method. Calculation of the uptake rate in living cells is more complicated because of cell movement and changes in cell shape during uptake i.e., the time series of intensities is no longer spatially invariant. Before the rate constants for uptake can be calculated, the image series must be corrected for cell movement and distortion. We collect a series of phase images at the same time as the series of fluorescence images. The morphological details in the phase images do not change substantially when cell movement is largely translational. The information from these images is used to specify tie points for geometric correction of the phase image. After correction, the morphological details of each image in the time series corresponds to those of the initial image. The same correction is then performed on the respective fluorescence images. Correction is performed recursively with polynomials of various degrees until the positional error is less than one pixel. The series of spatially normalized cell images are then suitable for calculating rate constants of uptake on a pixel by pixel basis.

**T-Pos370** COMPUTER SIMULATION OF THE EFFECTS OF ANTIFOLATES ON THE INTERCONVERSION OF AND INTER-ACTIONS AMONG CELLULAR FOLATE COFACTOR POOLS: A NETWORK THERMODYNAMIC STUDY USING SPICE2 Dean Hearne, David Trent, D.C. Mikulecky, and I.D. Goldman Depts. of Medicine and Physiology, Med. Col. Va. Com. Univ., Richmond, VA 23298

Jackson and Harrap's (*Arch. Bioch. Biophys.* 158:827-841[1973]) and White's models (*J. Biol. Chem.* 254:10889-10895[1979]) have been extended to test a number of hypotheses about the mechanism of action of antifolate drugs. The model utilizes the circuit simulation program SPICE2 and consists of 15 pools interconnected by enzymatic reactions modeled by controlled sources. Pools can be varied or clamped and some mimic the inputs and outputs to this particular set of reactions to approach as realistically as possible events in the intact cell. Michaelis-Menton kinetics and its various types of inhibition are modeled in auxiliary computing circuits and the results are fed into the appropriate steps in the reaction network. This model tests the relative effects of folate substrate depletion versus direct enzyme inhibition at multiple sites to account for the very rapid inhibition of thymidylate synthase following exposure to antifolates. Our results suggest that folate depletion alone cannot explain the experimental data and direct enzyme inhibition is equally important. (Supported by NIH grants CA39807, CA09564, & HL07110 and the MCV A.D. Williams Fund).

**T-Pos371** AN EXPERT SYSTEM FOR GLOBAL ANALYSIS OF TIME-RESOLVED FLUORESCENCE DATA IN TERMS OF DISCRETE AND DISTRIBUTED PHYSICAL MODELS. Joseph M. Beechem and Enrico Gratton. Laboratory for Fluorescence Dynamics (LFD), Department of Physics, University of Illinois at Urbana, 61801.

Theory and instrumentation are undergoing rapid change and development in time and frequency domain fluorescence spectroscopy. It is very desirable to develop a data analysis system flexible enough to keep pace with these rapid developments. The current generation of global analysis programs developed at the LFD have been designed so that new models and theories can be immediately incorporated into the analysis. Each fitting parameter is described using high level, "natural language" keywords. These keywords map into a table of mathematical formulas which are then properly utilized in the subsequent data analysis. Keywords are entered into an extensive "dictionary," which contains entries for the growing number of mathematical functions utilized in fluorescence analysis. The current dictionary of keywords allows for global nonlinear analysis of fluorescence data surfaces in terms of discrete/distributed: energy transfer distances, quenching enthalpies and entropies, activation barriers, lifetimes, Stern-Volmer constants, rotational rates, activation volumes, etc. A "linked-list" type of processing and indirection allows for extreme flexibility in the design and combination of many different types of experiments (e.g., multiple excitation/emission wavelengths, temperatures, viscosities, quencher concentrations, polarizations, steady-state data, etc.). As new theories are developed, they can be immediately incorporated into the analysis by creating new entries in the keyword and mathematical formula tables. Specific examples of the analysis of very high dimensional data surfaces obtained from tryptophan in solution and in proteins along with other model systems will be described. Supported by NIH grants RR03155 and GM11163.

**T-Pos372** DIRECT WAVEFORM COLLECTION AND ANALYSIS OF PHASE FLUOROMETRY DATA. Brett Feddersen, Joseph M. Beechem, Joshua Fishkin and Enrico Gratton. Laboratory for Fluorescence Dynamics, Department of Physics, University of Illinois at Urbana-Champaign, Urbana, IL 61801.

Multifrequency phase fluorometry measures time dependent fluorescence phenomena by collecting data which consists of a series of phase lags and modulation values. The phase and modulation data is determined by hardware/software manipulation of the signal emitted by the photomultiplier (PMT) observing the fluorescent sample. The total information content from a phase fluorometry experiment is contained in the waveform detected by the PMT. All subsequent transformations of this waveform can only reduce (for all waveforms with noise) the information content of the original signal. In addition, the noise characteristics on the original waveform (which may be well defined) are distorted by the conversion to the phase and modulation values. For these reasons (loss of information content and nonlinear error propagation), we propose the direct collection and analysis of the digitized cross-correlated waveform obtained from the PMT. By using the digitized forms of the excitation, reference and sample fluorescence, a highly flexible and PROPERLY WEIGHTED analysis can be performed. Utilizing reference deconvolution, or color shift approaches, the waveforms obtained at many different excitation frequencies are combined in a global analysis to recover fluorescence lifetimes, rotational rates, etc. Computer simulation studies will be described where waveforms are fit directly, bypassing the intermediate step of determining phase and modulation values. This type of analysis will prove to be very useful for the analysis of signals obtained from a parallel fluorometer, where the digitized waveforms will simultaneously contain all of the harmonic frequency content of the excitation source. Supported by NIH grants RR03155 and GM11163.

**T-Pos373** AN IMPROVED STIMULATION AND DATA ACQUISITION COMPUTER PROGRAM FOR SINGLE CHANNEL PATCH CLAMP EXPERIMENTS. Richard Wagner, X. Guo and S.H. Bryant, Dept. of Pharmacology and Cell Biophysics, U. of Cincinnati, Cincinnati, OH 45267.

We have developed a stimulation and data acquisition program in FORTRAN-77 and MACRO-11 optimized for single channel patch clamp recording on DEC 11/23 or 11/73 computers with VT220/Tektronics 4010/4015 compatible terminals. This system is considerably less expensive than comparable commercially available systems and has many other significant advantages. The program is single-character command driven and puts out up to 4 user-defined voltage pulses from a variable holding potential. Data may be acquired during any or all of the voltage pulses, at sampling rates as fast as 7  $\mu$ sec/point, with an integral number of blocks of data stored per trace. Acquired data is initially stored in virtual memory to increase program speed and decrease the number of writes to the hard disk. Using a 4 Mbyte memory board, over 4000 traces may be acquired at 2 blocks (512 pts/trace in one continuous file. The program makes use of several digital I/O switches to control various program parameters, including voltage pulse polarity (inside/outside-out patch), saving/erasing data in memory, and increasing the amplitude of the test pulse used in gigaseal formation. In addition, the program reads, displays, and records the bath temperature and the gain, filter, and headstage settings of the AXOPATCH patch clamp amplifier. The software utilizes an overlay structure, which allows the use of the RT11-SJ monitor for increased execution speed, and is completely soft-error trapped and essentially crash-proof. Recursive techniques are used for file transfer and other RT-11 commands, and all setup parameters may be saved when exiting the program. Program listings, operational software, and hardware suggestions are available from the authors. (Supported by NIH grants NS-03178, TG HL 07382-12; MDA and the Albert J. Ryan Foundation).

**T-Pos374** EXPLORING PROTEIN STRUCTURES ON AN IBM-PC  
Howard Robinson and Antony Crofts, Physiology and Biophysics,  
Univ. of Illinois, Urbana, IL 61801

We have developed a series of programs that run on the IBM-PC (with CGA, EGA or VGA) for visualizing protein structure. The program pdViewer is an atomic coordinate database manipulator for Brookhaven Protein Data Bank format structures. The coordinate databases are displayed as a red/green 3-D stereo image representing the atomic bonds of the structure. The image is viewed through red/green filtered glasses to perceive the 3-D structure. Standard templates specifying the atomic bonds for residues (amino acids and nucleic acids) are included and may be easily augmented to include unusual or modified structures. Residues can be highlighted by residue number or type. pdViewer can rotate, scale and slice the 3-D image. Structures can be drawn in full or backbone-only mode. A 3-D cursor identifies atoms and gauges interatomic distances. Two structures can be manipulated simultaneously or independently, then overlaid for comparison. Up to 14000 atoms may be manipulated. The program can selectively display water molecules, hydrogen bonds and prosthetic groups. Gradients such as electrostatic potentials can be represented as 3-D isopotential surfaces. The image from the screen may be plotted on an HP-GL pen plotter to produce high resolution stereograms. The atomic coordinates from the manipulated screen image may also be sent to a file to be used as input to the program SPHERE. SPHERE produces a CPK-like shaded atomic representation on the IBM-PCGA display. Coloring of the spheres and sphere radii can be adjusted to visually accentuate various structural features of the model.

**T-Pos375**      **COMPUTATIONAL ISSUES IN BACTERIAL CHEMOTAXIS** David Warland and William Bialek, *Departments of Physics and Biophysics, University of California, Berkeley, CA 94720*

Chemotaxis allows a bacterium to find regions of space where the concentration of various substances take maximal or minimal values. Mathematically this is just the problem of extremizing a function of three (spatial) variables. The classic strategy for such problems is gradient descent. If we think of the function to be minimized as the potential energy of a particle, then gradient descent is equivalent to diffusion in this potential at zero temperature. In fact bacteria adopt a strategy (running and tumbling) more closely analogous to diffusion at non-zero temperature, which is similar to recent proposals for the solution of complex optimization problems by 'simulated annealing.' In contrast to the conventional formulation of optimization problems, the bacterium does not have direct access to the function (concentration) it would like to minimize, but only to a noisy version of this function (1). We develop a theory of optimization in the presence of noise using the same statistical mechanics analogies which form the basis for simulated annealing. This approach suggests that there is an optimal balance of diffusion and gradient descent, and hence an optimal 'temperature,' which depends on the signal-to-noise ratio. If bacteria perform optimally these results should allow us to predict some aspects of run/tumble statistics and the variation of these statistics with signal level (adaptation).

(1) H.C. Berg and E.M. Purcell, *Biophys. J.* 20, 193 (1977).

This work is supported in part by grants from the NSF and the USPHS.

**T-Pos376** PULSED FIELD ELECTROPHORESIS: APPLICATION OF A COMPUTER MODEL TO THE SEPARATION OF LARGE DNA MOLECULES. - Marc Lalonde and Chantal Turmel, NRCC-Biotechnology Research Institute, Montréal, Canada, and Jaan Noolandi, Gary W. Slater, Jean Rousseau, Xerox Research Centre of Canada, Mississauga, Canada.

The biased reptation theory has been applied to the pulsed field electrophoresis of DNA in agarose gels. A computer simulation of the theoretical model which calculates the mobility of large DNA molecules as a function of agarose pore size, DNA chain properties and electric field conditions has been used to generate mobility curves for DNA molecules in the size range of the larger strain *S. cerevisiae* yeast chromosomes. Pulsed field electrophoresis experiments resulting in the establishment of an electrophoretic karyotype for *S. cerevisiae*, where the mobility of the DNA fragments is a monotonic function of molecular size for the entire size range which is resolved (200 to 2,200 kilobasepairs), has been compared to the theoretical mobility curves generated using the computer model. The various physical mechanisms and experimental conditions responsible for band inversion and improved electrophoretic separation are identified and discussed in the framework of the model. The size range of separation attainable using the experimental system has been extended to 9,000 kilobasepairs which corresponds to largest chromosome of the yeast strain *S. pombe*.

**T-Pos377** OPTIMIZING AGAROSE CONCENTRATION FOR RESOLUTION OF DNA FRAGMENTS. Francis H. Kirkpatrick and Brendan M. Duggan, FMC BioProducts, 5 Maple Street, Rockland, Maine 04841.

Separating DNA fragments by electrophoresis in agarose is a simple and reliable technique, but it is difficult to find convenient guides for choosing the correct agarose concentration to use, especially for a range of fragment sizes. We have separated a set of DNA fragments to known size (*Hae* $\phi$ x 174, *Hind* $\lambda$ , and  $\lambda$ ) on agarose gels of various concentrations, using a Serwer 9-lane cell. Plots of  $R_f$  vs log basepairs shows that the linear region typically lies between  $R_f$  of 0.2 to 1.0 (with bromophenol blue as standard).

We have found a useful way to replot such data. By interpolation, the agarose concentration at which a given DNA fragment has  $R_f$ 's of 0.2, 0.6 and 1.0, is found. By plotting this data on the log (basepairs) vs log (% agarose) plane, a trapezoidal band of "good resolution" is marked out. It is then easy to select an appropriate agarose concentration for a given fragment size or range of sizes.

These plots are useful for comparing the sieving of various media. They show clearly that borate buffers make all agaroses more sieving, as shown elsewhere. They confirm that SeaPlaque<sup>®</sup> agarose hydroxyethyl agarose is more sieving than SeaKem<sup>®</sup> standard agarose, but show that NuSieve<sup>®</sup> low-viscosity hydroxyethyl agarose sieves like SeaKem rather than SeaPlaque agarose. They demonstrate that variation in electroendosmosis has no effect on relative sieving, and affects only the velocity in the gel. Comparison of runs at 1V/cm vs. 5V/cm clearly shows the onset of reptation at less than 10 kBP. This method of plotting may be a generally useful tool for studying comparative sieving of various media.

**T-Pos378** ON LINE ELECTROPHORESIS OF NUCLEIC ACIDS RESULTS IN NOVEL APPROACHES TO MOLECULAR CLONING. M.A. Hediger (Intr. by E. M. Wright). Dept. of Physiology, University of California, School of Medicine, Los Angeles, CA 90024.

The preparative separation of nucleic acids in a continuous elution instrument has been used previously as an alternative to classical separation methods in molecular biology (Hediger, M.A., 1986, *Anal. Biochem.* 159:280-286). For example, preparative amounts of plasmid DNA have been obtained in high purity after only four hours of electrophoresis. Recently, this preparative scale method which I refer to as "on line electrophoresis" has been successfully used to facilitate the rapid isolation of a full-size cDNA clone of the intestinal Na/glucose cotransporter. Electrophoresis of mRNA in a non-denaturing gel system resulted in high resolution size fractionation. RNA from each fraction was tested using a functional expression assay with *Xenopus* oocytes. cDNA was then synthesized from the fraction of interest. Using "on line electrophoresis," full size cDNA was separated from partial transcripts to ensure the cloning of a full-size fragment. A small library was constructed and screened, and a functional clone was isolated.

I expect that size-fractionation of genomic DNA fragments by "on line electrophoresis" will be useful in constructing enriched genomic libraries and cloning DNA regions of a particular size. Using this procedure in conjunction with field inversion electrophoresis, the separation of nucleic acids larger than 50kb could be achieved.

**T-Pos379** THEORY OF GEL ELECTROPHORESIS OF WORMLIKE CHAINS. Stephen D. Levene and Bruno H. Zimm; Department of Chemistry, University of California (San Diego), La Jolla, CA 92093.

Calculations of the gel electrophoresis of wormlike chains, an appropriate model for the electrophoresis of DNA in concentrated gels such as polyacrylamide, are described. The mobility of a one-dimensional lattice model for the wormlike chain is calculated from a dynamical simulation employing a time-weighted average over the configurations of the chain, following a suggestion by Noolandi, et al., and the results are compared to those for a simple unweighted configurational average used previously. The simulation results reproduce the logarithmic molecular-weight dependence of the mobility typically observed in separations of DNA restriction fragments and SDS-poly-peptide complexes on polyacrylamide gels. The results also display the characteristic inflections and loss of resolution in the high and low molecular weight extremes that are observed experimentally.

Supported by an American Cancer Society Postdoctoral Fellowship PF-2541 to SDL and NIH grant number GM-11916 to BHZ.

**T-Pos380** TRANSIENT VELOCITY, DISPLACEMENT, AND ORIENTATION OF DNA DURING PULSED-FIELD GEL ELECTROPHORESIS. G. Holzwarth, Kevin J. Platt, Richard W. Whitcomb, and Chad B. McKee, Dept. of Physics, Wake Forest Univ., Winston-Salem, NC 27109

The instantaneous velocity and local helix orientation function  $\langle 3\cos^2\theta - 1 \rangle / 2$  of T4 and  $\lambda$  DNA stained with EB have been measured in 1% agarose gels for E between 4 and 14.6 V/cm. In response to a square pulse with E=14 V/cm, the velocity of T4 DNA rises steadily to an overshoot of 10  $\mu\text{m/s}$  at 4 s, then declines to a plateau of 8.8  $\mu\text{m/s}$ . At the time of the overshoot, the center of mass of the DNA has moved 25  $\mu\text{m}$ , about half its contour length. The orientation function reaches a peak value of +0.40 at 3 s before declining to a steady 0.35, indicating a substantial stretching of the DNA chain in the direction of the field. The overshoot in both velocity and orientation function is nonlinear in E and moves to longer times as E decreases or molecular weight increases. Reptation models for the equilibrium conformation can explain the value of the orientation function and velocity but have not anticipated the overshoots, which can be harnessed for DNA separations by pulsed-field electrophoresis.

\*Supported by grants from Chevron Research Corp., Research Corp., the NC Biotechnology Center, and the NSF.